University of Texas at El Paso

ScholarWorks@UTEP

Open Access Theses & Dissertations

2022-08-01

Trade Study Analysis Of The Janus Moon Lander Vehicle

Omar Vazquez
University of Texas at El Paso

Follow this and additional works at: https://scholarworks.utep.edu/open_etd

Part of the Aerospace Engineering Commons, and the Translation Studies Commons

Recommended Citation

TRADE STUDY ANALYSIS OF THE JANUS MOON LANDER VEHICLE

OMAR VAZQUEZ

Master's Program in Mechanical Engineering

APPROVED:

_____

Jack Chessa, Ph.D., Chair

_____

Angel Flores, Ph.D.

_____

Luis Rene Contreras, Ph.D.

_____

Stephen Crites, Ph.D.
Dean of the Graduate School

Dedication

To my family that has always supported me. To my friends and people that have

believe in me since I started this chapter.

It didn't become a dream, the goal has been achieved.

TRADE STUDY ANALYSIS OF THE JANUS MOON LANDER VEHICLE

by

OMAR VAZQUEZ, B.S. M. E.

THESIS

Presented to the Faculty of the Graduate School of

The University of Texas at El Paso

in Partial Fulfillment

of the Requirements

for the Degree of

MASTER OF SCIENCE

Department of Mechanical Engineering

THE UNIVERSITY OF TEXAS AT EL PASO

August 2022

Acknowledgments

I would like to thank my parents (Paulin and Carmen), siblings (Ivan and Itzel), grandmother (Juanita) and Tias (Claudia and Yovanna), for all the love and support that they have given me. For always been there when I need them the most.

My sincere gratitude to Dr. Chessa and Dr. Adams for all the help and mentorship that I have received from them to complete my tasks as a research assistant and for pushing me out of my comfort zone.

I would like to thank the cSETR staff and faculty for all the help and guidance. Luz for believing in me and giving me the opportunity to work as a research assistant. Dr. Quintana for all the help with the electrical hardware at Fabens and all the knowledge and experience shared, for being more than a professor. Dr. Flores for the guidance to present my final work. Luis Orozco, Jose Hernandez and Rick Keller for being such a great help and friends at Fabens in the most stressful times.

To my mentor Marissa Garcia, Paul Gradl, and Darren Tinker for making my first internship at NASA such a great and unforgettable experience. For all your knowledge, help, mentorship, and patience.

To all the LOX/LCH4 team members that have work along my side. To my first team lead Gerardo, and my friends Raul, Jazmin, Dominic, and Rodrigo to whom I work with during the harsh times of the pandemic. To Jazmin for all the advice, help and her friendship. To my friends Raul, for all the help and his friendship since my first assignment in the lander, Iram and Cruz for all the help in the CAD of the lander designs and other tasks assigned. To Perla for all the unconditional support in the most stressful and hard times that I had as a team lead. To Isaac

for being my companion all summer in the lab during the completion of this work. To Jesus, Kristina, Cesar, Lalo, Adam and James for all the help during testing, the support during the stressful times and the funny moments that we went through together. Thank you for making my time at the LOX/LCH4 team such a blast! You'll be forever in my heart.

To my friends that crossed my path at EPCC and have been along my side in the completion of my bachelors degree and pursuing my masters degree. The friends who shared with me the most stressful, funny, and happy moments of my career: Jesus, Jerry, Erick, Rene and Daniel.

Lastly, to my hometown friends and family that have been always with me, that have believed in me since I started college and who always give me their sincere affection when I go back home. Agustin, Uriel, Zilvano, Jesus N., Daniel, Jonathan, Hector, Erick and Jesus Acevedo.

Thank you for believing in me.

Abstract

Liquid Oxygen (LOX) and Liquid Methane (LCH4) has become a propellant combination of interest in the recent years, especially for leading aerospace companies with the sight set on mars such as SpaceX and Blue Origin in their heavy thrust engines (the Raptor and BE-4 respectively) since methane can be more stable than hydrogen, can be stored at more manageable temperatures and can be produced locally, at mars, using in-situ resource utilization (ISRU) [1].

The Center for Space Exploration and Technology Research (cSETR) has developed a 500 lbf throttleable (4:1) thrust chamber (CROME) using the aforementioned propellant combination with the intention of validating the current design and develop a throttleable (4:1) thrust chamber capable of delivering 2000 lbf of thrust (CROMEX). CROMEX will be used as the main engine of the flight vehicle (JANUS) current under development by cSETR, for which its main design requirement is to be able to deliver 130 lbm to the lunar surface. JANUS will also utilize 12X5 lbf reaction control engines, developed in house by cSETR with the same propellant combination of LOX/LCH4, for maneuvering. In addition, JANUS will have a gimbal system, an electronic system capable of operating autonomously the required electronic hardware and for data acquisition and a leg system intended for landing.

In this thesis, a trade study comparing properties such as mass and moments of inertia of different design configuration was performed to select the best design option. In addition, an FEA analysis was performed to determine the magnitude of the stresses as well as the natural frequency of the JANUS main lander design once the best design was chosen. Different iterations were performed to manipulate the structure to reduce the stresses and increase the natural frequency. In the FEA analysis loads such as pressure, G forces in the lateral and vertical

directions and a modal analysis were performed to analyze the results of interest already mentioned.

Table of Contents

List of Tables

List of Figures

Chapter 1: Introduction

1.1 INTRODUCTION

At the end of WWII both nations, the US and the USSR were submerged into what is known as the cold war. This was not a direct confrontation since the conflict only involved competition in political influence, arms development and eventually the space race. In 1957 the USSR launched the Sputnik 1 on a modified R7 ICBM, making it the first spacecraft to ever be launched to space [2], giving birth to the space race. Right after the launch of the Sputnik 1, both countries began space missions launching spacecraft to the moon.

1.2 US SPACECRAFTS

In 1958 the US began their space program with the Pioneer Project that had the objective of sending space craft to orbit moon, detect cosmic radiation, provide the first map of the interplanetary magnetic field, make measurements of the solar wind, solar magnetic field and cosmic rays, visit Jupiter and Saturn, observe Venus' atmosphere and provide in-situ measurements in Venus [3]. In 1961 the US continued with the Ranger Project which obtained images of the lunar surface, these increasing in resolution as the spacecraft neared the surface until impact. The main goal of the project was to gather data and help in the design of future spacecraft that would land on the moon [4]. Nine spacecraft were part of this project, Ranger 1 and 2 failed due to launch failures, Ranger 3 and 5 missed the moon, and Ranger 6-9 successfully impacted the moon with the exception that the camera system failed in Ranger 6. The images obtained with the Ranger program showed that the lunar surface had craters, most likely due to impacts, and that the "intercrater areas were sufficiently level and smooth to allow for the landing of a spacecraft" [4].
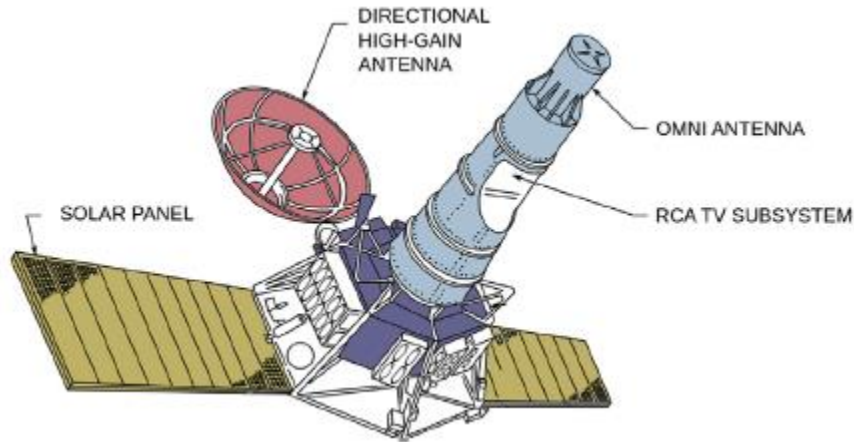
Figure 1. Ranger Spacecraft [4]

Unlike the previously stated programs, the series of spacecraft used in the surveyor program had the capability to make soft landings on the moon. The main objective of the surveyor spacecraft series was to determine if the lunar surface was safely for manned missions and take close-up images of the lunar surface [5]. The surveyor spacecraft was a three-meter-tall vehicle on a 27-kilogram thin walled aluminum triangular structure with three legs attached to each corner. At the center, attached, there was a solid-propellant retro-rocket engine. Doppler velocity-system to control the decent to the surface, aircraft-type shock absorbers, and strain gauges for data on landing characteristics were some of the components that were equipped into the surveyor spacecraft series [6]. The spacecraft was similar in design for all seven vehicles with the exception of the mass (995.2 kg, 997.9 kg, 1037 kg, 1006 kg, 1008.3 kg and 1040.1 kg for Surveyor I & II, III, IV, V, VI and VII respectively) and the specific instruments on the spacecraft such as TV camera, surface sampler, imaging system, alpha-scattering instrument, footpad magnet and stereoscopic and dust detection mirrors that were part of some Surveyor vehicles.
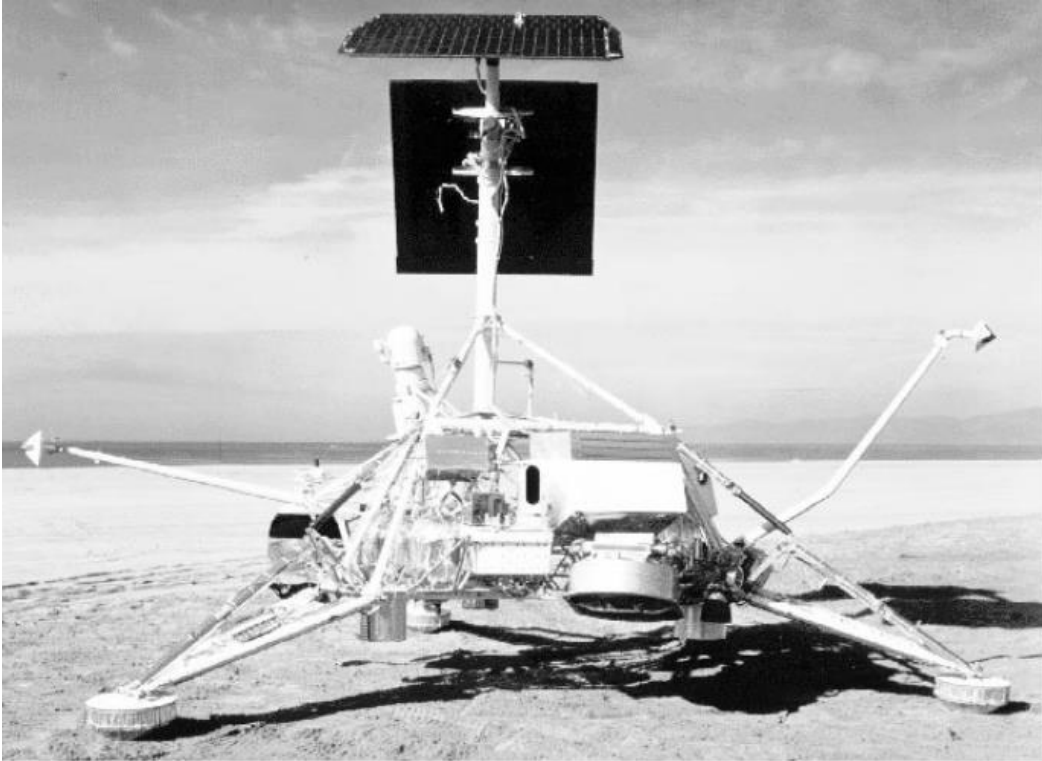
Figure 2. Surveyor Spacecraft on terrestrial beach [7]

The apollo program began in 1967 with the apollo 1 mission, which unfortunately ended in tragedy when three astronauts lost their lives in the command module due to a fire. After that, the program continued with the apollo 4 mission, which was the first launch of the Saturn V, having no apollo 2 and 3 missions [8]. Apollo 5 was the first test of the lunar module, having the objectives to test the spacecraft structure, propulsion system, restart operations and the ascent and decent stage of the spacecraft [9]. Eventually the apollo missions continued with different objectives and preparations such as the simulation of putting the spacecraft into translunar injection (apollo 6), demonstrate rendezvous capability, among other objectives, of the Command Service Module (apollo 7), refine the systems and procedures for future lunar operations (apollo 8), engineering tests of the first crewed lunar module (apollo 9) and the simulation of a crewed moon landing down to 9 miles off the lunar surface. All these

preparations made possible the landing of the first man on the moon on apollo 11. Subsequent apollo missions, apollo 12-17, successfully landed humans in the lunar surface, except for apollo 13 which had to circle the moon and return to earth due to an explosion in the oxygen tank of the service module. The vehicle that was used to land the first man in the moon was the lunar module, developed by Grumman Corporation, now knows as Northrop Grumman. Once the company was awarded the contract to develop more than a dozen of lunar modules, nearly 3000 engineers were working on such system that incorporated lightweight metals and unique electronic and electric systems [10].

The spacecraft was a two-stage vehicle, the descent and ascent stage, that was covered with silver, gold and black thermal shielding making the vehicle look fragile. In addition, the vehicle was made from light thin metal that helped reducing the amount of propellant needed for landing [11]. The crew cabin was in the ascent stage, along with the controls air and water. The ascent stage's engine was developed by Bell AeroSystems, able to deliver a nominal thrust of 3500 lbs. In contrast to the descent stage engine, the ascent stage engine had a fix thrust since the main task of this stage was to put the astronauts into the predetermined orbit from lunar surface [13].

Table 1. Ascent Stage Engine Assembly Parameters

Thrust (lbs.)	3500
Chamber Pressure (psia)	120
Propellant Injection Ratio (oxidizer to fuel)	1.6 to 1
Approximate Weight (lbs.)	200
Overall Length (in)	47
Nozzle Expansion Area Ratio	45.6 to 1
Nozzle Exit Diameter (in)	31

The descent stage stored the scientific equipment and the support materials, along with the landing gear and, in the case of apollo 15, 16 and 17, the lunar rover vehicles [12]. The descent stage's engine was designed by Space Technology Laboratories [15], being capable of throttle from 1280 to 9900 lbs. of thrust. Due to the complexity of the descent stage's task, maneuvering and hovering over the lunar surface as the astronauts select the proper landing spot, the engine was designed to be throttleable and gimbaled making it capable of delivering enough thrust for the landing of the complete lunar module vehicle but also to have thrust control and thrust vector control [13].

Table 2. Descent Stage Engine Assembly Parameters

Thrust (lbs.)	1280-9900
Chamber Pressure (psia)	103.4
Propellant Injection Ratio (oxidizer to fuel)	1.6 to 1
Approximate Weight (lbs.)	348
Overall Length (in)	95
Nozzle Expansion Area Ratio	47.4 to 1
Nozzle Exit Diameter (in)	63

Both engines were pressure feed engines having helium as the pressurizing fluid. In addition to that, both engines used hypergolic propellants Aerozine 50 as fuel and nitrogen tetroxide (N2O4) as the oxidizer.

Chapter 2: Analysis

2.2 LANDER CONFIGURATIONS MASS AND MOMENT OF INERTIA PROPERTIES

The stability of spacecraft is one of those requirements that must be meet otherwise the mission is intended to failure. Preceding spacecraft, such as Ranger 5 (US) and Luna 4 (USSR) failed to successfully complete their objectives due to malfunctions in their control and navigation system respectively [2]. For this reason, stability is of such importance to engineers involved in the design. In stability, one parameter that must be known is the moment of inertia (MOI). The moment of inertia shows "an object's amount of resistance to any change in its rotational rate about an axis" [16]. The MOI plays and important role in attitude control of the spacecraft (defined as the prediction of and reaction to a vehicle's rotational dynamics [17]). One example on how the torque needed to stabilize a space craft can be estimated is using Euler's rotational equations of motion, which are dependent on the MOI, angular velocity, and angular acceleration as shown below.

$$\begin{bmatrix} \tau_x \\ \tau_y \\ \tau_z \end{bmatrix} = \begin{bmatrix} I_{xx} & I_{xy} & I_{xz} \\ I_{yx} & I_{yy} & I_{yz} \\ I_{zx} & I_{zy} & I_{zz} \end{bmatrix} \begin{bmatrix} \alpha_x \\ \alpha_y \\ \alpha_z \end{bmatrix} + \begin{bmatrix} \omega_x \\ \omega_y \\ \omega_z \end{bmatrix} \times \begin{bmatrix} I_{xx} & I_{xy} & I_{xz} \\ I_{yx} & I_{yy} & I_{yz} \\ I_{zx} & I_{zy} & I_{zz} \end{bmatrix} \begin{bmatrix} \omega_x \\ \omega_y \\ \omega_z \end{bmatrix}$$

Equation 1 [37]

The moment of inertia tensor is a 3X3 matrix that lists the magnitudes of the moments of inertia of the same object around the three different axis, since, the moment of inertia will not be equal around the three axes unless the body is symmetrical about all axes. The diagonal components of the matrix such as I_{xx}, I_{yy} and I_{zz} are the principal moments of inertia whereas the rest of the components are called the products of inertia.

$$I = \begin{bmatrix} I_{xx} & I_{xy} & I_{xz} \\ I_{yx} & I_{yy} & I_{yz} \\ I_{zx} & I_{zy} & I_{zz} \end{bmatrix}$$

Equation 2 [37]

Another parameter of interest when analyzing the stability of a spacecraft is the center of mass (CM). The CM is the point in the body "through which any plane will divide the mass moment evenly" [17]. If a force is applied at the CM, there will be no torques generated, that is why "freely rotating bodies rotate about their centers of mass" [17]. The center of gravity (CG) is defined as an imaginary point in a body where the total weight of the body is concentrated [18]. In a uniform gravity field such as the one on earth, the CM and CG are in the same location, but this cannot be true in a gravitational field where the magnitude is not the same in all directions, such as in the free fall of a space orbit [17]. For elongated or flattened objects in orbit the CM may not be in the same location as the CG, generating a torque, which is critical when modeling of spacecraft and the understanding of the torque environment [17].

Because of the importance of these parameters (CM, MOI and CG) a trade study was performed to four different configurations (tank arrangements and different tank shapes) of the JANUS lander at two scenarios, wet, including the mass of the propellant and pressurizing fluid, and dry, without these fluids. The objective of the trade study was to analyze the pros and cons (structural weight, location of CM, MOI tensor, etc.) of each configuration and eventually choose the configuration that best meet the requirements of the weight budget, properly perform maneuvers with thrust generated by the Reaction Control System (RCS) and was stable enough and allow for a simple gimbal system design (MOI is a crucial parameter for the algorithms used

in the Thrust Vector Control (TVC)) [19]. These parameters can be easily calculated/obtained through the use of a CAD software, in this case the configurations were CAD using Fusion 360.

The configurations had components of similar properties to allow for a good comparison between each other. The material for the propellant tanks was chosen to be aluminum 6061 since aluminum is less dense than stainless steel and stronger, making it suitable for a light and strong pressure vessel, whereas for the pressurizing tank titanium was chosen (since it will not react with helium as it would with oxygen) because of its strength and low density making it a good material for a resistant pressure vessel at high pressures but also of low weight allowing for a greater margin to increase its thickness if needed. The thickness of the oxidizer tanks used for the first two iterations was chosen to be 1/8", based on the hoop stress calculations that yielded a thickness of 0.09 as the minimum thickness required, and ¼" in the oxidizer tank for the last two configurations since the oxidizer thank was placed in the bottom and, thus, will get more load than the fuel tank in the last two configurations. For the fuel tanks, in all iterations, the thickness was chosen to be 1/8", and for the pressurizing tanks a thickness of ¼" was chosen since the operating pressure will be 4000 psi, making more conservative even though the required thickness to withstand the pressure is 0.120". Fusion 360 has the ability to calculate the moment of inertia, all principal and products of inertia, about the center of mass of the CAD and about the origin, which can be arbitrary since any can change the origin at any location. For this reason, the moment of inertia used for this analysis were the moments of inertia about the center of mass.

The first configuration designed consisted of four spherical tanks, two for the propellants and two for the pressurizing fluid. The tanks are arranged opposite to each other meaning that the propellant tanks are arranged next to each other and in opposite directions the pressurizing tanks as shown in the figure below.

Figure 3. First Configuration. Methane tank (L); Oxygen Tank (R); Pressurizing Tanks (Front

and Back)

In this configuration, at the dry case, the center of mass is located at the origin (17.15" from the

ground in the positive z-direction and 10.22" from the center of the front pressurizing tank in the

positive y-direction), of the CAD but 0.22" off from the origin in the negative z-direction. For

the wet case, the center of mass was shifted to the right, x-direction, by 8.197", and went to -

0.04" in the z-direction (from the origin).
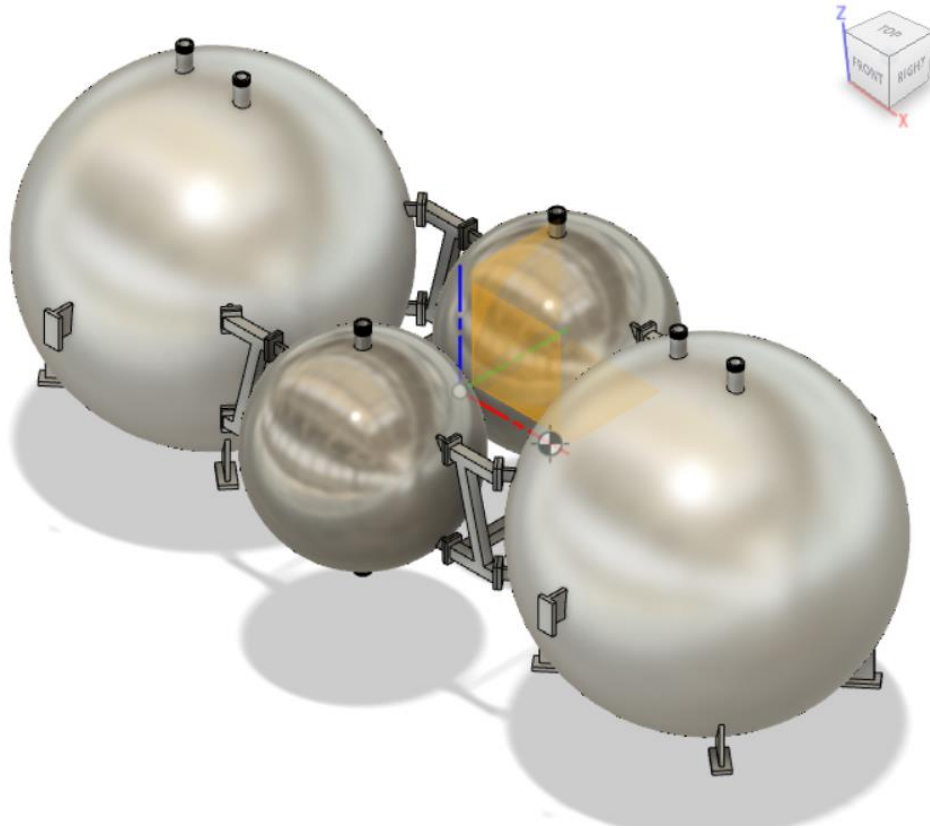
Figure 4. First Configuration. Origin and Center of Mass at Wet Case

The mass (lbm) and the moment of inertia (ouncemass in^2) of this configuration were also determined for the two cases already mentioned. First, the mass at the dry case was 168.6 lbm, including the supporting structure to hold the pressurizing tanks and the supports that are part of the propellant tanks for the leg system and pressurizing tanks. The mass for the wet case went up to 996.6 lbm, which now includes liquid oxygen, liquid methane and helium that is pressurized at 4000 psi and at a temperature of 70° F. The moment of inertia, including the products of inertia, were also calculated. For simplicity in the analysis, the principal moments of inertial will be listed. For the dry case the principal moments of inertia were $I_{xx} = 4.22E05$, $I_{yy} = 1.09E06$, $I_{zz} = 1.24E06$, whereas for the wet case the principal moments of inertia increased to $I_{xx} = 1.64E06$, $I_{yy} = 9.44E06$, $I_{zz} = 9.62E06$ ouncemass in^2.

The second configuration analyzed is similar to the first configuration presented, with the difference that cylindrical tanks were used instead of spherical tanks for the pressurizing gas.

Figure 5. Second Configuration. Center of Mass at Dry Case

As in the first configuration, the methane tank is at the left side, oxygen at the right, and the pressurizing tanks at the front and back of the picture. Also, the origin (17.38" from the center of the methane tank in the positive x-direction and 17.15" from the ground in the positive z-direction) was placed at the center of the geometry. For the dry case the center of mass is at the origin except 0.254" off in the negative z-direction.
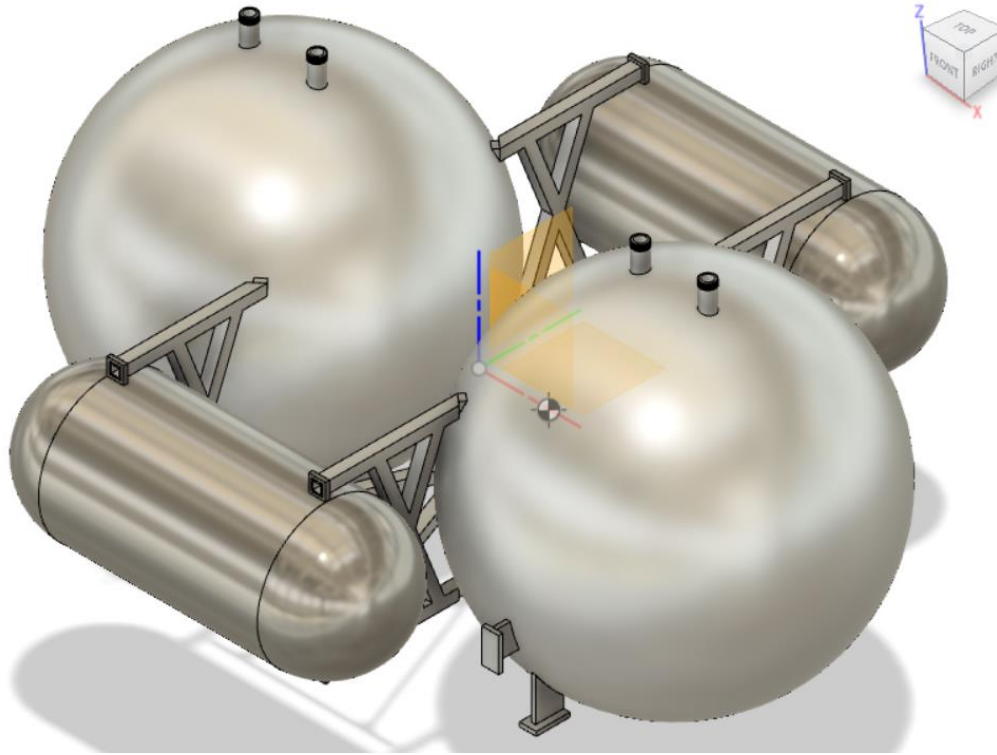
Figure 6. Second Configuration. Origin and Center of Mass at Wet Case

As in the first configuration, at the wet case the center of mass was shifted to the right, 6.293",

positive x-direction due to the weight of the liquid oxygen and went up to 0.088" in the positive

z-direction (measured from the origin).

As well as in the first case, the mass and the moment of inertia were calculated for this

configuration to allow for a comparison between the first iteration and the second iteration since

these two are similar in the propellant and pressurizing tanks arrangement. The mass for the dry

case was 184.55 lbm and for the wet case it increased to 1012.57 lbm. The principal moments of

inertia were calculated to be $I_{xx} = 1.13E06$, $I_{yy} = 7.07E05$, $I_{zz} = 1.59E06$ for the dry case and $I_{xx} =$

2.53E06, $I_{yy} = 5.12E06$, $I_{zz} = 6.24E06$ ouncemass in^2 for the wet case.

12

Table 3. Parameters Comparing the First and Second Configurations

Parameter	First Configuration (Figure 3)	Second Configuration (Figure 5)
Center of Mass$_{Dry}$ (in)*	(-0.05, 0.02, -0.22)	(0, -0.03, -0.25)
Center of Mass$_{Wet}$ (in)*	(8.2, 0.02, -0.04)	(6.3, -0.03, -0.05)
Mass$_{Dry}$ (lbm)	168.6	184.5
Mass$_{Wet}$ (lbm)	996.6	1012.6
I_{xx_Dry} (ounces in^2)	4.22E05	1.13E06
I_{yy_Dry} (ounces in^2)	1.09E06	7.07E05
I_{zz_Dry} (ounces in^2)	1.24E06	1.59E06
I_{xx_Wet} (ounces in^2)	1.64E06	2.53E06
I_{yy_Wet} (ounces in^2)	9.44E06	5.12E06
I_{zz_Wet} (ounces in^2)	9.62E06	6.24E06

*Dimensions are measured from the origin of that particular configuration

As seen in table 3, the second configuration shifts its center of mass at the wet case 6.3" in the positive x-direction, 1.9" less than the first configuration, which can be an advantage for stability if the engine is going to be located under the origin/geometrical center of the configuration. The mass was less for both cases for the first configuration, making it more suitable in terms of having a configuration with as less mass as possible. The moment of inertia was also less for the first configuration than for the second configuration in all principal moments of inertia for the dry case, even for I_{xx_Wet}, but increased for I_{yy_Wet} and I_{zz_Wet} which can result in more thrust needed for the reaction control engines since they will be providing the torque needed to maneuver around the z-axis. Even though the first configuration seems more suitable in terms of having the lower mass from those two configurations analyzed, having the lower magnitude in the moments of inertia except for I_{yy_Wet} and I_{zz_Wet}, none of these two configurations were chosen to be the final design due to the center of mass constantly shifting, as the propellants are being burned with time, from start location, 8.2" and 6.3" in the x-direction for the first and second configuration respectively, to the final location, -0.05" and 0 for the first

and second configuration respectively. As mentioned earlier if a force is applied at the center of mass there would no torques generated, meaning that if one of those two configurations were to be chosen, the engine will have to move in the same direction, x-axis, and same location at the same time to avoid any torques, which would result in a complex gimbal system.

Due to the center of mass problems in these two configurations and the complexity in the gimbal system that would have to be designed, another two configurations were created to be compared, similarly as the previous two configurations. The third configuration created is similar to the second configuration, where the propellant tanks are spherical and the pressurizing tanks are cylindrical, but the with difference that the configurations has been "shifted up" as seen in Figure 7.

Figure 7. Third Configuration Center of Mass at Dry Case

As mentioned earlier, in this configuration the thickness of the oxygen tank was increased from 1/8" to ¼" since it will be supporting the fuel tank and the pressurizing tank, meaning that it will be at the bottom. The fuel tank is at the top and next to both propellant tanks there are two cylindrical tanks that are mounted and supported by these propellant tanks. For this configuration, the origin was placed in the at the center of the distance that separates both propellant tanks, which is 39.8" from the ground. The center of mass does not experience a significant change in location, moving only 0.135 from the dry case (-7.45") to the wet case (-7.57") in the negative z-direction (center of mass is measured from the origin).
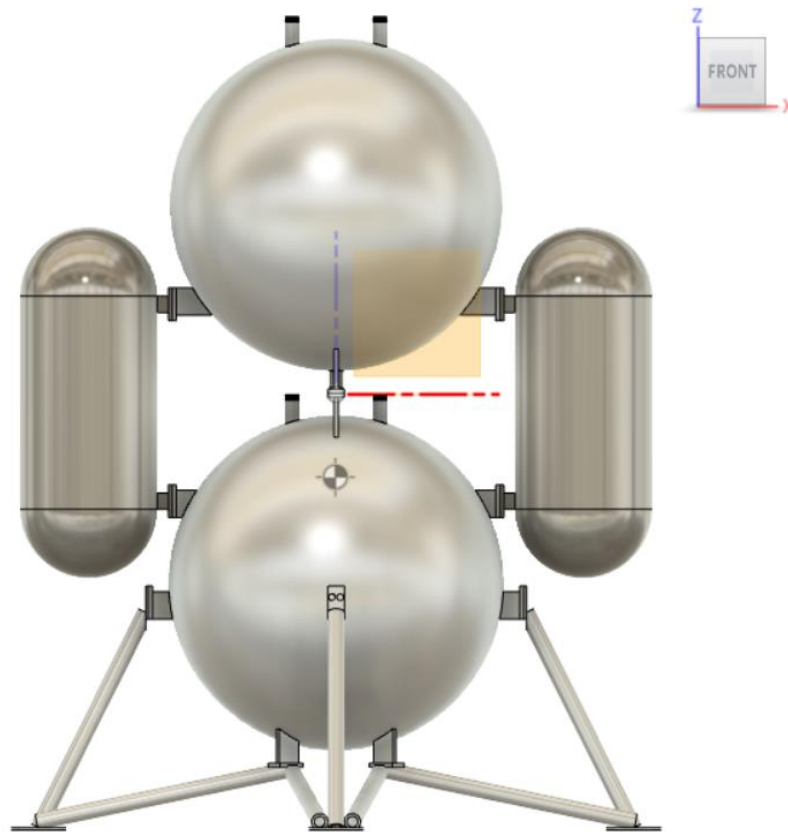
Figure 8. Third Configuration Center of Mass at Wet Case

The mass of the configuration at the dry case came up to be 241 lbm, increasing to 1069 lbm once the propellants and the pressurizing gas were added (wet case). The principal moments

15

of inertia for this configuration were $I_{xx} = 1.42E06$, $I_{yy} = 2.22E06$, $I_{zz} = 1.30E06$ for the dry case, and $I_{xx} = 5.63E06$, $I_{yy} = 6.66E06$, $I_{zz} = 2.69E06$ ouncemass in^2 for the wet case.

For the fourth configuration the propellant tank arrangement was kept the same, oxygen on bottom and methane on top of oxygen. Also, the thicknesses were kept the same as in the third configuration for both propellant tanks, the only difference in this configuration is that instead of two cylindrical pressurizing tanks, only one tank was used, also the shape was changed to spherical instead of cylindrical.

Figure 9. Fourth Configuration Center of Mass at Dry Case

The origin for this configuration was chosen to be at the center of the oxidizer tank, 29.15" from the bottom supporting ring. The center of mass at the dry case is located 0.3" in the positive x-direction, 0.19" in the negative y-direction and 26.2" in the positive z-direction, all

16

these measurements from the origin. For the wet case the center of mass moves to 0.06" in the negative x-direction, 1.9" in the negative y-direction and down to 14.45" in the z-direction.
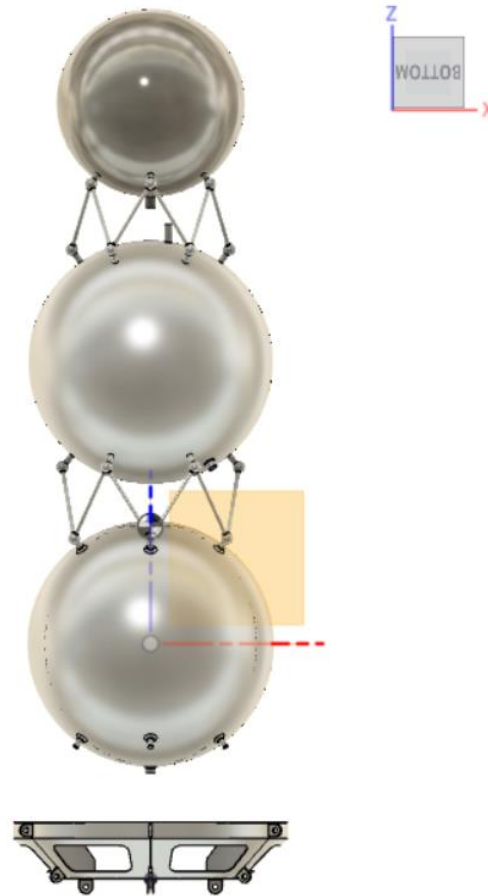
Figure 10. Figure 10. Fourth Configuration Center of Mass at Wet Case

The mass for the fourth configuration was 227 lbm at the dry case and increased to 1051.8 lbm once the propellants and pressurizing gas were added. The principal moments of inertia were calculated to be $I_{xx} = 4.04E06$, $I_{yy} = 4.05E06$ and $I_{zz} = 4.69E05$ for the dry case. For the wet case the principal moments of inertia were $I_{xx} = 1.02E07$, $I_{yy} = 1.02E07$ and $I_{zz} = 1.64E06$ ouncemass in^2.

Table 4. Parameters Comparing the Third and Fourth Configurations

Parameter	Third Configuration (Figure 7)	Fourth Configuration (Figure 9)
Center of Mass$_{Dry}$ (in)*	(-2.3E-05, -0.02, -7.4)	(0.3, -0.19, 26.4)
Center of Mass$_{Wet}$ (in)*	(-5.16E-06, -0.005, -7.6)	(0.06, -1.9, 14.5)
Mass$_{Dry}$ (lbm)	241	227
Mass$_{Wet}$ (lbm)	1069	1051.7
I_{xx_Dry} (ounces in^2)	1.42E06	4.05E06
I_{yy_Dry} (ounces in^2)	2.22E06	4.05E06
I_{zz_Dry} (ounces in^2)	1.30E06	4.69E05
I_{xx_Wet} (ounces in^2)	5.63E06	1.02E07
I_{yy_Wet} (ounces in^2)	6.66E06	1.03E07
I_{zz_Wet} (ounces in^2)	2.69E06	1.64E06

*Dimensions are measured from the origin of that particular configuration

"Shifting up" the second iteration and the fourth iteration where all the tanks are in top of each other, allows for the center of mass move in the z-direction as the propellants are being consumed but still be at the center in the x and y axis. Since the engine will be in the center in the x and y axis, locations (0,0), but colinear in the same axis, the z-axis, as the center of mass, no torques will be created, making it stable and with the possibility to have a simple gimbal system. For the mass, the fourth iteration is the best choice since is it lighter than the third iteration by 14 lbs. and 17.3 lbs. in the dry and wet case respectively. For the moment of inertia, the third iteration would be thought to be better since the magnitudes of all principal moments of inertia, except I_{zz} for the dry and wet cases, are greater in the fourth iteration, but since those configurations require no rotation, or else the vehicle would fail, about the x and y axis, having a greater moment on inertia in those axes would be beneficial. In addition, the fourth iteration has a moment of inertia, I_{zz} for the wet and dry case, of less magnitude than the third iteration, which makes it a better option since rotation about the z-axis will performed for maneuvers with the

RCS system and, having less moment of inertia about that axis would result in less thrust needed to generate the torque to rotate the vehicle.

Because of the problems with stability and having to develop a complex gimbal system in the first and second configurations, they were discarded to be the final configuration for JANUS. Having a configuration that would allow for the center of mass to move in the axis colinear to the engine would be the best option. Both the third and the fourth configuration allow for the center of mass to move only in the axis that is colinear to the engine as the propellants are consumed, making them stable and not torque generating. Comparing those two configurations allowed to choose a configuration/design that would be best suited for the mission requirements, weight budget and design specifications on systems such as RCS and gimbal. In this case, the fourth configuration was chosen to be the configuration for JANUS. As progress is made, systems such as gimbal, propellant delivery and legs will be added to this configuration and give form to the JANUS moon lander.

2.2 JANUS FEA ANALYSIS

2.2.1 Approach

2.2.1.1 Importing Geometry and Midsurfaces

To be able to determine if the current JANUS lander structure will be able to support the loads of the propellants and forces generated by the thrust, an FEA analysis was performed to simulate weights, stresses, G forces, etc. This section describes the approach taken to be able to import the geometry from the CAD software, create the surfaces where the mesh will be created, load conditions and some common errors found during the creation of this simulation.

The first step taken was to import the CAD model into hypermesh since a CAD can be used to create surfaces or solids that will be meshed to perform the FEA analysis. For this case, surfaces were created using the geometry of the components to create shell elements (mesh). Shell elements were used since the geometries in this model are thin, making it simpler to use 2D elements to reduce computational time [20] and use simplifications such thin wall structures, where the stress and strain are considered not to vary significantly throughout the thickness [21]. As show in figure 11, clicking on the fourth icon from left to right we can import the CAD.
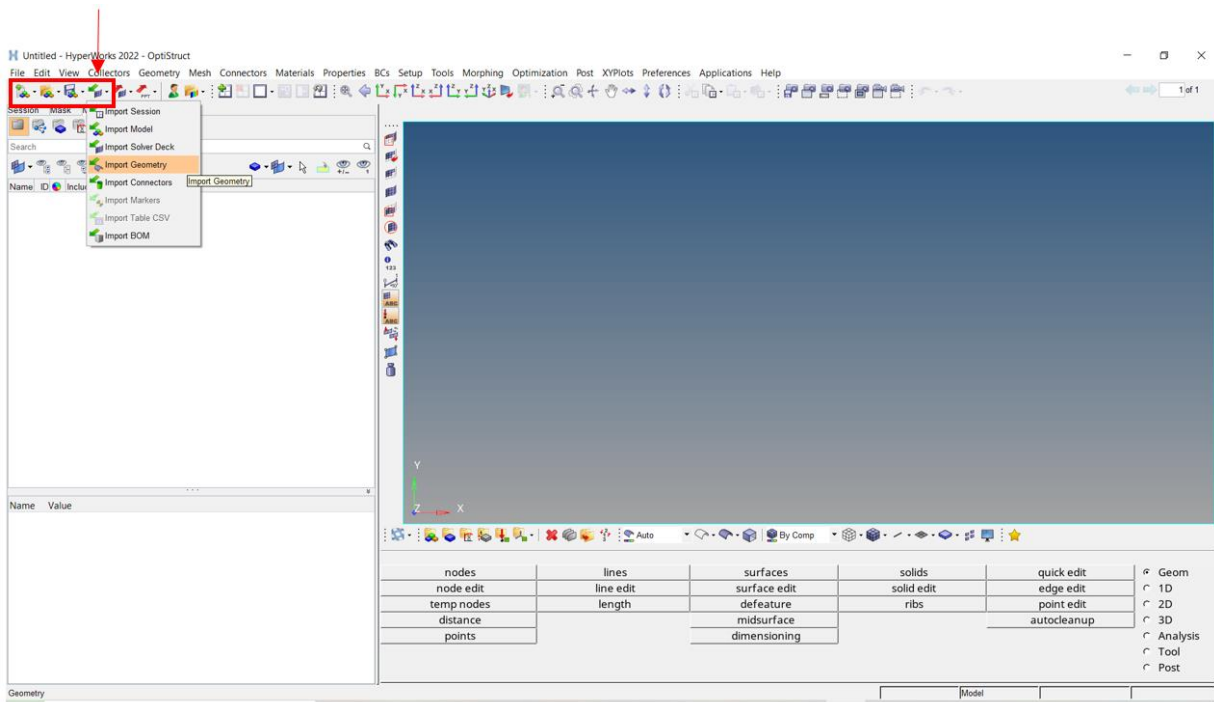
Figure 11. Importing Geometry

Once clicking on "Import Geometry" the yellow folder can be selected to select the file downloaded into the personal PC (the other two icons can be used to delete a single file or delete all of the files selected, since previous/multiple files can be stored in the box and uploaded to be used). It was found that for this CAD model the best type to use was SAT file. Other formats such as STEP and IGES can also be useful if Fusion 360 is being used.
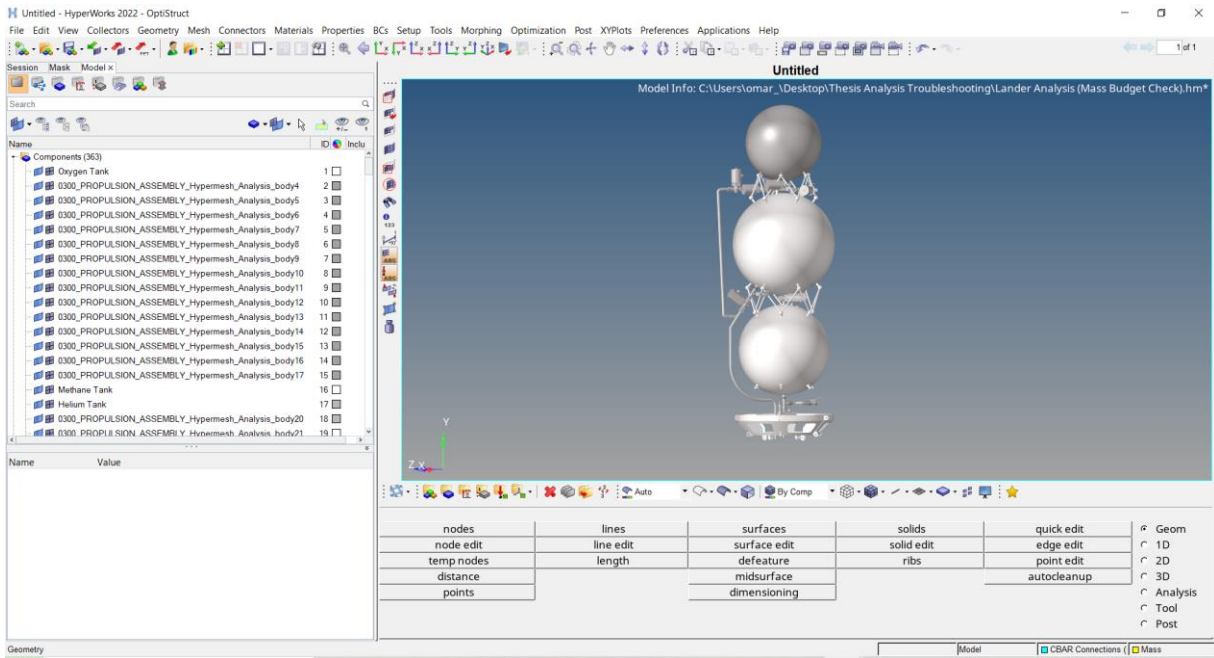
Figure 12. CAD Model and Components List

Once the CAD model has been imported the CAD model will be displayed in the blue window, along with the components that make up the hole CAD model. They will appear in the left window named as components.

As seen in figure 12, in the components section the components that make up the entire CAD model are being displayed. Besides that, small icons, similar to little "flags", are being displayed. The left smooth "flag" means the surface/solid, in other words you can hide the entire body by clicking on the icon. The squared "flag" refers to the mesh, meaning that if a mesh has been created in that component the mesh can be displayed or hidden. Also, at the right side each component has a number displayed identifying the component along with a "little square" that allows the user to change it to any color desired, this can be used to keep components organized and easy to identify. In addition, in the bottom central window there are several sections that have different functions to perform an analysis, throughout this section some of those sections

will be mentioned on how they were used to perform different tasks at the time when the model was being setting up for the analysis.

The first feature being used was "midsurface" in the "Geom" section. The midsurface command allows the user to create a surface with a thickness, given through a property, out of a solid body. This surface can be used to create a 2D mesh later in the process.
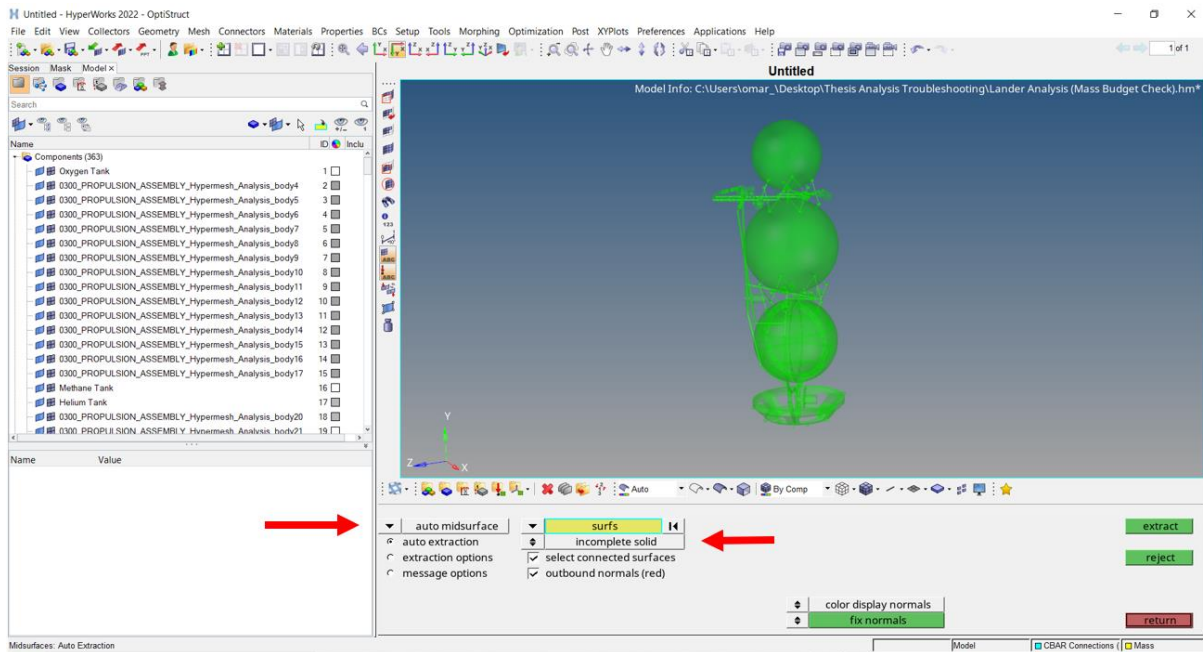
Figure 13. Midsurface Feature

As seen in Figure 13, the midsurface feature allows the user to create a midsurface by different options. The first option is the default mode, where if a subcomponent of the component selected is connected to the component of interest, they will be midsurfaced automatically. The second option is by unchecking the box "select connected surfaces". This allows the user to select manually the surfaces of interest. The third option is by clicking in the box "incomplete solid", this will change the selection to entire components (not allowing for the selection of subcomponents). Depending on the geometry of component of interest some of the

options explained earlier can work better than other. When creating a midsurface by default a new component is created. This can be useful in some instances when the solid components might be removed and to prevent confusion and overlapping of solid components, surfaces and meshes. But in some instances, surfaces might be created and still be conserved in the same component, this is where the dropdown arrow in the "auto midsurface" can be selected. When selecting the arrow there are several options ("auto midsurface", "interim edit tools", "final edit tools", "review thickness", "sort") in which the user can explore and determine the best way to create a good midsurface. In the "final edit tools" the software allows the user to select whether the new midsurface will "result in Middle Surface component" or if it will result in "current component".
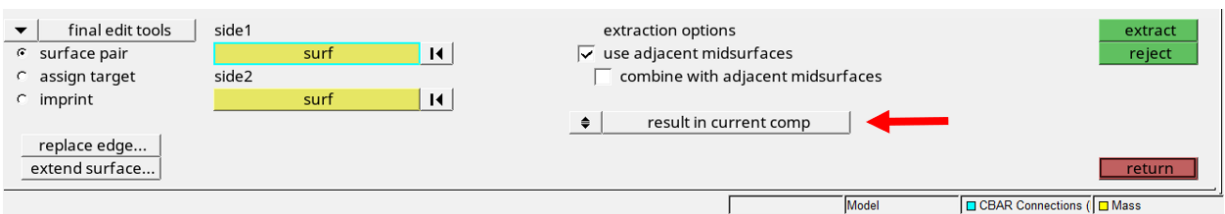
Figure 14. Selecting the Component Destination for a Middle Surface

To extract a middle surface the software offers a vast variety of options that can be tried to create a midsurface with the less possible imperfections. It is encouraged to dive into these different options and explore how each one of them affect the middle surface extraction.

As mentioned, the use of "middle surface" will not always create a perfect surface. Sometimes the middle surface has imperfections that can be, in some instances, be fixed using other features in the "Geom" section.

As seen in Figure 12, there are several features that can be used to fix surface imperfections. The most common used features for this analysis were the "surface edit" and "quick edit" features.

23
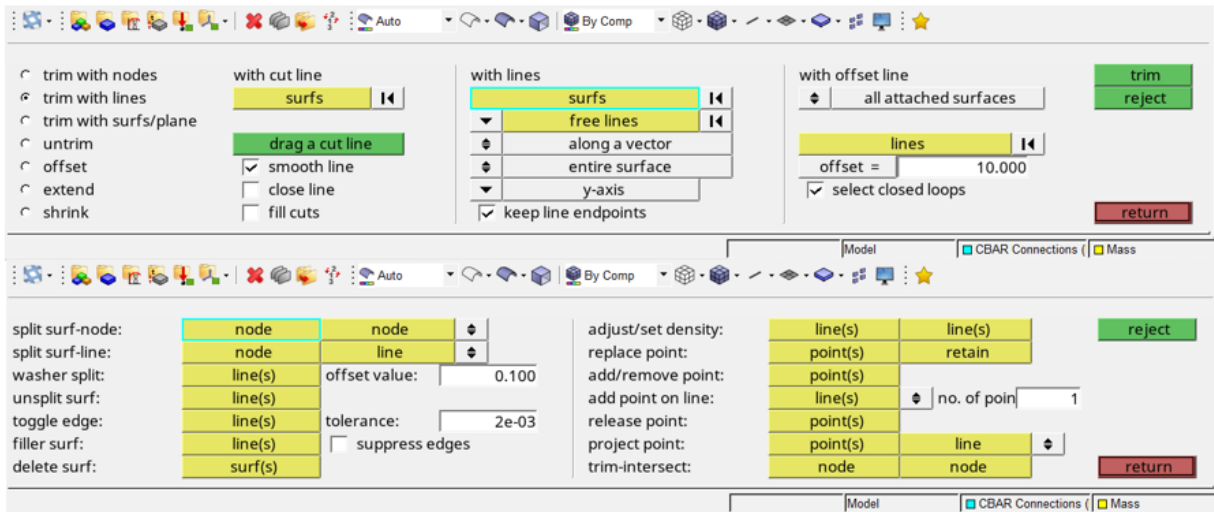
Figure 15."Surface Edit" (Top) and "Quick Edit" (Bottom) Features

As seen in Figure 15, in the top side, the "surface edit" feature can be seen, this is where the surface can be modified by using different commands such as trimming it using nodes, lines, and surfaces. Sometimes trimming a surface allows the user to control the number of elements desired when creating a mesh as well as making easier the creation of elements of better quality. Reference [22] is a good example of how surfaces can be split using lines, nodes and how the mesh can be controlled easier by using these two features ("surface edit" and "quick edit"). Besides that, the "untrim" can be used, by left clicking an edge, when there are edges created in the surface extraction, as part of the imperfections already mentioned, that will create undesired elements affecting the quality of the mesh. Also, the untrim option can be used in some instances to make a surface sharing two edges (green lines) into a single surface. It is common that when a midsurface has been created out of a complex shape geometry, some surfaces are not connected, making the surface being split into multiple surfaces. The "extend surface" option allows the user to connect surfaces by allowing the maximum distance and the surfaces that will be extended and the target surfaces to where they will be extended to.
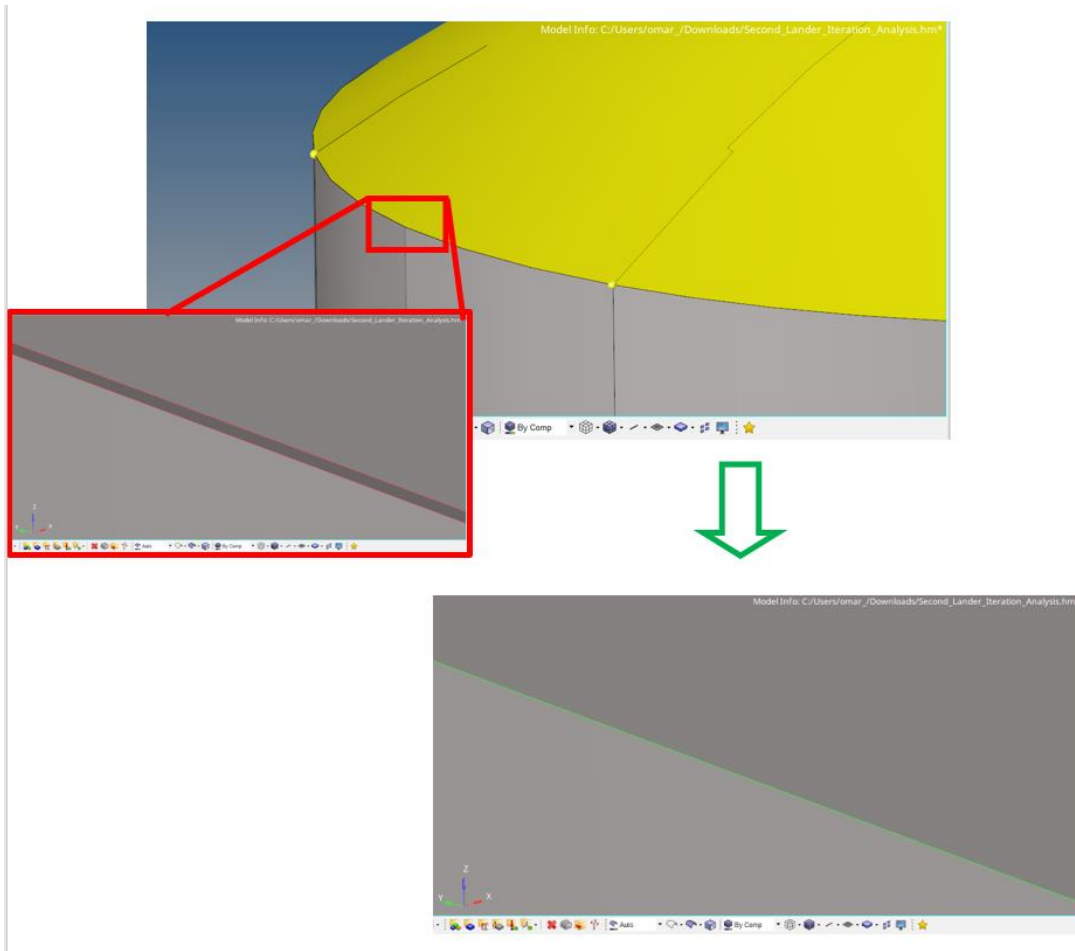
Figure 16. Extending Surfaces Not Connected (Middle Left) and Surfaces Extended (Bottom

Right)

Besides that, there are additional options in the "surface edit" feature not utilized in the analysis

(offset, shrink) that can be helpful if changes/fixes will be performed to a surface.

In the bottom part of Figure 15, there are several options in the "quick edit" feature that can be

used to edit/fix a surface. Although there are several options that are similar to the ones in the

"surface edit" panel (trim with nodes, trim with lines & untrim) the difference between these

options is that trimming will separate the surfaces in all the surfaces involved/intersecting,

whereas splitting will only separate the surfaces selected. The washer split allows to create an

identical edge to the one selected in two directions, making a washer like split. The "toggle" edge" option can be useful because it allows to make free edges to shared edges, by one left click, and also to suppressed edges, with two left clicks. In addition, it allows to make a suppressed edge to shared edge or a shared edge to make it free. One aspect to consider is that the edge being toggled must meet the criteria for the type of edge you wish to change it to, as an example if a free edge is changed to a shared edge it requires the presence of a similar edge within the distance you specify [24]. The filler surface allows to fill gaps in between surfaces. These gaps can be filled by setting the right tolerance and distance allowed to fill this gap, same parameters used in the "toggle" option. Lastly, the "delete surface" option allows to delete unwanted surfaces. For this analysis, the rest of the options in the right side of the "quick edit" panel were not used, but it is encouraged to interact with them and see how these options can be of potential use if a surface is being fix/created.

Figure 16, shows two surfaces that have not been connected, and because of that, their edges appear red. Once the surfaces have been connected these edges change from being red to green.
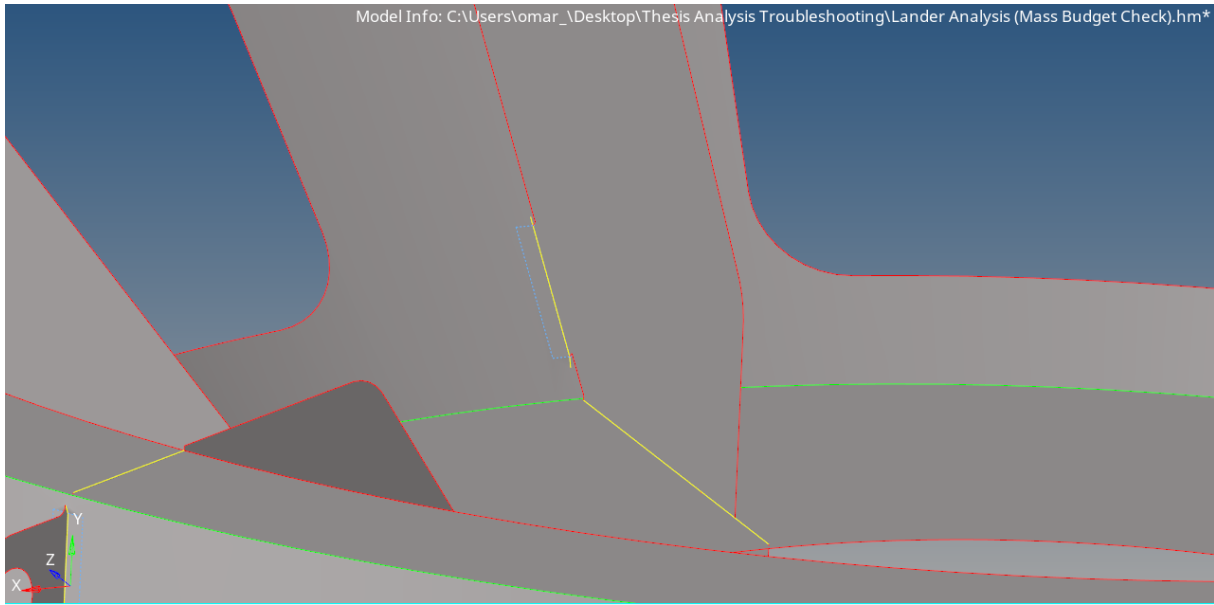
Figure 17. Edges at Different Colors

In figure 17, a surface is shown having different edge colors. Each color means a different edge behavior:

- Free edges (red lines): edges that is owned by only one surface.

- Shared edges (green lines): edges that are shared or are owned by two adjacent edges.

- Suppressed edges (blue lines): edges that are shared by two edges but are being ignored.

- Non-manifold edges (yellow): edges that are owned by three or more surfaces, typically occur at T intersections between two surfaces or when two or more duplicate surfaces exist.

Free edges usually appear at the outer perimeter of the geometry or interior holes. If free edges appear between two adjacent surfaces, it means that there is a gap between them. The automesher will leave the gap in the mesh if the surfaces are not connected (the mesh will not be continuous. Shared edges indicate that there is no gap or overlap between the two surfaces, resulting in a continuous mesh. Suppressed edges indicate that the edge is shared by two

27

surfaces, but unlike shared edges, the automesher will ignore the edge as if it didn't exist, this can be advantageous to combine surfaces into a large surface, resulting in better-quality elements. Non-manifold edges indicate that the edge is part of three or more surfaces, the automesher will always place a node in the edge. This can sometimes be problematic since the node placed in the edge will disrupt the mesh, causing it to have low quality elements. Suppressing the edge (using the "toggle" option, right click to release the edge, turning it red, then left click to share the edge, turning it green, then left click to suppress it, turning it blue. Note that this process can work in some instances) might be the best option, depending on how it affects the mesh being created. Reference [24] offers more information about edges and how can they affect the meshing process.

There will occasions where the best option will be to create a surface manually. This is where the "surface" feature can be helpful.

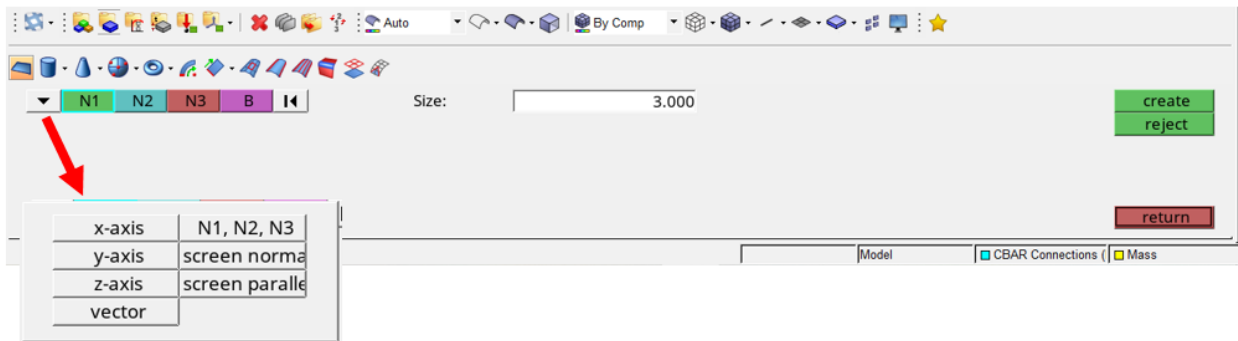Figure 18. "Surfaces" Feature

As seen in Figure 18, there are multiple options that can be helpful to create a surface. In the first option a square shape surface can be created by either following a vector, which is default, or having a base node, where its center will be, and rotating it about the three axes. Also, options

such as creating it normal or parallel to the base node are also available. Note that these options are very common throughout the different surface options in the "surfaces" feature.

Shapes such as a cylinder, cone, sphere can also be created by specifying dimensions such as height and radius, all three of them allow to be created partially or fully. Also, shapes such as "donuts" can be created by specifying the minor and major radius, its center (a node) and a node that specifies its direction normal to the hollow center. Surfaces can also be created using lines. A line can be either be revolved around the options already mentioned and shown in Fig 17, to create a washer like surface or they can be dragged the same options already described to create a surface. The last method used in this analysis is the 12th option (counting from left to right) which allows the user to create a surface from a mesh. It creates a surface that will take the shape of the elements selected. Other options such as spline/filler, ruled, skin, fillet and meshline were not used in this analysis but it is encouraged to try those options and determine how they can be helpful/used to create surfaces.

2.2.1.2 Nodes and Lines

Nodes can become very useful when it comes to creating/editing a surface or a mesh, but also to place elements in a desired position. Nodes can become very handy to create a line that needs to follow a certain direction and distance. To create nodes and lines there are features in the "Geom" section where nodes and lines can be created and edited using different options.

29
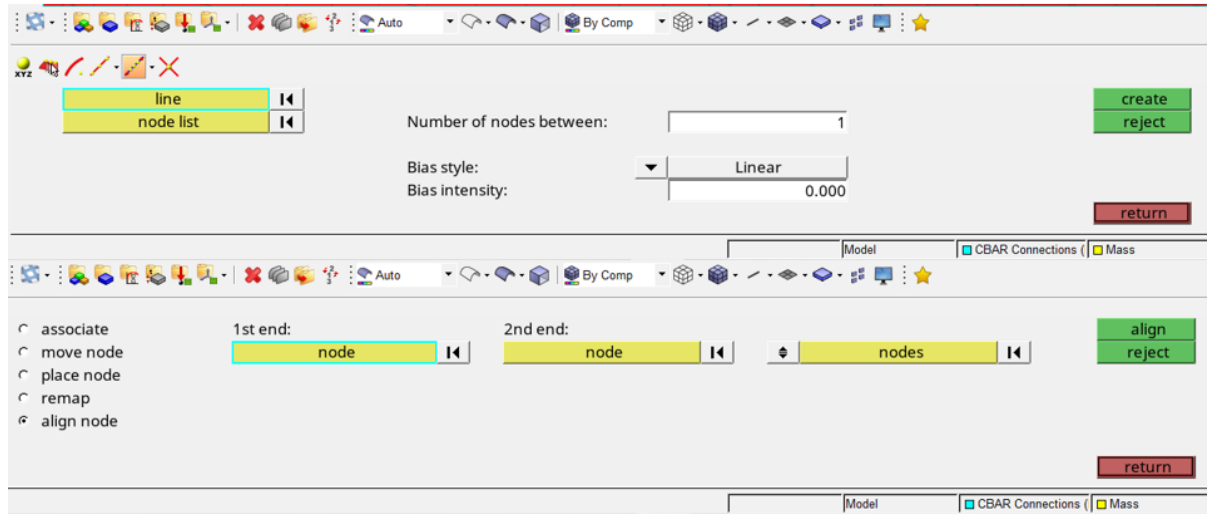
Figure 19. "nodes" (Top) and "node edit" (Bottom) Features

Figure 19 shows the two different features that can be used in the "Geom" section to create and

edit nodes. In the first option a node can be created by using coordinates. One advantage of that

is that if a node is selected, coordinates will appear on each box, letting the user know the

coordinates of the node, this can be used to place a node a distance on each axis from that node

by only adding/subtracting the desired distance on the desired direction. The next option allows

the user to freely create nodes on points, lines, surfaces and planes, depending on the option

selected. The third option allows to create a node that will be at the center of any curvature. One

thing that can be used, is that multiple lines can be selected, whether they are arcs or straight

lines, and a node will be created in the middle of the lines selected. One example is that if a node

is to be created in the center of a square, two parallel lines can be selected and a node will be

created at the center of these lines. The fourth option allows the user to extract nodes from a line

in different forms of bias (linear, exponential or bell curve) and bias intensity and the number of

nodes desired. The next option allows the user to interpolate nodes freely (in the same axis),

nodes in the same line, and nodes in the same surface. Lastly, the 6th option creates nodes on the

intersection of two lines. In the "node edit" feature, there are two options that were used in this analysis, move node and align node. The move node option allows to move a node in a variety of different directions (options similar to shown in Figure 18) in the positive and negative directions. The node has to be part of a surface, otherwise there will be an error not moving the node. The align node option allows to align a node with two other nodes in the same axis, note that even if nodes have been created in a line or surface they will move out of the line or surface and align with the target nodes. The associate, place node and remap options were not utilized in this analysis.

As mentioned, lines can be helpful to fix/create surfaces. There are different options that can be used to create lines as well as to edit lines already created.
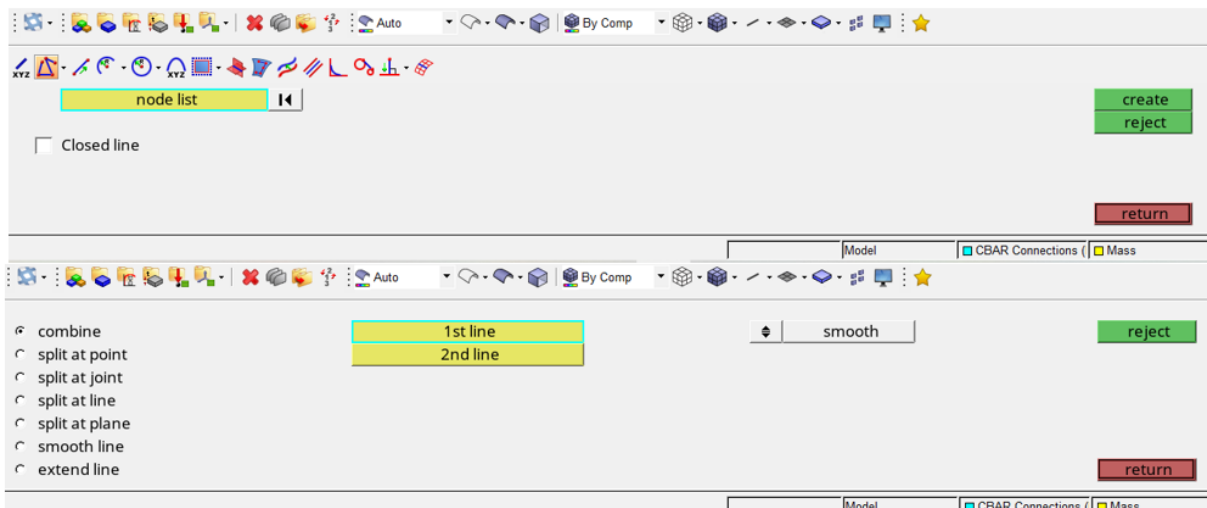
Figure 20. "lines" (Top) and "line edit" (Bottom) Features

As shown in figure 20, there are 15 different options that can be used to create lines depending on its position and shape. The first option allows to create a line from a starting point to an ending point by specifying coordinates in the x, y and z directions. The second option allows to create a line using nodes. There are 3 more options that specify the type of node (standard,

smooth and controlled), the most common option used is linear nodes. The fourth option allows to create an arc line by three different ways, the first two by specifying the radius, the angle, vector normal to the center of where the arc will be created, and the last option by selecting three nodes, giving the desired magnitude to the arc. The fifth option is the same as with the arc option, the only difference is that the line will be a full circle. The ninth option allows to create a line between two nodes, similar to the second option, but with the difference that it will follow the surface shape and not be a straight line. The options split at point, split at joint, split at line, split at plane, smooth line were options not used.
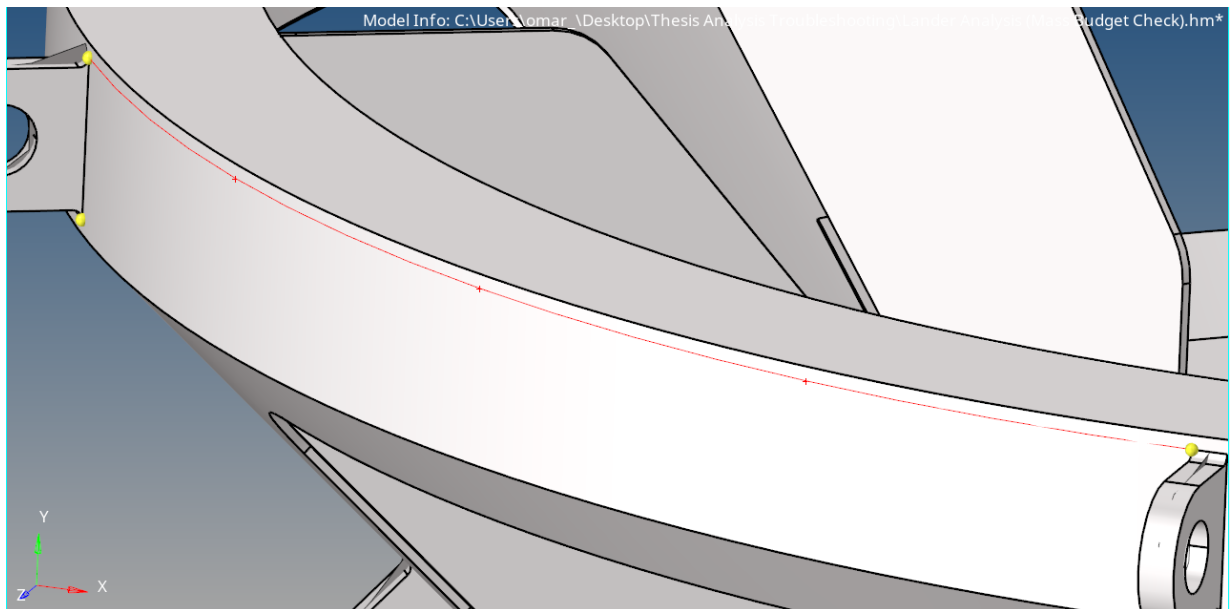
Figure 21. "Manifold" Line

Options such as conic, intersect, offset, midline, fillet, tangent, normal to geometry were not used for this analysis, but it is encouraged to explore and see how they can be used to create lines in different and more efficient ways.

When a line needs to be modified the "line edit" feature can be useful. As seen in figure 20, there are numerous ways in which a line can be edited. The first option allows to combine two

different lines. The last option allows to extend a line by specifying the distance desired and the direction of the extension, positive or negative direction. It also allows to extend the line following a curvature, such as the case of Figure 21, or not to follow it.

2.2.1.3 Meshing

Once the surfaces have been created and/or modified/adapted, if imperfections were present, the mesh can be created. The "Geom" section was mostly used to fix/create surfaces, to create a mesh the "2D" and "3D" sections can be used, depending on the type of analysis and element types desired, "2D elements are used when two or more of the dimensions are very large in comparison to the third dimension" [26].
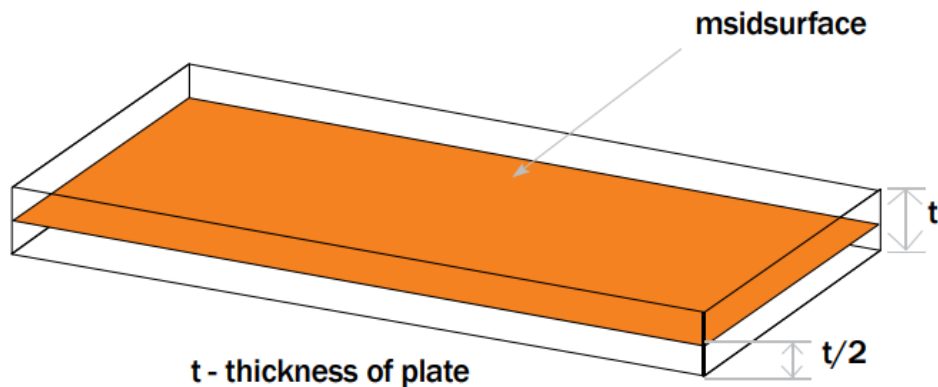
Figure 22. Common Geometry Dimensions for 2D Mesh [26]

Figure 22 shows a geometry in which one dimension is very small compared to the other two dimensions (thickness) which is typical in thin-walled structures such as pressure vessels. For this analysis, 2D elements were used since 2D elements are best suited since thicknesses of some of the components were small compared to other dimensions. To start the mesh, the automesh feature needs to be selected in the "2D", this is where the element type, element size and desired surfaces will be selected.
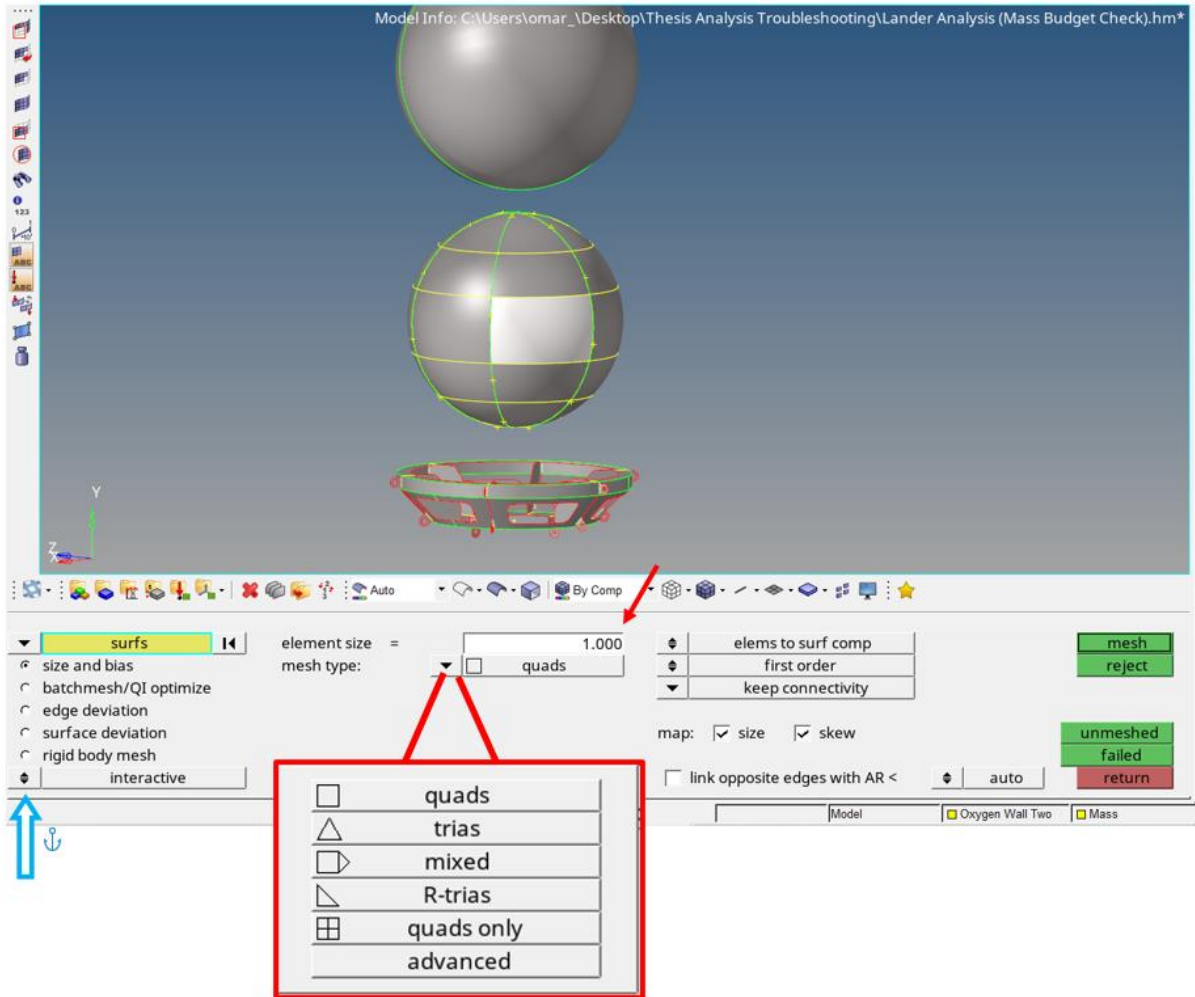
Figure 23. "automesh" Feature and Element Type Options

As already mentioned, the elements used in this analysis were quads, since they will have better accuracy in the stress results, which is of great importance since the pressure vessels will experience stress that will dictate the thickness and, thus, the weight of the pressure vessels. The blue arrow shows a button that has two options, interactive and automatic. The interactive mode allows the user to modify the mesh once it has been automatically created, whereas the automatic mode will terminate the mesh process once the mesh has been created, not allowing to modifications.
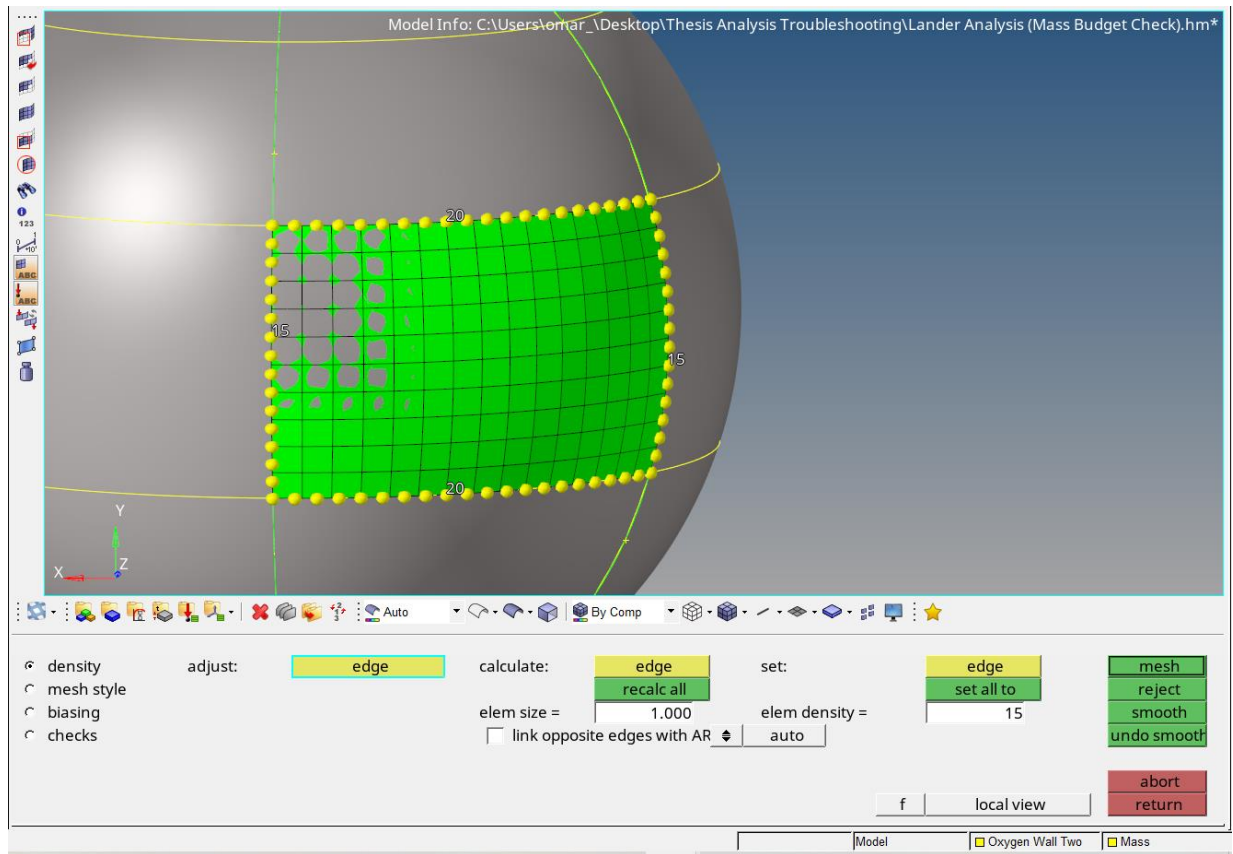
Figure 24. Meshing Density

As already mentioned, once the mesh is created automatically, the user can modify the mesh in different manners depending on the analysis being performed. The first option is the mesh density. The user can increase or decrease the number of elements per edge. As shown in Figure 24, numbers will be displayed in the edges, letting the user know that that number is the amount of elements present in that edge. Left click, to increase, right click, to decrease, in the numbers and the yellow nodes will pop-up or disappear. Note that the first yellow button, "edge" is selected. The third yellow button, "edge", allows the user to increase the number of elements automatically to a given value. For example if 15 elements will be created in multiple edges, just type the amount in the white box, below to "set all to", and select "edge", the third yellow box, and click on the number in the desired edge, this will increase the number of elements desired in

that edge, if the user wants to return to the default mode just select the firs "edge" button, this will allow to increase/decrease the number of elements manually. The "reject" button will cancel the mesh and the "abort" button will take the user out of the window. If the mesh is not rejected or aborted and the "return" button is hit, the mesh will be accepted. To delete elements or a mesh, the delete option will need to be selected in the "tool" section.
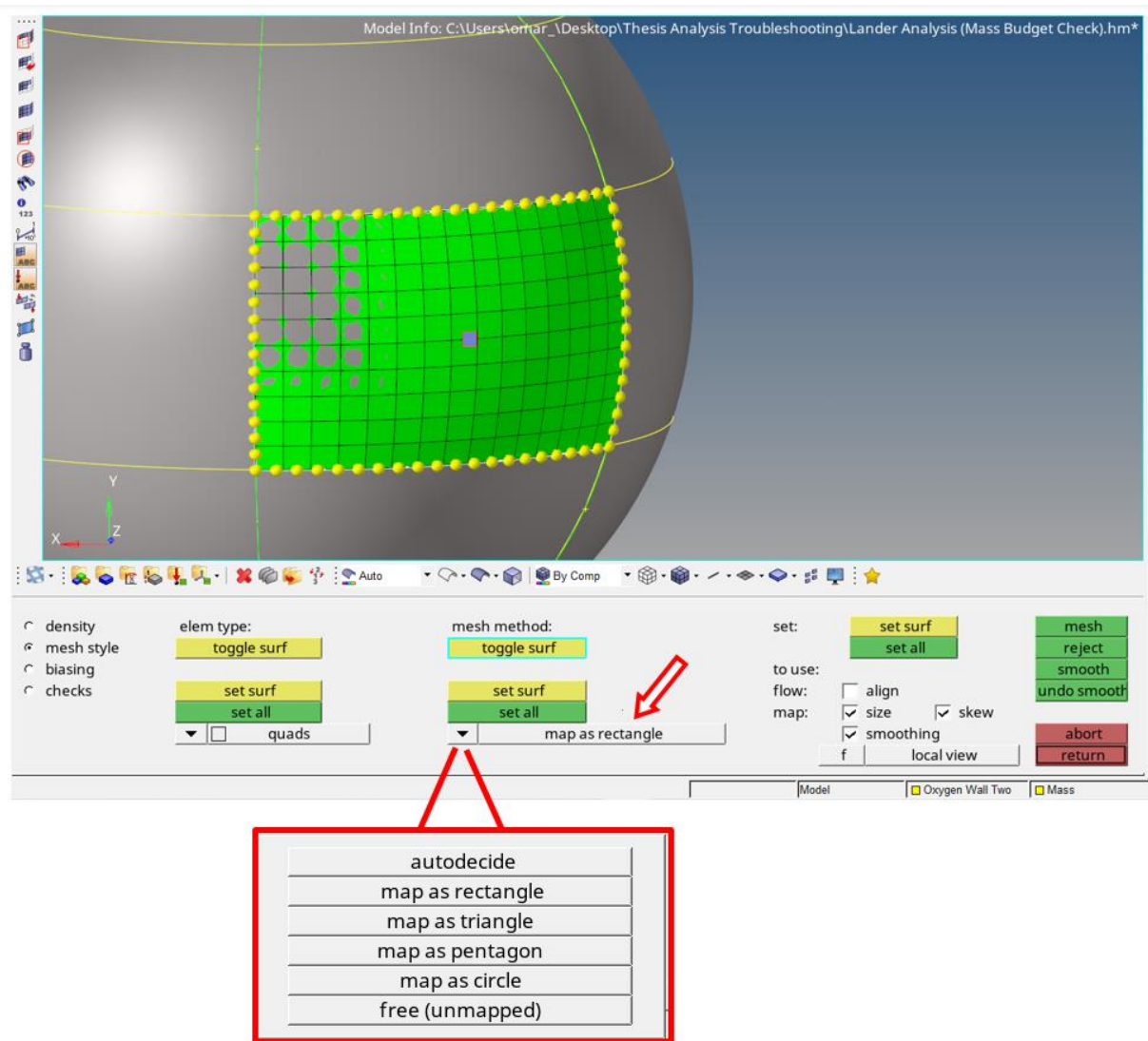
Figure 25. "meshing style" Option

Another option that can be of great advantage when creating a mesh is the "mesh style" option. The mesh style option allows the user to change the element types and to map the mesh in different shaped surfaces. Figure 25 shows the option that allows to map the mesh in different geometries such as, rectangle, triangle, pentagon, circle or automatically. The selection of the option should be made based on the geometry of the surface. For example, if a surface has 5 sides (doesn't have to be a perfect pentagon) the pentagon option might be the best option to use. Once the shape has been selected, click on "set all" for all the three green buttons shown, this will map the mesh into the desired shape style. Reference [27] provides helpful information about how to use the "density" and "mesh style" options as well as splitting surfaces to have a good quality mesh.

The third option that is useful to edit/create a mesh is the "bias" option. This option allows to move the elements to one side (concentrate the elements in one side).
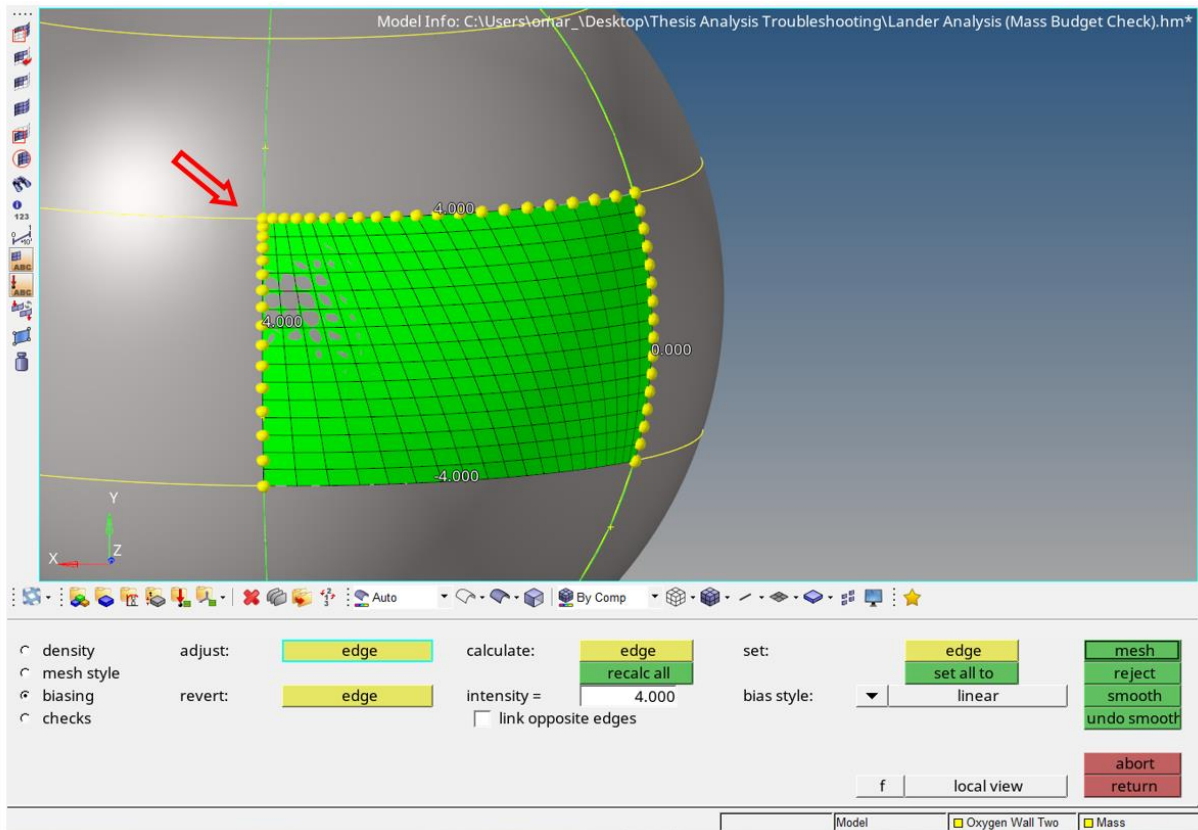
Figure 26. "biasing" Option

Figure 24 displays the biasing option being used. Biasing allows to "shift" the same quantity of elements to one side. The red arrow shows the top edge elements are being centralized to the left side, as well as the elements of the left edge. The bottom edge is biasing the elements to the right side and the right edge has a bias of 0.0 which is not shifting elements to neither side. The biasing can be controlled by left and right clicks, similar to the element density. One can also enter a desired bias value and automatically bias an edge, just like the option explained in the density section. Lastly, bias style can be changed from linear to exponential or bell curve in the drop-down arrow.

The last option is the "checks" option. This option allows to check some parameters such as maximum and minimum element interior angles, length, and Jacobian among other parameters.
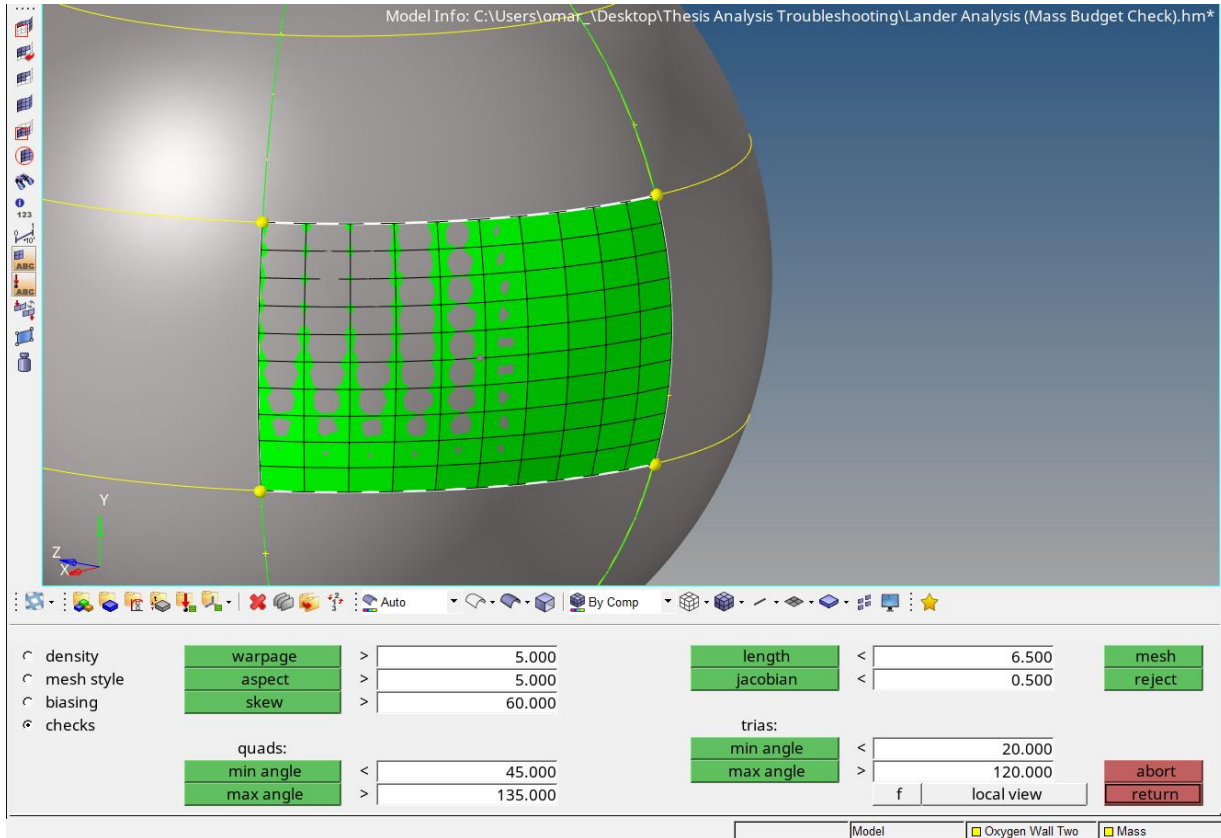
Figure 27. "checks" Option and Bottom Left Corner Message Window

The values shown are default values, but they can be manually changed to check for parameters of interest. Once the parameter has been set, click on the green button and a message will appear in the bottom left corner of the window giving the minimum value found in the mesh being created (mesh displayed in green). For this analysis, a Jacobian check of less than 0.5 was performed since there were quality errors running the simulation and having elements with a Jacobian of less than 0.5 meant that these elements have a poor quality. If there is an element with a value on a parameter less than the one entered, the elements will turn red.

Simple shaped surfaces are common but that will not be the case for most of the analyses performed. There will be occasions in which the surface will have a complex geometry. Also, in some instance the creation of a detailed mesh will not be possible due to time constrains since fixing/creating a surface can become time consuming. In some instances a simple mesh can be helpful if the only goal of the analysis is to have an idea of the loads happening in the design. For these cases, meshes can become "unorganized" and coarse. In the same section, "2D" there is a tool that can be helpful to manually fix elements of low quality, allowing to perform a quick analysis and with relatively good quality elements. "quality index" allows the user to display, in red, the elements based on a set of parameters selected with a given range (similar to the "checks" option in the "automesh" feature). Note that elements will appear red if they meet the value specified in the box. Uncheck the "min value" box to clearly see low quality elements. For this analysis elements shown in yellow and red were fixed to prevent any quality errors when running the simulation.
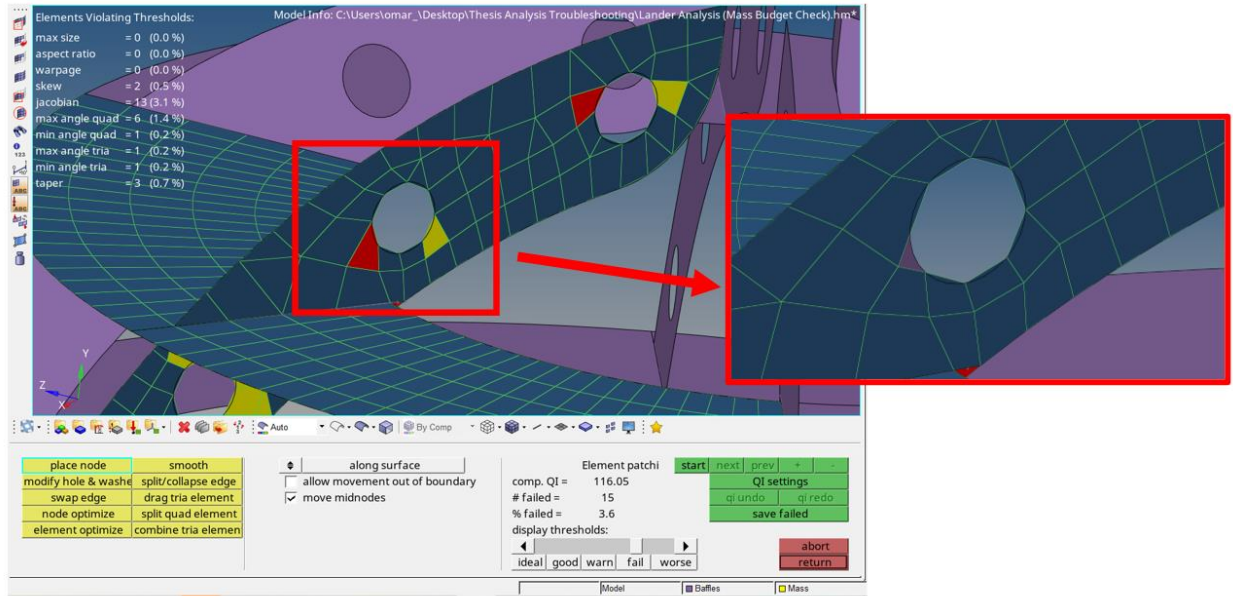
Figure 28. "quality index" Tool and Fixed Elements

Figure 28 shows the window that enables the fixing of low-quality elements manually. This window is not shown as default, the user needs to click on "clean up tools" to be able to see the window shown in figure 28. Once in the window, the user can manually move the element, changing its shape, until the element turns navy blue. This process can be tedious since sometimes the elements turn blue but adjacent elements turn yellow or red. This tool can be helpful, but patience will be needed.

2.2.1.4 Equivalence

It was mentioned that edges are colored in four different ways, red, green, yellow and blue and each color represents the edge being shared by one or more surfaces or if it is being ignored or free. This can be helpful to determine if the mesh will be continuous (if the nodes will be connected) through adjacent surfaces. This can sometimes not be true because surfaces can be connected but the mesh will not. In the "tool" section there is a feature that allows to check if the nodes are connected in a given range and connect them if they are not.

41
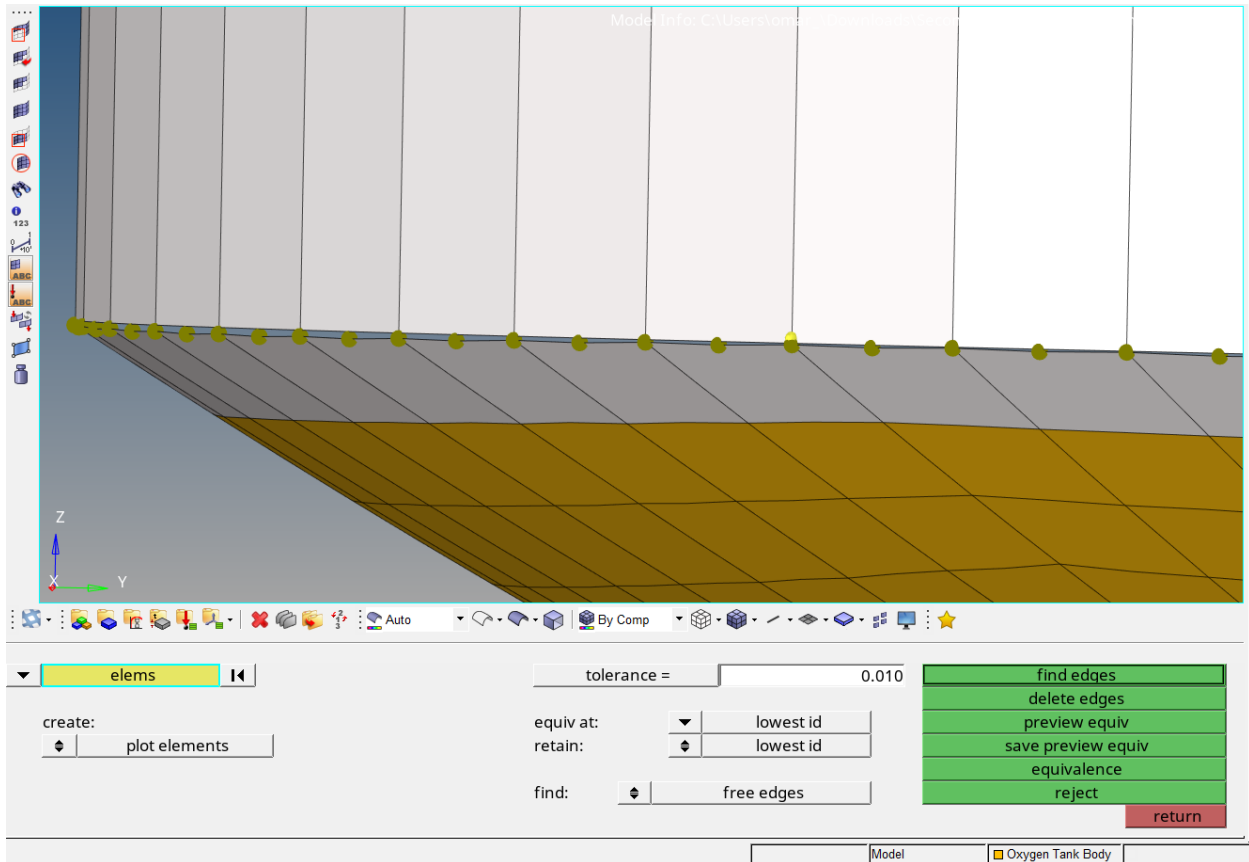
Figure 29. "preview equivalence" and "equivalence" Options to Connect Elements

Figure 29 shows a similar case as shown in Figure 16 where two surfaces were not connected. When the mesh was created for the bottom surface, the density of elements, was allowed to be edited for the bottom surface (when surfaces are shared this is not possible) this means that the surfaces are not connected and that the elements are not connected. This is a problem that needs to be avoided since the loads will not be transferred to the other elements, thus giving no results. The "edges" feature allows to check for connectivity between elements at a given range. As an example, Figure 29 shows the elements selected that need to be connected. A range of 0.01 was given, then "preview equiv" was selected. This will show the nodes that have a gap less or equal to the tolerance given. Then equivalence was clicked to connect the nodes.
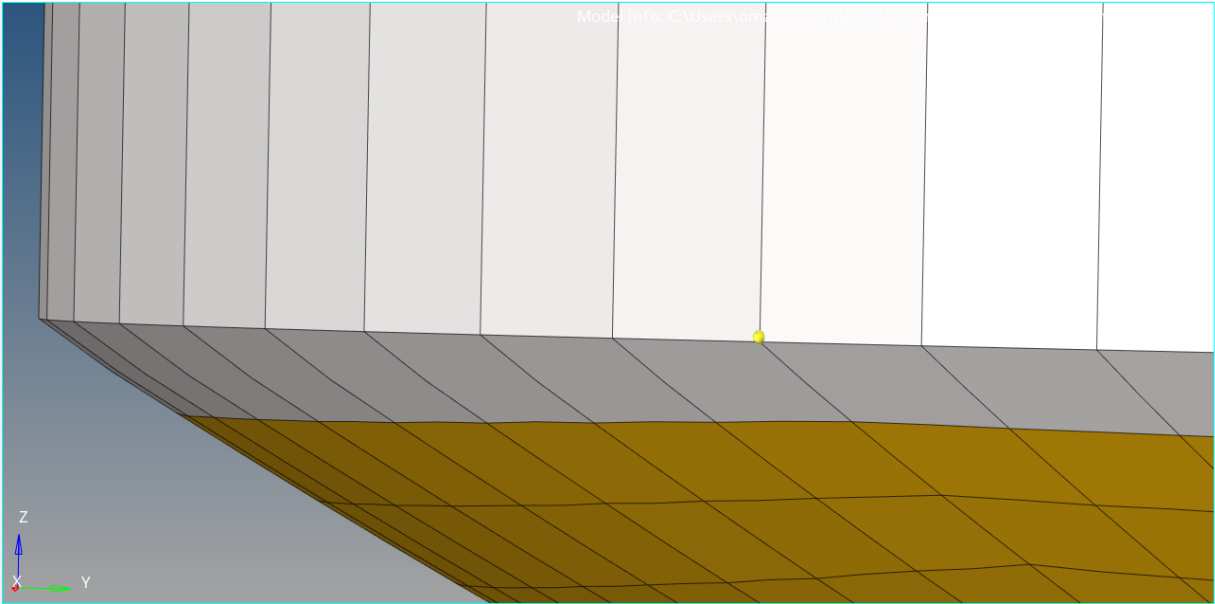
Figure 30. Elements Connected Through the "equivalence" Option

If the gap between elements is more than 0.5 connecting the surfaces will be the best option or narrowing the gap between elements (one way can be by using the "translate" option under the "tool" section. Elements can be moved in the x, y and z directions as well as other options). If the gap is considerable the elements will be connected but they will be distorted, increasing the chance of making these elements of poor quality.

Big gaps in between unconnected elements can lead to element quality problems and unexpected errors. If big gaps are present in between elements, the tolerance value can be increased until the "preview equiv" option displays the nodes that will be connected. One problem that can result from that is that, if the tolerance value is too high, not only nodes that will be connected will be highlighted, also nodes from different sides of the elements will be highlighted as shown in Figure 31.
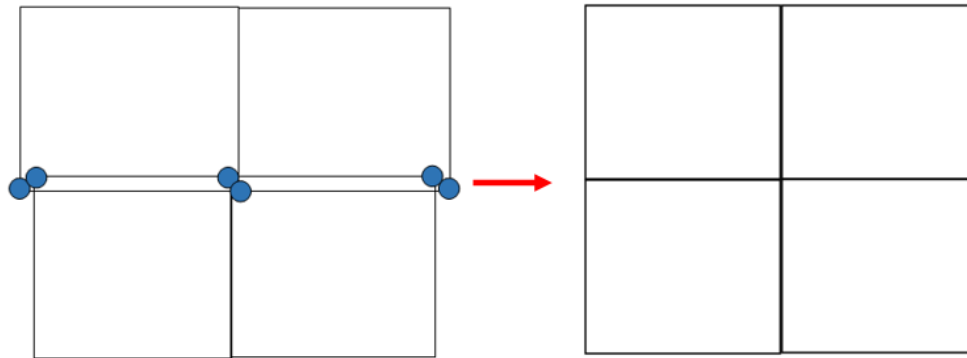
Low Tolerance Value
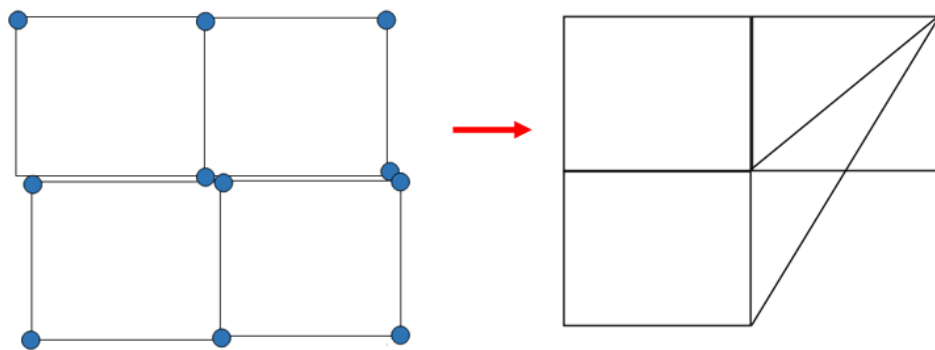
High Tolerance Value

Figure 31. Equivalence Example at Low and High Tolerance Values

Figure 31 shows elements not being connected, left side, and being connected, right side, when the "preview equiv" and "equivalence" options are selected respectively. If the tolerance value is high the chances that two nodes connect to one node (bottom right picture) increase. This will generate errors when the simulation is being run as shown in Figure 32.
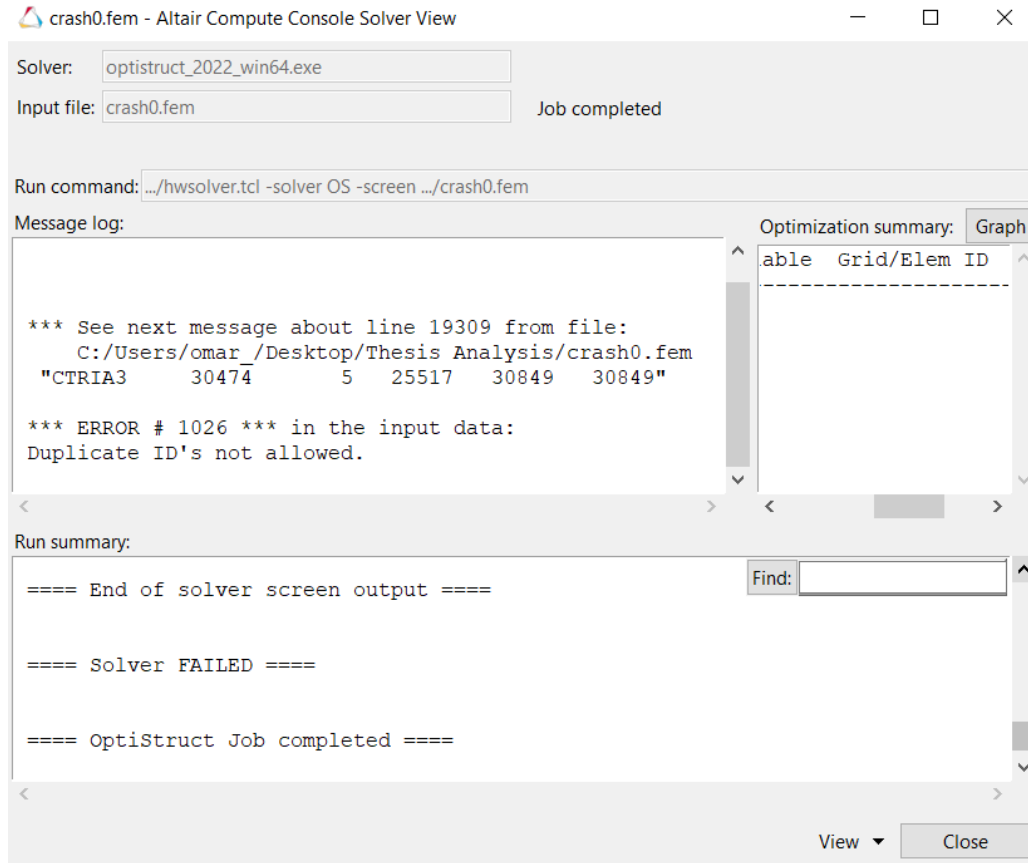
Figure 32. Error # 1026. Duplicate Id's Not Allowed

Figure 32 shows a typical error when a node is being connected to multiple nodes as shown in figure 31. It shows the nodes that are being connected; it is also shown the node where there has been a connection more than once. One solution would be to delete the element and create another element manually going to the "2D" section > "edit element" > "create". To find the nodes that have been connected repeatedly in the "tool" option select the "find" option > "find entities" (which is default) > nodes (note that the first dropdown arrow allows to select elements, lines surf, etc.) > "nodes" (yellow box) > "by id" (this will allow to enter the id of the node of interest) > press enter > "find".

45
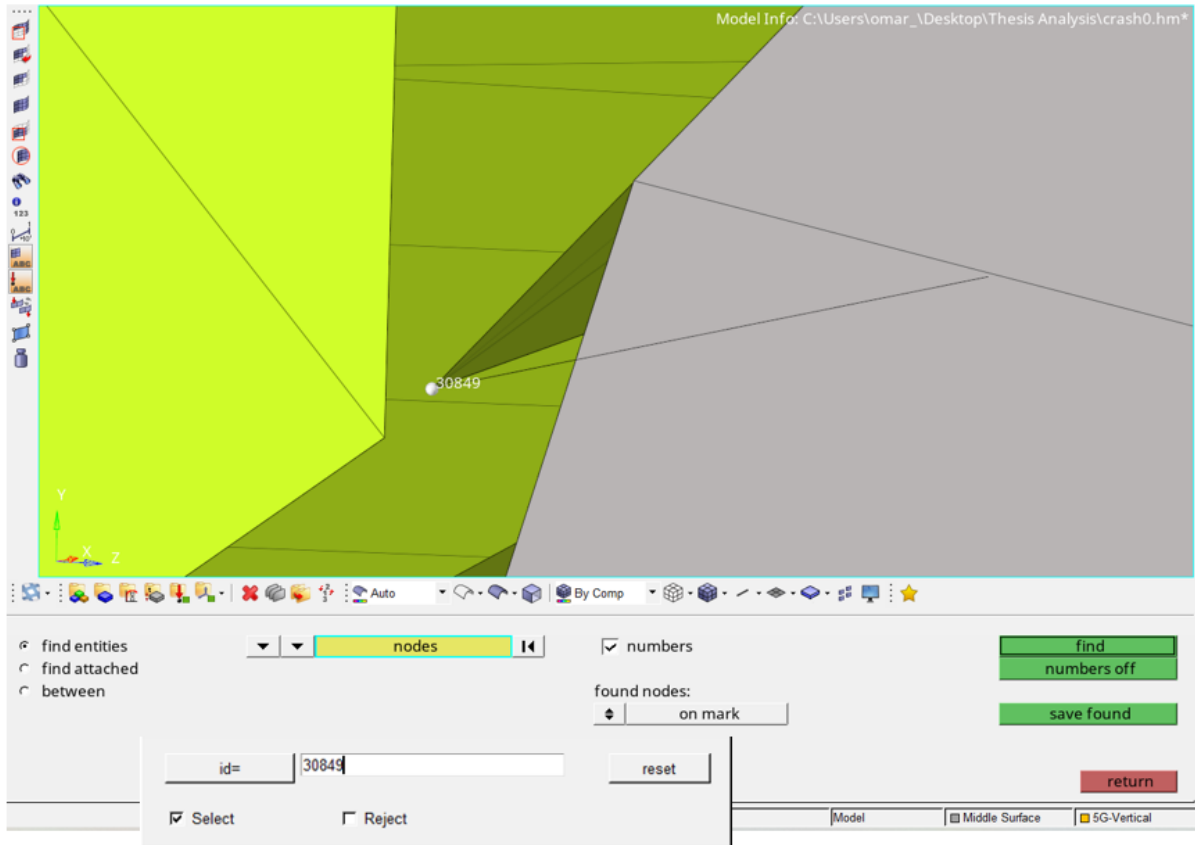
Figure 33. Finding Nodes Through "by id" Option

It is shown on Figure 31 how a node can be found using the "by id" option. This will save time finding the node and will allow to inspect the element, visually and through the "quality index" option.

2.2.1.5 1D Elements

1D elements are, similar to 2D elements, commonly used if one if the dimensions is very large in comparison to the other two. They are practical if long shafts, beams, pin joints, connection elements are used [28].
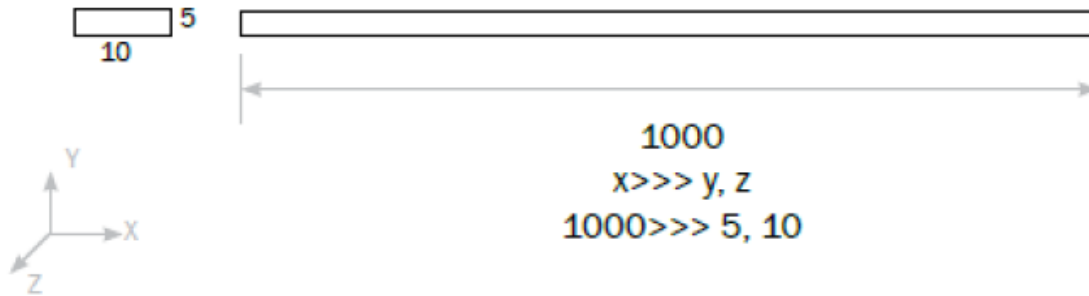
Figure 34. 1D Elements Example [28]

In this analysis, four types of 1D elements were used. CROD elements were used in the structure (the rods) that supports the tanks (helium, methane and oxygen). The structure, the rods, supporting the tanks was designed with the goal to prevent any bending stresses, allowing for simpler and lighter supports. In hypermesh, CROD elements allow only tension and compression [28], making them suitable to model the rods connecting the helium to methane tanks, methane to oxygen tanks and oxygen tank to the base ring.
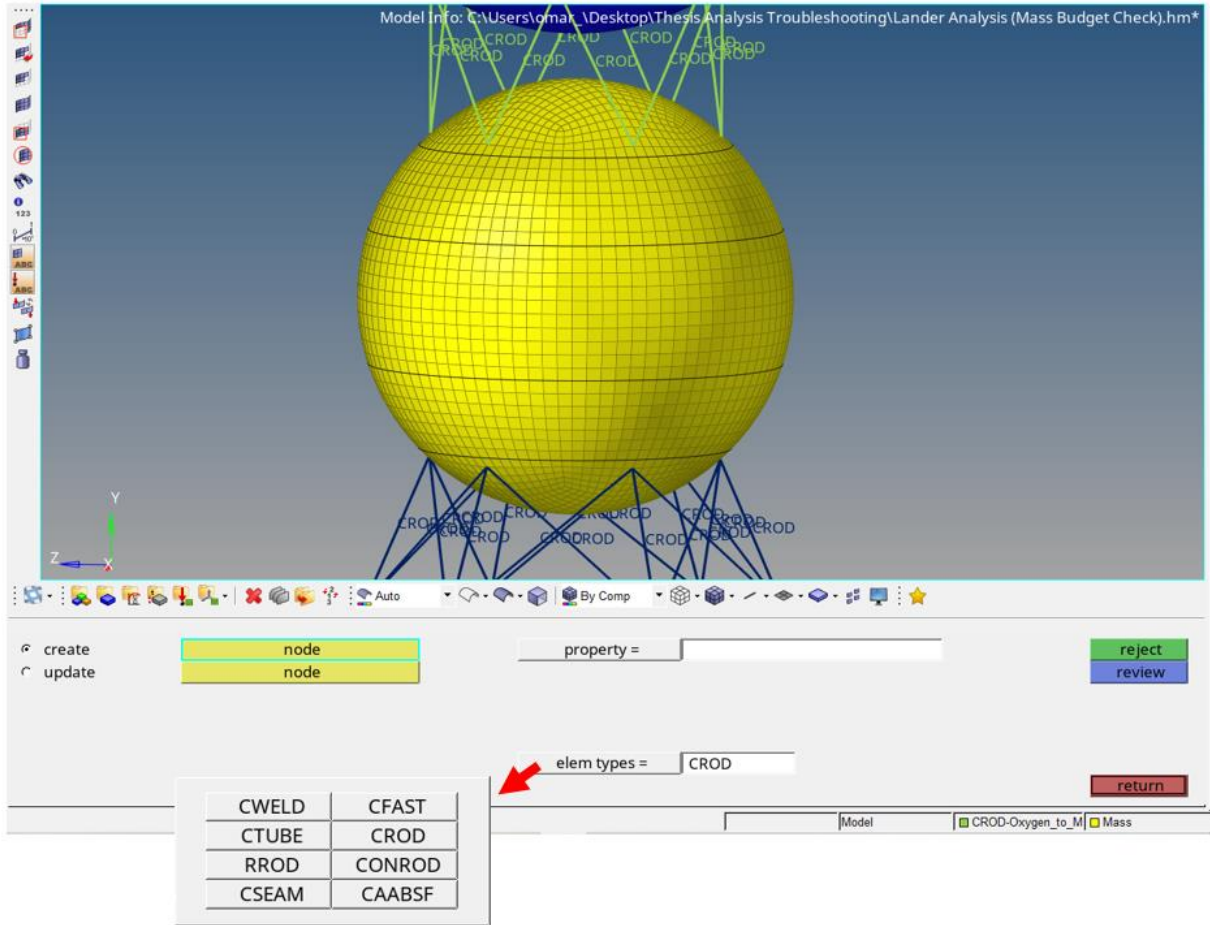
Figure 35. CROD Elements Window

The elements can be found in the "rods" option in the "1D" section. Note that there are different elements, with different functions, that fall in this category and that can be selected by clicking on element types. For this case CROD was selected. Then the element can be created by using two nodes. The property will be entered manually differently and will be explained in the next sections.

CBAR elements were another element used in this analysis. Besides being interested in the stresses generated in the rods, stresses generated in the piping system, which is going to be affected by the instrumentation such as solenoid valves, manual valves and any other connection and fittings, is of great interest since it will experience loadings due to the maneuvers and

vertical takeoff. Knowing the stresses and behavior of the piping system will be crucial to design

structures to minimize the piping movement and stresses. CBAR and CBEAMS elements allow

tension, compression and bending [28], allowing to model the piping system and determine how

bending stresses will affect the delivery system as well as the pressure vessels.
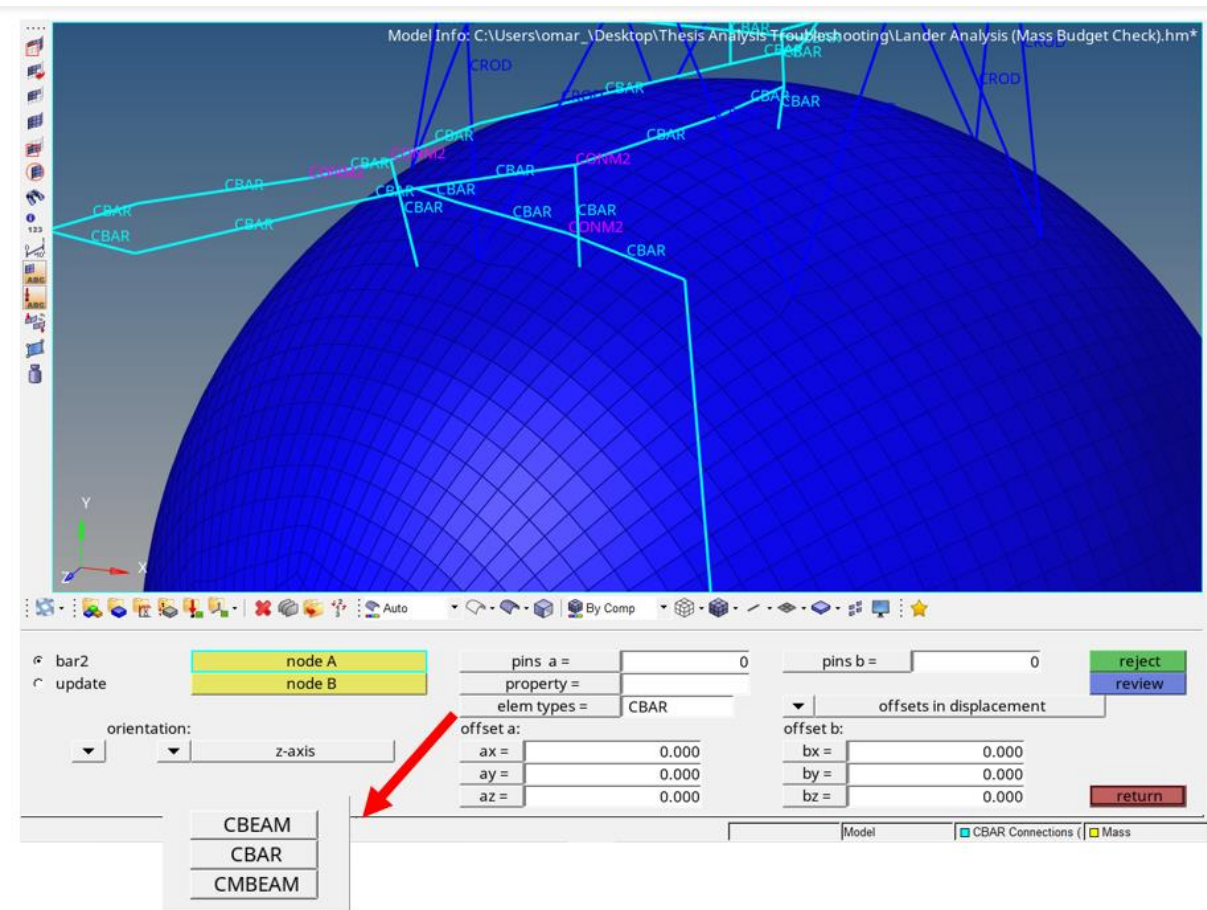
Figure 36. CBAR Elements Window

Similar to the CROD elements, the CBAR can be found in the "bars" option in the 1D

section. As well as with CROD elements, there are multiple elements that fall in this category

with different functions that can be selected. For the gimbal system rods, CROD elements were

selected since most of the stresses will be tension and compression.

RBE3 elements are also 1D elements that allow the distribution of loads. In this analysis the mass, another 1D element, of the propellants and pressurizing fluid are accounted for since their weight will also generate stress in the pressure vessels. Since RBE3 elements allow the distribution of loads evenly and do not induce stiffness [28], they were used to distribute the mass evenly throughout the wall of the pressure vessels.
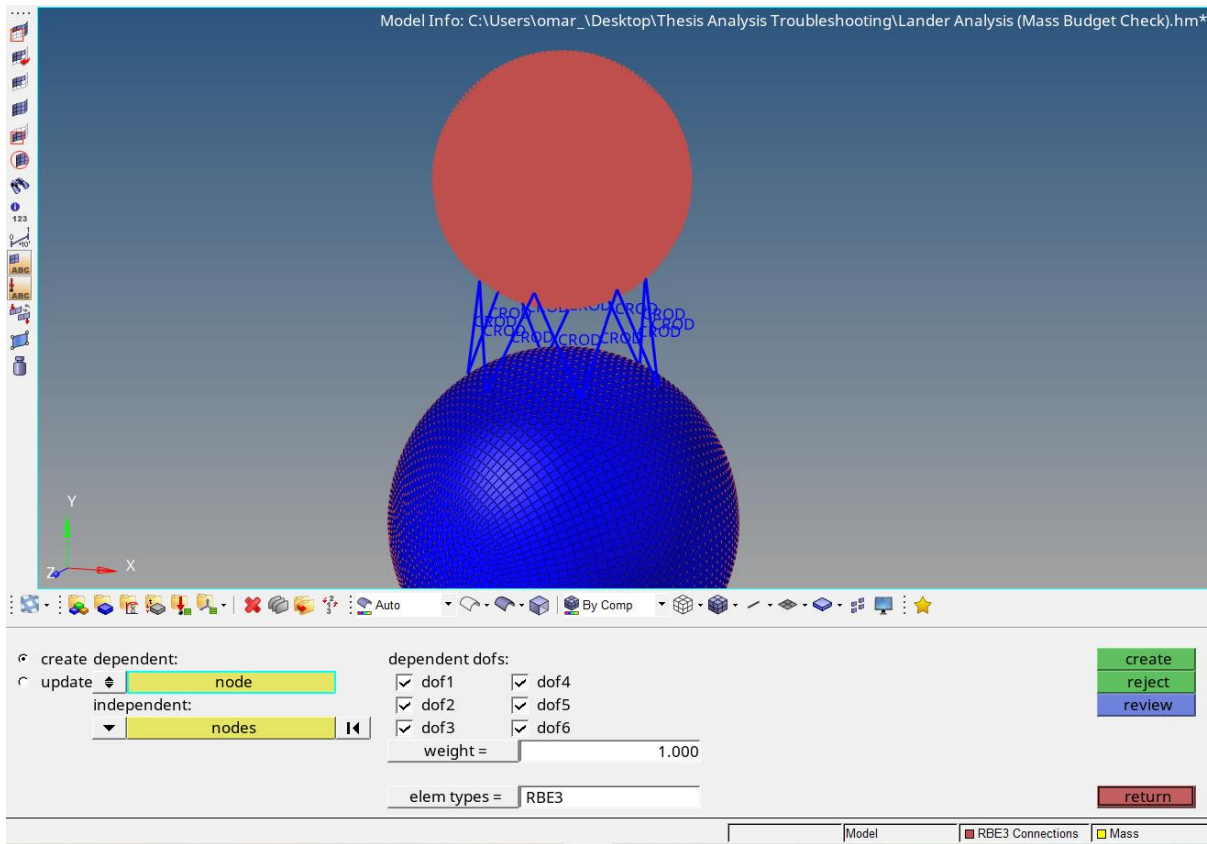
Figure 37. RBE3 Elements Window

Differently than CROD and CBAR elements, RBE3 elements can be found in a section with the same name, "rbe3". RBE3 elements have degrees of freedom and weight (which is the proportion of the force and moments that are distributed to the dependent node from the independent nodes for the degrees of freedom selected [28]) that can be modified. For this

50

analysis these were set as default and the dependent node was selected to be the CONM2 (mass) and the independent nodes the nodes in the structure (where it is there were the load is desired to be distributed). The nodes can be selected by using the "by window" option (allows to draw a window and nodes inside will be selected) or the "displayed" option (allow to select all the nodes that are displayed).

As mentioned, the mass is another 1D element used in this analysis. There are 20 types of masses that can be used, card images that can be assigned, but for this case the mass, card image, selected is CONM2. This type of mass allows to model a concentrated mass about its center of gravity. Reference [29] can help to model and understand more about rigid masses.
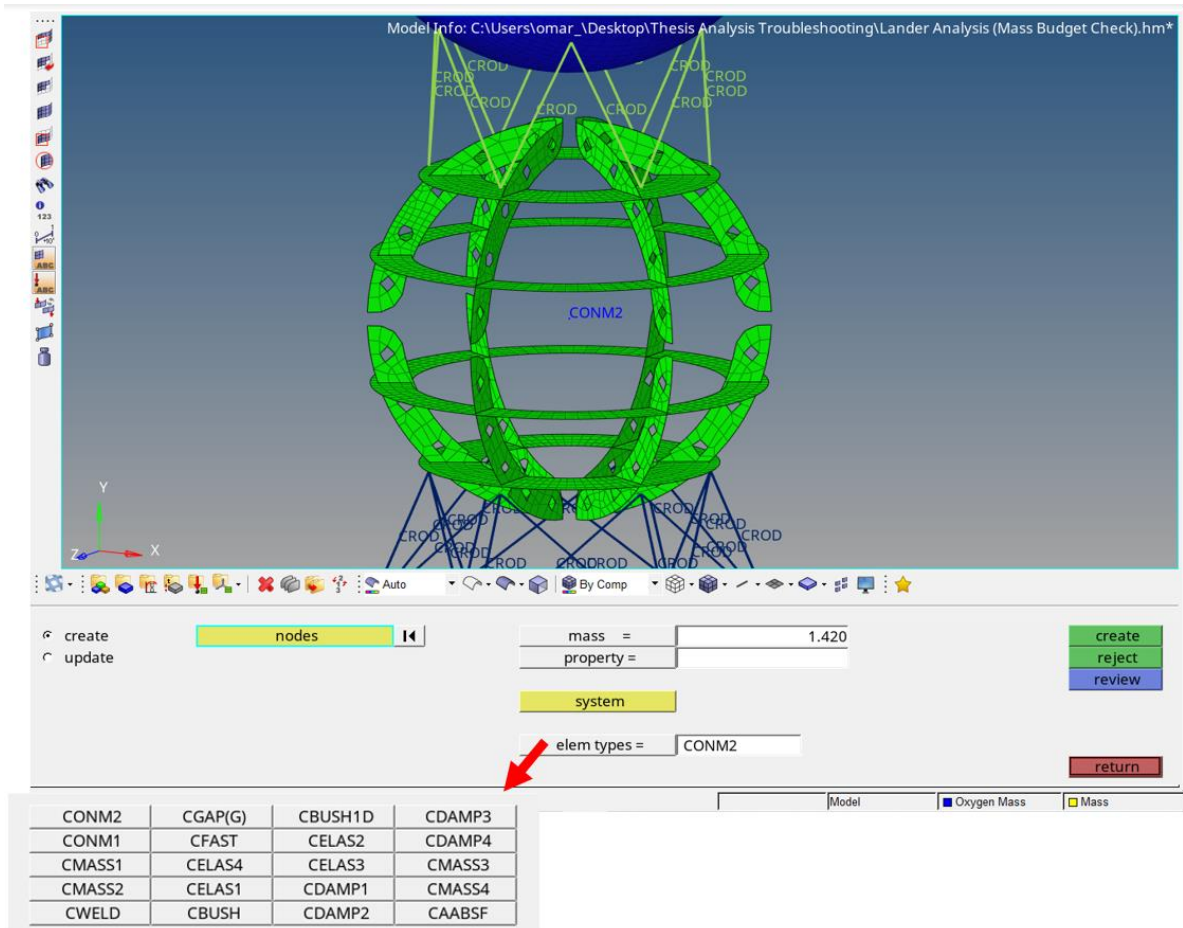
Figure 38. CONM2 Element Window

The window shown in Figure 38 can be found in the "masses" option in the "1D" Section. The magnitude of the mass can be entered in the mass box, which for this case was entered in slinches. The mass is created by selecting a node. In this analysis the nodes were created at the centroid of the sphere (tanks). Also, CONM2 elements were also used to model the heavier instrumentation of the delivery system (solenoid valves), engine and the actuators of the gimbal system. The nodes were created at approximately their geometrical center.

2.2.1.6 Property Cards and Materials

It was mentioned that for each part of the model there was an individual component created, this is of good practice since it allows for an organized analysis. Each component created represents a structure, physical quantity or an element to distribute forces. Each component requires what is called a property card. The property card allows to assign the material, the type of structure, dimensions and other parameters to the component.
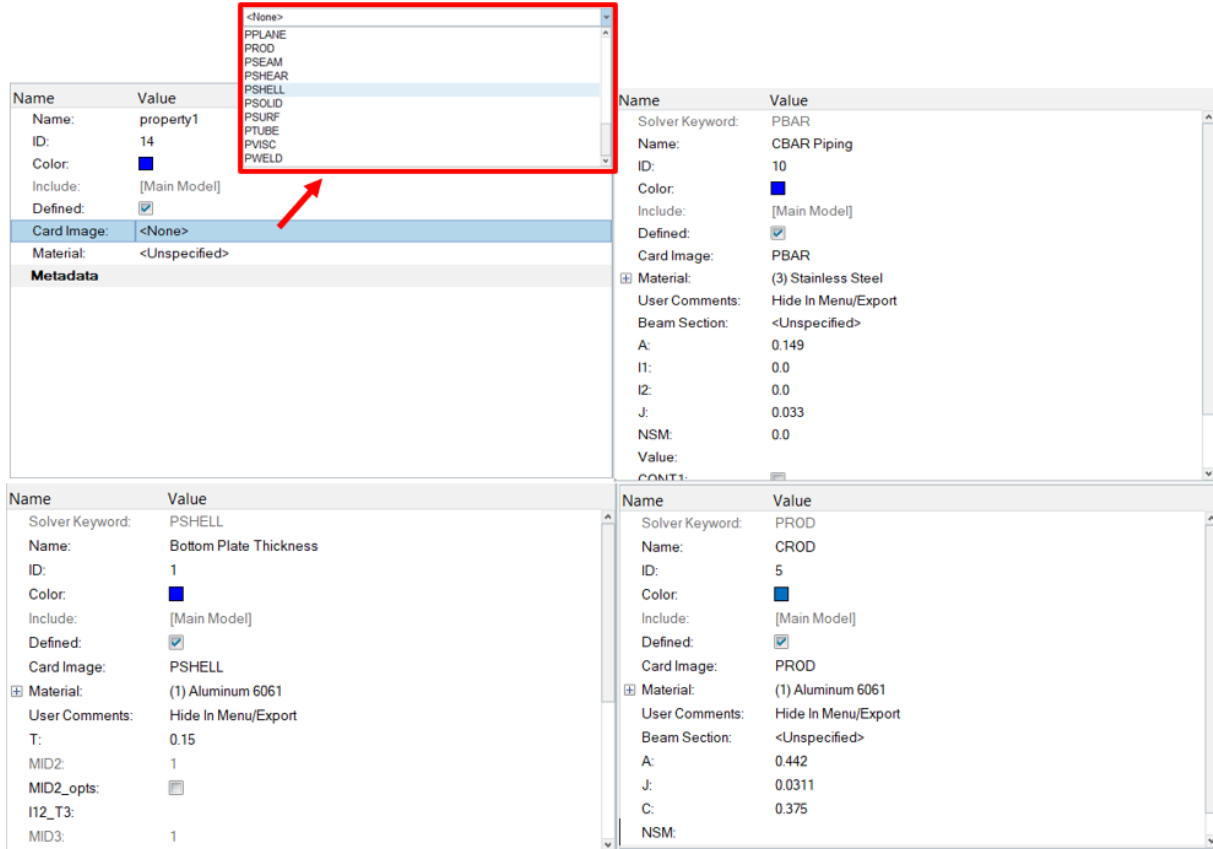
Figure 39. Property Cards

Figure 39 shows how a property card typically is displayed. To create a property card right click anywhere in the panel in the left side where all the components are stored, can be seen in figure 13, and select create allowing to create properties, components, load collectors, materials and more. Once a property has been created, the name, color and ID can be changed. Card image will depend on the function of the component that will have the property card. Parameters will be different for each type of property card. For this analysis, four different card images were used. PSHELL was used in meshed components that represented structures such as the baffles, the tanks, the bottom plate and the avionics box. This image card allows to enter the thickness of the component (T). PROD was used for CROD elements. This card image requires parameters such as the cross-sectional area, polar moment of inertia and the torsional stress coefficient. There are

two card images PBAR and PBARL that are used for CBAR elements but can also be used for CBEAM elements but with a difference that PBAR is used for simple elements (bars) and PBARL, L means that the library is activated, is used for elements that have a cross-section that is different than a bar. For the PBAR image parameters such as area, A, polar moment of inertia, J, and area moment of inertia about two planes, I1 and I2, will need to be specified. For the PBARL card image the cross-section will have to be specified and a beam section collector needs to be created, same approach as when creating a component or property card.
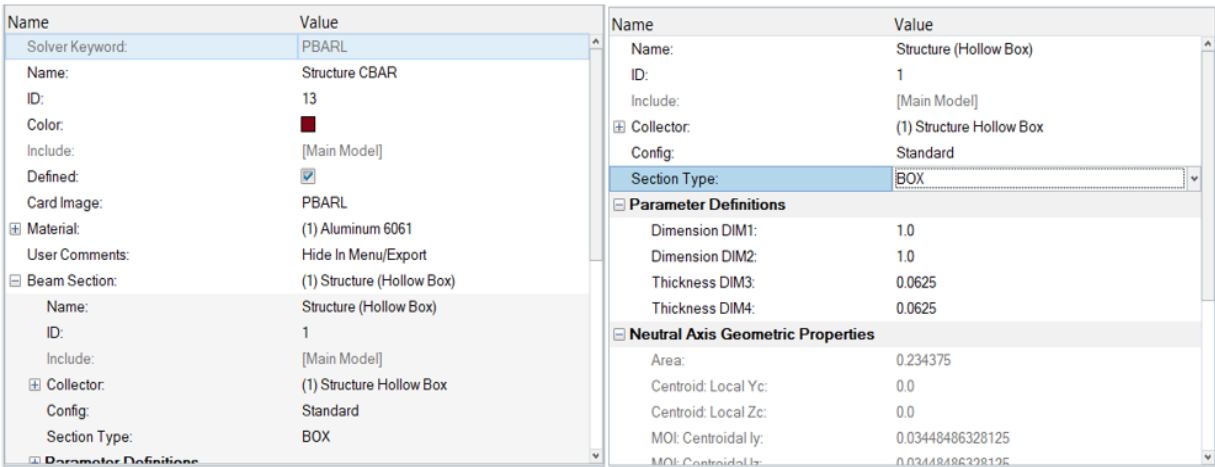
Figure 40. PABRL Property Card (Left) & Beam Section Collector (Right)

Figure 41 shows a bar and a box cross-section with the reference parameters to specify the dimensions. For this analysis two different cross-sectional areas were used, a circular tube to simulate the piping of the propellant delivery system and a box to simulate a hollow square aluminum tube that will be used to analyze how the structure supporting the avionics and other components will behave under the loads applied.
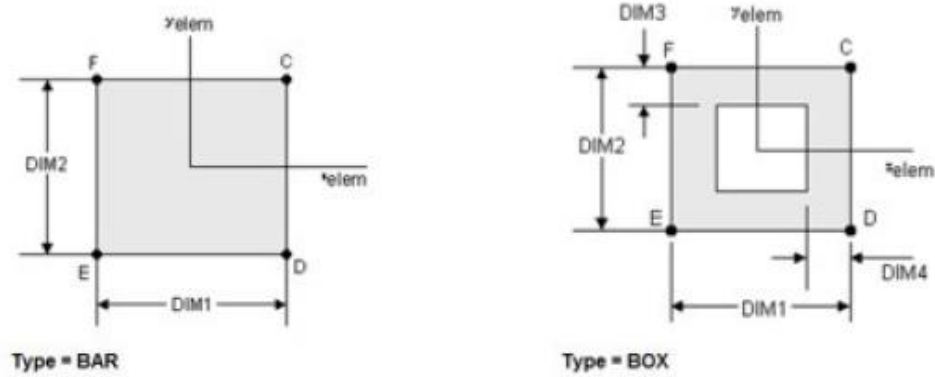
Figure 41. Bar and Box Cross-Sections [28]

Once the dimensions, DIM's, were referenced, the values were specified in their corresponding DIM box in the beam section collectors. Reference 28, starting in page 161, has different shapes that can be modeled using CBAR and CBEAM elements, with their corresponding DIM's.

It is noticed that there is also a box in the property card for the material. A material must be created to assign it to the properties. A material can be created in the same way components and property cards were created. Once the material has been created two independent material constants, for example E and NU, need to be specified for a linear static analysis, and for gravity, centrifugal and dynamic analysis the density needs to be specified [28]. In addition, a card image also needs to be specified to the material. When a new material is created the card image given to the material is MAT1, which is used for linear, temperature independent and isotropic materials [30].
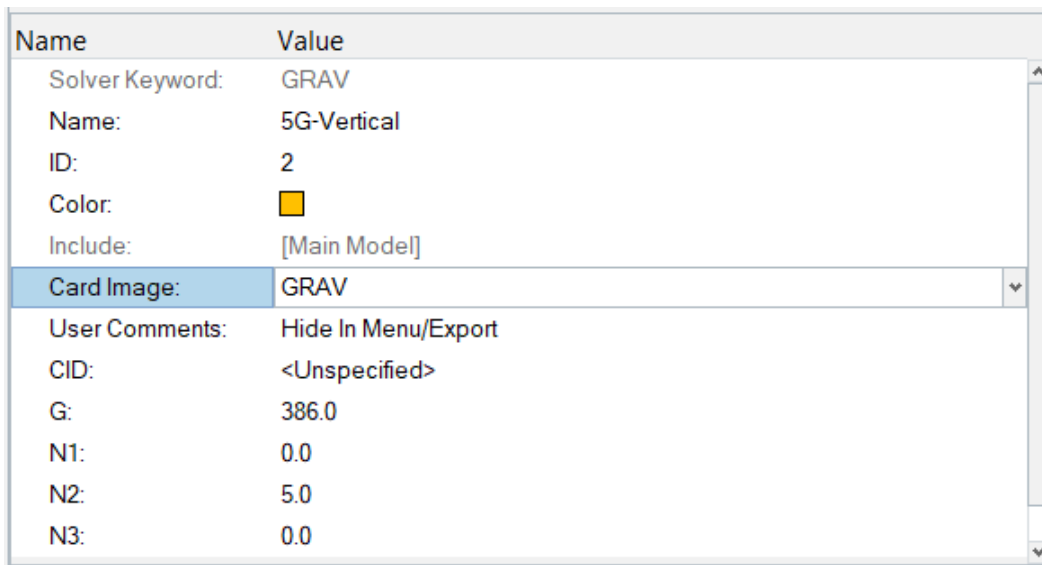
Figure 42. Material Component

When creating a material, it is strongly recommended that either E or G must be specified. Also from the parameters E, G or NU is also recommended that only two of these parameters are specified, in this analysis only E (psi) and NU were specified, including RHO (slinch/in^3). Care needs to be taken when assigning the values to the materials. When the cursor is hover over any parameter a number, default value, can be seen but once the cursor is removed it disappears. When entering a value, the enter key must be hit to always display the number as in figure 42, otherwise the software will give a 0 value to the parameter, even if a number has been entered to the parameter, which can affect the results of the analysis. Once a material has been created, it can be assigned to the property card desired.

It should be mentioned that there are components that do not need a property to be specified. In this analysis components such as mass and RBE3 elements did not have a property card assigned.

2.2.1.7 Load Collectors and Load Steps

The load collectors allow to create the boundary conditions and loads needed to perform an analysis. A load collector and a load step can be created in the same way that components, materials and properties were created. Similar to the property card, the load collectors also require a card image that will have different parameters to assign values to, depending on the image card type. For this analysis 6 different load collectors were created. The first two load collectors were for a G-force analysis, one in the vertical direction and the other for a lateral direction. The card image used was GRAV, which is used for gravity analysis. This card image allows to enter the gravity value, as well as the number of G's desired in the x, y, and z directions.

Name	Value
Solver Keyword:	GRAV
Name:	5G-Vertical
ID:	2
Color:	▯
Include:	[Main Model]
Card Image:	GRAV
User Comments:	Hide In Menu/Export
CID:	<Unspecified>
G:	386.0
N1:	0.0
N2:	5.0
N3:	0.0

Figure 43. G-Force Load Collector

For this analysis, 386 (in/s^2) was specified for the G force and the desired direction for the vertical G force was in the y direction (N2). Note that N1 is the x direction, N2 is the y direction and N3 is the z direction and the amount of G's can be specified in each slot, also the direction (negative or positive direction) for this case, the analysis was 5G's vertically in the positive y direction. The same approach was taken with the 3G's lateral direction with the only difference that the amount of G's was 3 in the N1 slot (positive x direction). [36] is a good reference to perform a static G-analysis.

The next load collector created was to fix the geometry at the bottom end (in the base plate of the lander). For this load collector no card image was specified. For this load collector the boundary conditions need to be created and then assigned to that load collector. In the "analysis" section, there are multiple options to assign different types of loads such as forces, pressures, moments, constraints, temperatures, etc. For fixed points/ends, the "constraints" option can be selected.
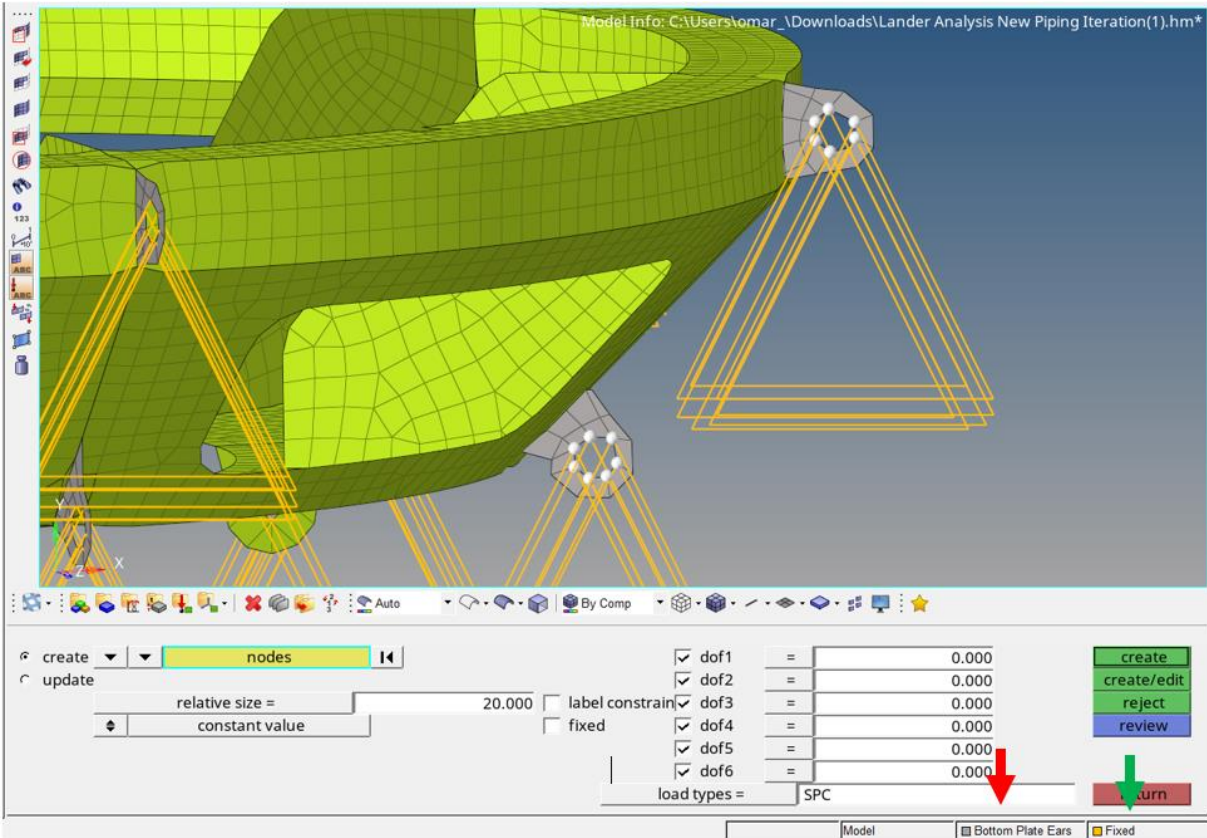
Figure 44. Constraints

Figure 44 shows the "constraints" option. Note that the load collector is selected before the constrains are created. This will allow the forces, pressures, constraints or any other type of loads to become part of the load collector desired. The green arrow shows the load collector selected (that is the spot where the load collectors are shown) and the red arrow shows the component selected (that is the spot where the components are shown). One way to make sure that the component or load collector is assigned to the right component or load collector is by selecting the "By Comp" option. As seen in figure 44, the constraints were assigned to the load collector created for the fix ends. For constraints the SPC load type was selected (default) and all the dof (degrees of freedom) boxes are checked out (this means that the node will be constrained in that degree of freedom). After that the nodes that will be constrained were selected.

59

Similar to the fixed ends (constraints), another load collector that does not require a card image but needs to be assigned to a load is pressure. As mentioned, pressure can also be found in the "analysis" section in the "pressures" option.
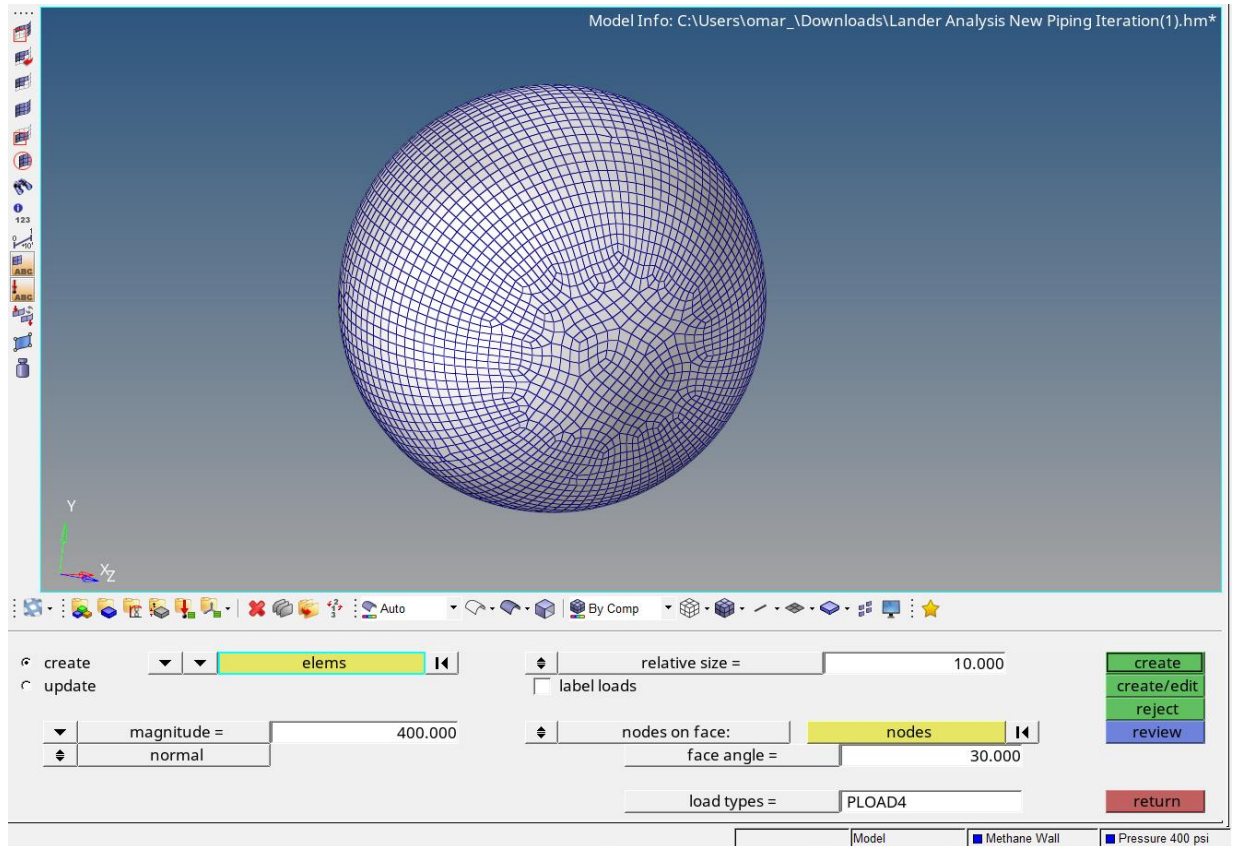
Figure 45. Pressures

As shown, the elements where the pressure is going to be applied are selected. The magnitude of the pressure (psi for this case) is specified in the magnitude box. Also, for this analysis the load type used was a PLOAD4, which defines a load on a face of a HEXA, PENTA, TETRA, PYRA TRIA3, TRIA6, QUAD4 or QUUAD 8 element [31]. Note that in the component and load collector boxes the corresponding component and load collector are selected before the load is created. The same approach was taken for the pressure applied in the helium tank, with the only difference that the magnitude was 4000 psi. Since the same pressure will be applied to the

oxygen tank, the same load collector was used when the pressure elements were created for the oxygen tank.

Another load collector created allows to have multiple load collectors in the same load collector. This load collector uses the card image LOADADD. The LOADADD load collector can be used to combine multiple forces and see the results of these multiple forces combined.
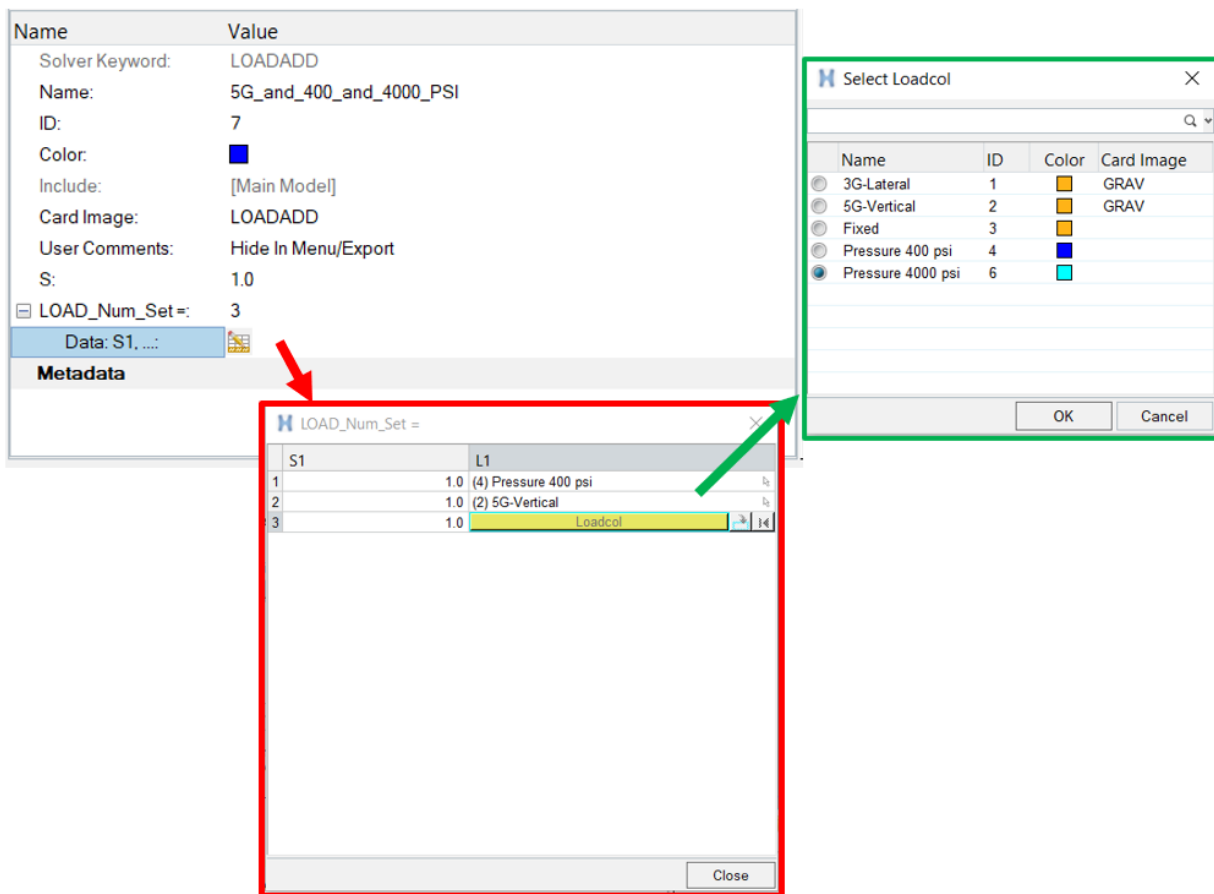
Figure 46. LOADADD Collector

Figure 46 shows the load collector with the card image LOADADD. The parameter LOAD_Num_Set allows to enter the number of load collectors that will be used. For this case 3 different load collectors were used, the pressure applied to the methane and oxygen tanks, the 5G

vertical force and the pressure applied to the helium tank. Once the amount of load collectors is entered, a list with the slots available is shown, then in L1 the load collector can be selected from the load collectors already created.

The last load collector created allows to perform a modal analysis, required in this analysis. A Normal Modes Analysis (Modal Analysis) "is a technique used to calculate the vibration shapes and associated frequencies that a structure will exhibit" [28]. The modal analysis can help in determining the frequencies at which the structure can resonate, leading to the failure of the structure (similar to the Tacoma Bridge incident). In this version the load collector can be created by creating a "Load Step Input", in the same way the load collectors were created. In previous versions a load collector can be created and use the EIGRL card image.

Name	Value
Solver Keyword:	Real Eigen Value Extraction
Name:	EIGN
ID:	1
Include:	[Main Model]
⊟ Config type:	Real Eigen Value Extraction
⊟ Type:	EIGRL
V1:	1.0
V2:	150.0
ND:	25
MSGLVL:	
MAXSET:	
SHFSCL:	
NORM:	MASS
Metadata	

Figure 47. Load Step Input for a Modal Analysis

As shown in figure 47, the configuration type selected for this analysis is Real Eigen Value Extraction since the EIGRL card is selected (EIGRL defines the data that allows to perform a

real eigen value analysis, buckling or vibration, with the Lanczos method [33]), allowing to perform a vibration analysis using the Lanczos method [32]. V1 and V2 is the range of the frequencies desired and in the NORM field, MASS was selected since it is the default option for a normal modes analysis. [34] and [35] can be a good reference to perform a modal analysis.

Load Steps allow to select the loads and boundary conditions created in the Load Collectors and perform the analysis with those loads and boundary conditions applied. The Load Steps can be created in the same way the Load Steps were created. Then the boundary conditions and loads can be selected for each of the options displayed.
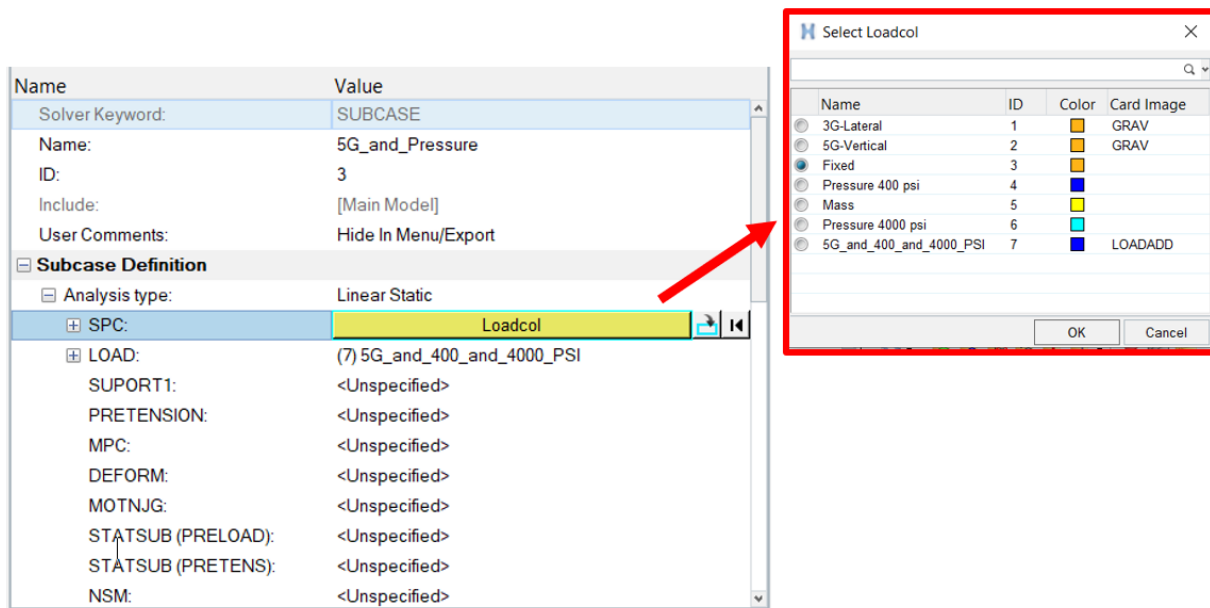
Figure 48. Load Steps

Figure 48 shows the options of the when selecting the boundary conditions and loads that will be applied. The SPC box allows to select the boundary conditions, for this case the "Fixed" load collector is selected since it fixes the lander at the bottom base plate. In the LOAD box is where the loads desired can be selected. In figure 48, the loads selected were the 5G in the vertical direction and the pressures in the propellant and pressurizing tanks. Note that those loads were

selected in the Load Collector using the LOADADD card image, only one load Collector can be chosen, since it was desired to determine the stresses and displacement of the structure at a 5G force vertically while the tanks were pressurized the Load Collector with these loads was created. For this analysis 4 Load Steps were created, two for the G-forces in the vertical and horizontal directions, one with the pressures in the tanks and the G-force vertically and the modal analysis. These load steps will allow to see results at these conditions. For the "SUBCASE OPTIONS" the "ANALYSIS" and "OUTPUT" boxes were selected. For the "ANALYSIS" the "STATICS" option was selected in the "TYPE" box since it allows to perform a linear static analysis and for the "OUTPUT" the "STRESS" option was selected. The "OUTPUT" option allows to select the type of reactions that are desired to be displayed in the results, "STRESS" is of great interest for this analysis.

2.2.1.8 Help Tool

Throughout the setup of this analysis, the help tool has been used several times to consult the applications of different elements and image cards and how to use them having references [30] and [33] as an example. The use of the "help" tool is encouraged since, as explained, can be useful to know the application of different elements and image cards, and based on the type of analysis, what card images or elements are the best to use. The "help" tool is located in the horizontal line of options displayed at the top of the window below the title of the model being worked on. The "help" tool is located at the far end, next to "applications". Once clicked, "HyperWorks Help Home" should be selected. That option will take the user to the web page were any element or property card, in the search bar, can be searched. In detail explanations are given, which are helpful and increase the experience of the user.

Chapter 3: Results

3.1 DISPLACEMENT AND STRESSES ITERATIONS

The goal of this analysis was to determine the best arrangement of the supports (connecting rods), piping and avionics, to have a structure with the highest natural frequency possible and, as mentioned in the previous sections, to determine if the structure, mostly the tanks and their supports, would be able to withstand the stresses generated with the current dimensions.

To have a perspective on how the arrangement of the rods as well as the spacing between the tanks and total height of the lander would affect the parameters of interest some equations were used. The first equation used was the flexure formula which tells the maximum stress generated by relating the furthest point apart from the neutral axis (c), resultant internal moment (M) and the moment of inertia of the cross-sectional area about the neutral axis (I).

$$\sigma = \frac{Mc}{I}$$

Equation 3 [38]

Since stress is desired to be minimal, the only parameter that can be changed/manipulated would be the I. The only component of the vehicle that can be rearranged easily are the supporting rods. The rods are not at the center of gravity, which means that the parallel axis theorem needs to be applied

$$I = I_G + md^2$$

Equation 4 [39]

Where I_G is the moment of inertia, in this case the rod, at the center of gravity plus the mass (m) times the distance from the center of gravity (d).

The natural frequency of a cantilever beam is given as

$$f = \frac{k_n}{2\pi} \sqrt{\frac{EIg}{wl^4}}$$

Equation 5 [40]

Where k_n is the mode, E the modulus of elasticity, I the moment of inertia, g gravitational constant, w the weight of the beam and l the length of the beam. Also, from Hooke's law, the displacement of a beam, which can be modeled as a spring, is

$$k = \frac{F}{x}$$

Equation 6

Where F is the force and x the displacement. The displacement x can be taken as the deflection of a cantilever beam. The deflection of a cantilever beam fixed at one end is

$$\delta = \frac{PL^3}{3EI}$$

Equation 7 [41]

Where P is the force applied, L is the length of the beam, E the modulus of elasticity, and I the moment of inertia. From these equations natural frequency can be affected by the length of the "beam", lander in this case, and also by the moment of inertia of the structure, which for this case can be increased by manipulating the supporting rods. In addition, bending stresses also depend on the moment of inertia I which as already said, can be increased by manipulating the supporting rods.

66

Several iterations were performed, starting by analyzing the original design imported from Fusion 360. The goal of the results from the first analysis was to validate the approach taken and the setup of the FEA analysis to perform other iterations with the goal of improving the design.
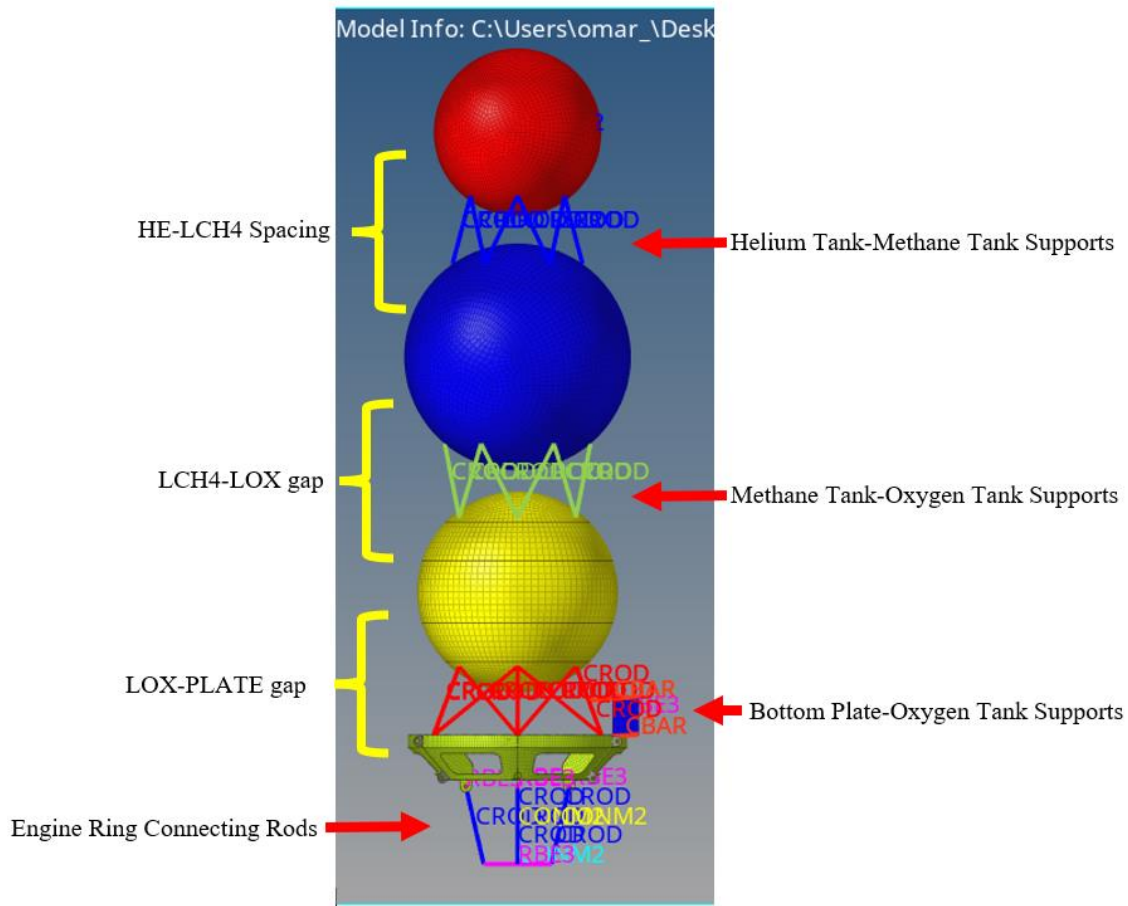
Figure 49. Lander Components Labeling

In the results of the first analysis performed, the highest displacements, 2D stresses and stresses in the CBAR elements were located at the 3G lateral load case, except for the CBAR stresses, which were higher for at the 5G with pressure case. The firs mode of the modal analysis showed a frequency of 6.51. Also, the mode first mode showed a bending mode similar to the one seen in the 3G case. In that mode, the support connecting the bottom plate and the engine

ring are oscillating and being displaced showing that those spots displace the most. The 2D

stresses are also the highest at the 3G case, where they concentrate in the tank walls, oxygen tank

and bottom side of the methane tank, where the supports connect to the tanks. For the CROD

elements, the highest compression and tension is located at the elements connecting the bottom

plate and the oxygen tank, most precisely, the rods that are in the x-direction, which is where 3G

load was applied. The CBAR elements, show the highest compression and tension at the 5G with

pressure case, being the elements that are vertically positions and simulating the purge and

delivery lines for the oxygen and methane. Elements simulating the delivery lines for oxygen and

methane show the highest tension and compression respectively.

Table 5. Original Iteration Analysis Results

Original Iteration	5G	3G	5G With Pressure	Modal Analysis (First Mode)
Original Position				6.51 (Frequency)
Displacement (in)	0.040 - 0.36	0.11 – 1.05	0.033 - 0.30	NA
2D Stresses (psi)	0.20 - 19320	0.23 - 57050	0.26 - 113500	NA
1D CROD Stresses (psi)	-370.4 - 2665	-7447 - 6680	-1318 - 3709	NA
1D CBAR Stresses (psi)	-708.5 - 173.0	-357.9 – 329.3	-1321 - 417.9	NA

As mentioned earlier, the goal of this analysis is to analyze and optimize the structure of

the designs that are being considered for the JANUS moon lander. The natural frequency and the

bending stresses can be increased and reduced respectively by reducing the height of the

structure and increasing the distance of the supporting rods from the axial direction. Several

iterations were performed by reducing the distance in between the tanks and the bottom plate. Also, the connecting rods were moved inside and outside (shrunk and extended) as well as kept in their original position when the distances were reduced to determine how the location of the rods and the distance between the tanks and the bottom plate affect the natural frequency and stresses in the structure.

For the first iteration, the gaps were reduced by 6 in (between oxygen tank and bottom plate), 1 in (between the methane and oxygen tanks) and 1.5 in (between the helium and methane tanks), shown in figure 50.
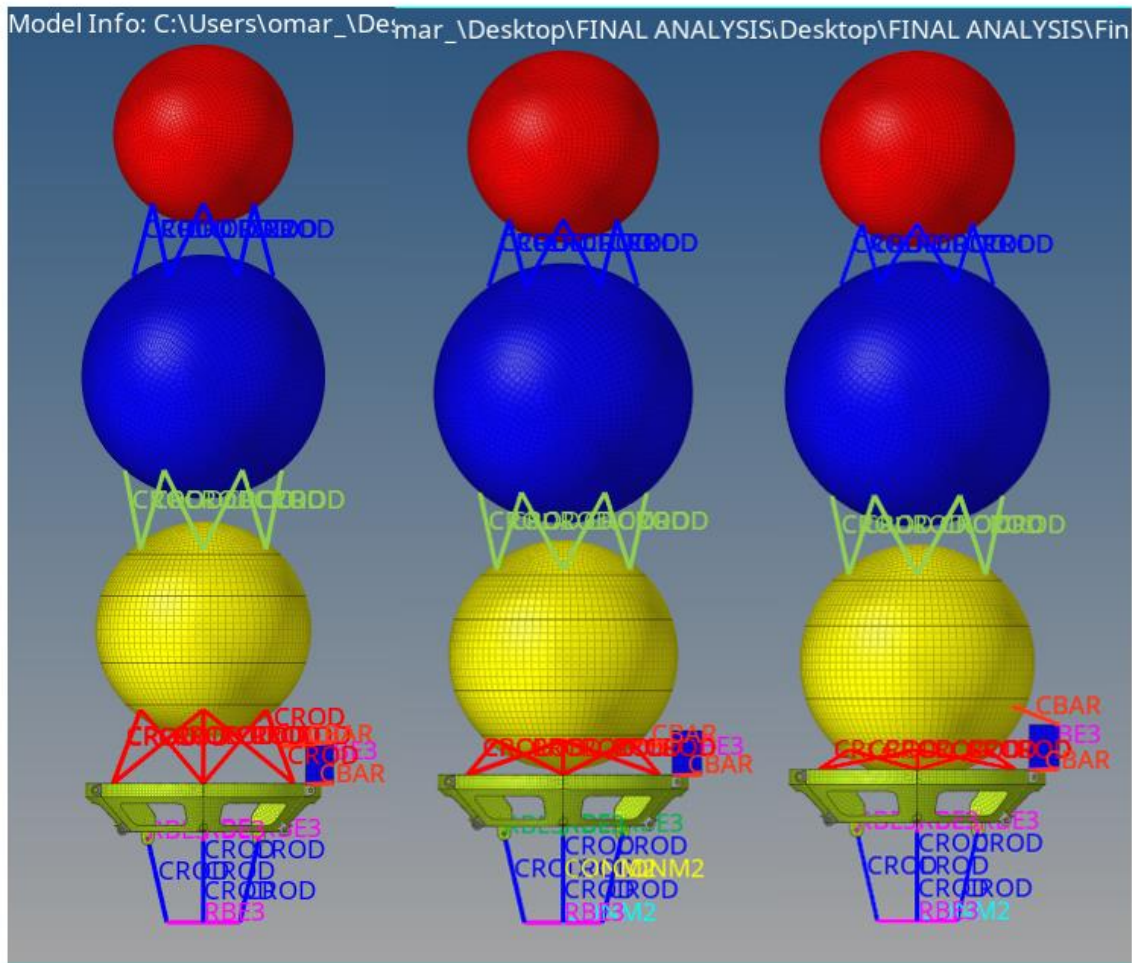
Figure 50. Iterations Performed. Original (Left), First Iteration (Center), Second Iteration (Right)

In the first case the rods were kept at their original location, which shrunk to 10.34 in in the HE-LCH4 gap, 11.85 in in the LCH4-LOX gap and 14.08 in (diagonal rod) and 6.48 in (vertical rod) for the LOX-PLATE gap. The same approach and analysis were performed to the other two cases, shrunk and extended supports rods. For the second case the rods were shrunk in, reducing their lengths to 7.15 in in the HE-LCH4 gap and 8.94 in in the LCH4-LOX gap from the length at the original location. The connecting rods in the LOX-PLATE gap were kept same as previous iteration. For the extended supports case the connecting rods were extended out, increasing their length to 13.14 in in the HE-LCH4 gap, 14.73 in in the LCH4-LOX gap and 19.04 in (diagonal rod) and 10.81 in (vertical rod) for the LOX-PLATE gap.

Figure 51. Original Supports (Top Left), Shrunk Supports (Top Right), Extended Supports

(Center)

The displacement and stresses are displayed at Table 6 at the three different support cases:

original, shrunk and extended for the four different load cases performed: 5G vertical, 3G lateral,

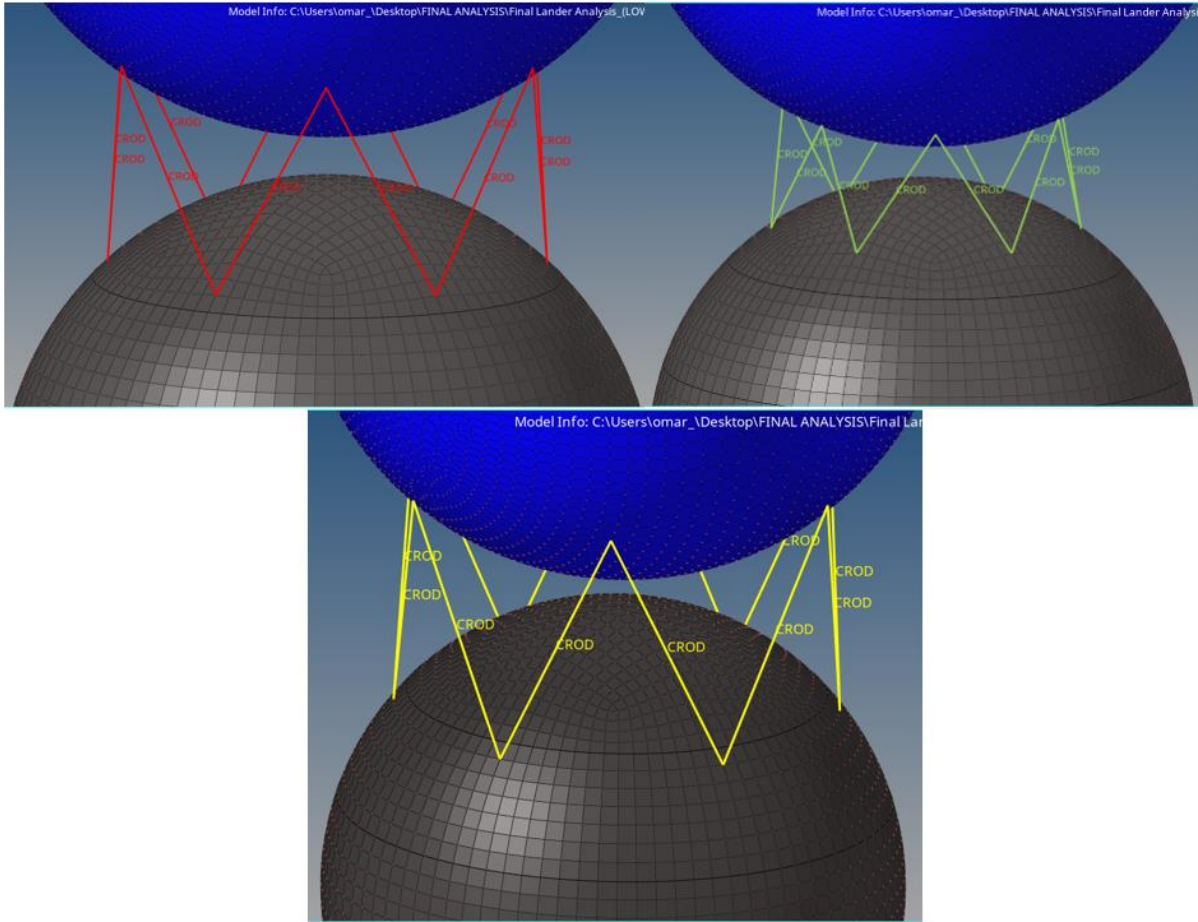5G with pressure and modal analysis (where only the frequency at the first mode is displayed).

Table 6. Displacement and Stresses (Highest to Lowest) for all Load Cases and First and Last Modes of First Iteration

Supports Cases	5G	3G	5G With Pressure	Modal Analysis (First Mode)
Original Position				6.37 (Frequency)
Displacement (in)	0.043 - 0.38	0.13 – 1.19	0.047 - 0.42	NA
2D Stresses (psi)	0.20 - 16720	0.23 - 50570	0.26 - 114000	NA
1D CROD Stresses (psi)	-236.8 - 3012	-8083 - 8319	-293.7 - 3932	NA
1D CBAR Stresses (psi)	-668.2 - 477.0	-577.1 – 701.6	-1508 - 573.5	NA
Shrunk Elements				5.62 (Frequency)
Displacement (in)	0.041 - 0.37	0.16 - 1.5	0.047 - 0.42	NA
2D Stresses (psi)	0.20 - 15950	0.39 - 50350	0.26 - 112900	NA
1D CROD Stresses (psi)	-236.8 – 3005	-8035 - 8288	-308.1 - 3926	NA
1D CBAR Stresses (psi)	-728.9 - 476.9	-912.0 – 1117	-1677 – 617.7	NA
Extended Elements				9.96 (Frequency)
Displacement (in)	0.022 - 0.20	0.085 - 0.77	0.042 - 0.37	NA
2D Stresses (psi)	0.19 - 15920	0.20 - 21800	0.26 - 112900	NA
1D CROD Stresses (psi)	-236.8 - 1301	-2761 - 2794	-236.8 - 2318	NA
1D CBAR Stresses (psi)	-637.7 - 161.3	-481.2 – 574.7	-1415 – 544.7	NA

*Dimensions in red mean compression stress

For the first iteration, the displacements of greater magnitude happen at the 3G case for all the support cases, where they go above 1 in, except for the extended supports case where the biggest displacement is 0.77 in. The elements that see that displacement are the rods connected to the engine due to oscillations in these elements. Besides that, for the original supports and shrunk supports cases the top part of the helium tank also experiences the greatest displacement due to the bending of the whole structure due to the 3G lateral force applied.

Figure 52. First Iteration, Extended Supports (Left), Original Supports (Center) and Shrunk

Supports (Right), Displacements at 3G Case

From the results, the first mode appears to be what is call a bending mode, where the structure bends in a similar fashion as in the 3G case. As the supports are extended, the tanks move less but the supports connecting the engine and the bottom plate oscillate in a more aggressive manner due to the increase in the frequency of the mode.

For the 2D stresses the highest stresses were present at the 3G lateral direction and 5G with pressure case. For the 3G lateral, these stresses are concentrated at the walls of the tanks where the rods connecting the tanks are connected. This is due to the bending that is being caused by the force being applied in the lateral, x, direction.

Figure 53.First Iteration, Extended Supports (Left), Original Supports (Center) and Shrunk

Supports (Right), 2D Stresses at 3G Case

In the 5G with pressure case, the stresses increased in the pressure vessels due to the pressure at
which the propellants and the helium are being stored. From the results it is seen that helium,
pressurized at 4000 psi, cause stresses of 112,900 psi and the propellants stored at 400 psi cause
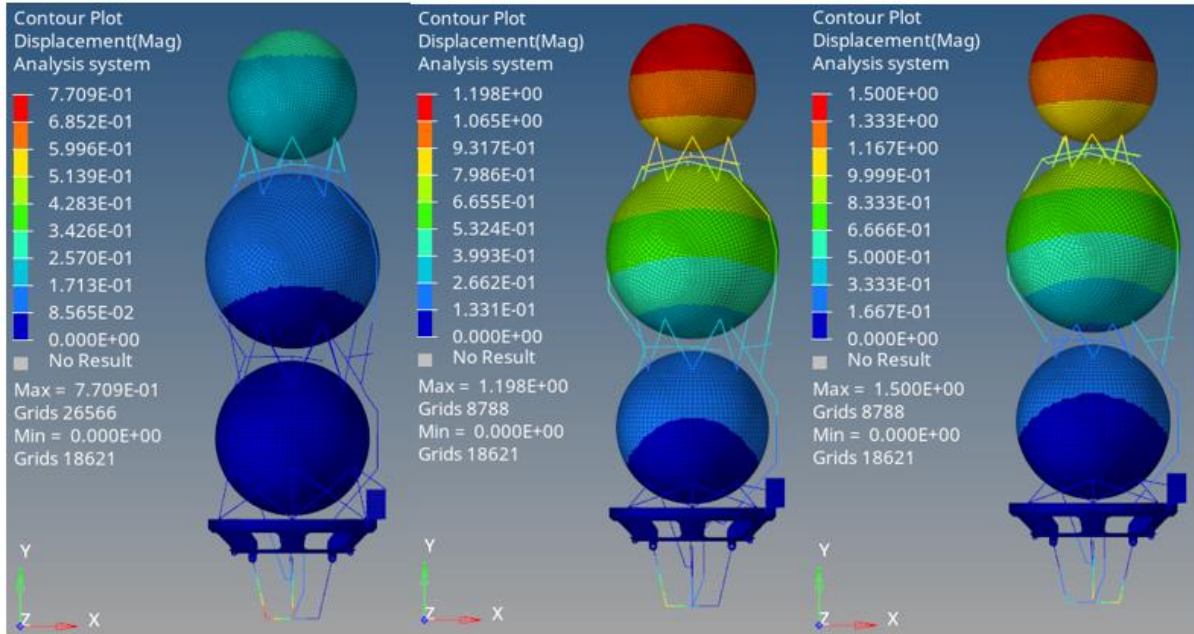stresses of 37,600 psi in the methane and oxygen tank.

Figure 54. First Iteration, Extended Supports (Left), Original Supports (Center) and Shrunk

Supports (Right), 2D Stresses at 5G With Pressure Case

First Iteration, Extended Supports (Left), Original Supports (Center) and Shrunk Supports (Right), 2D Stresses at 5G With Pressure Case

For the CROD elements, stresses near the 10,000 psi are spotted to be at the 3G due to the bending that is being caused by the lateral force applied. These stresses decrease in magnitude for the 5G case but are higher at the 5G with pressure case.
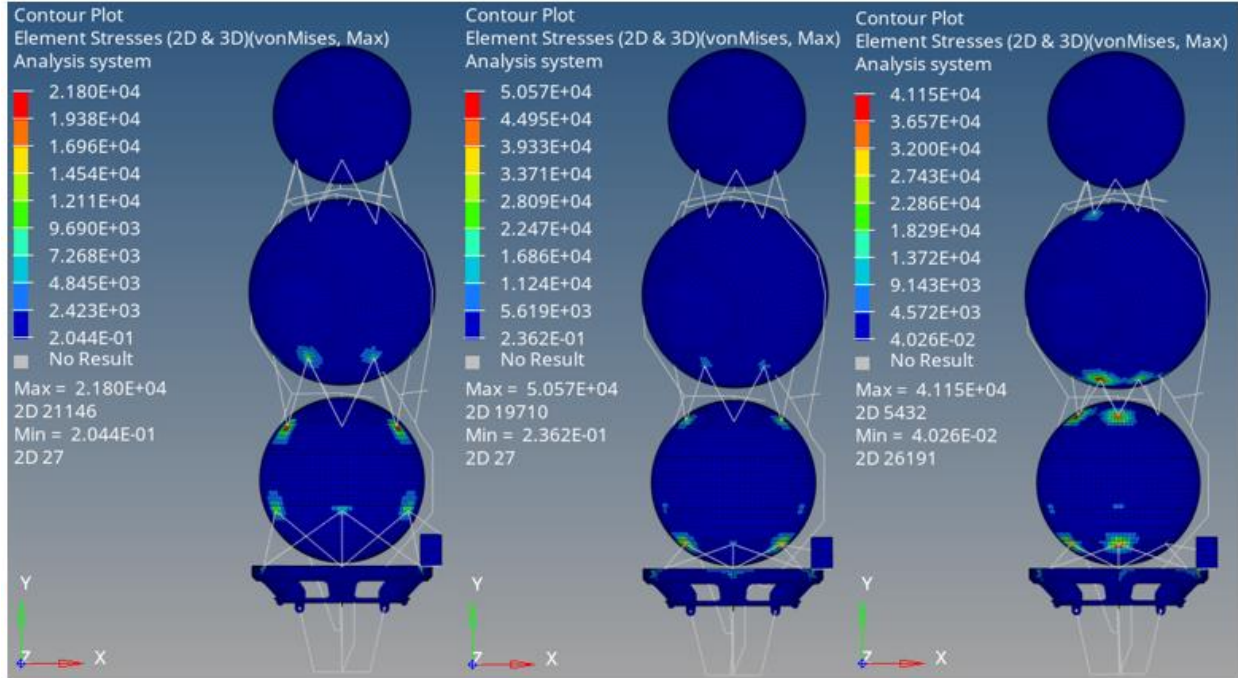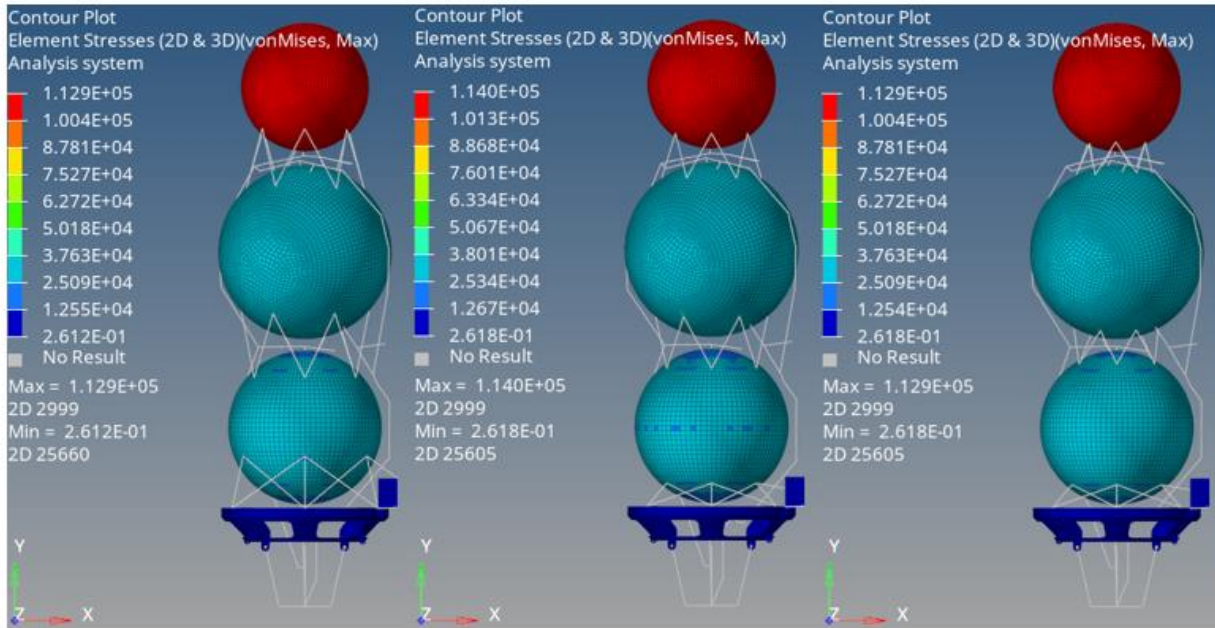
Figure 55. First Iteration, Extended Supports (Left), Original Supports (Center) and Shrunk

Supports (Right), CROD Stresses at 3G Case

These stresses are mostly located at the elements connecting the bottom plate and the oxygen tank.

Lastly, stresses of high magnitudes for CBAR elements seem to be more experienced at the 5G with pressure case for all the supports cases and decrease in magnitude for the 3G case. For the stresses in the 5G with pressure, the highest stresses are in tension at around 1700 psi. These stresses decrease as the supports are extended which can be due to the less bending that is seen in the animation as the supports are extended and the vertical movement in the 5G with pressure case.
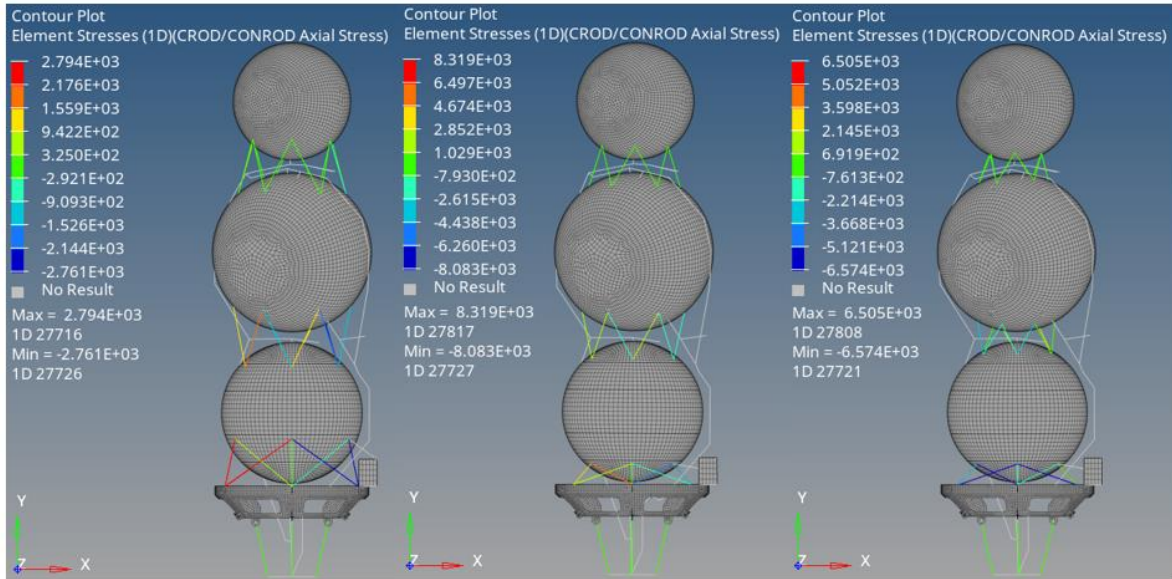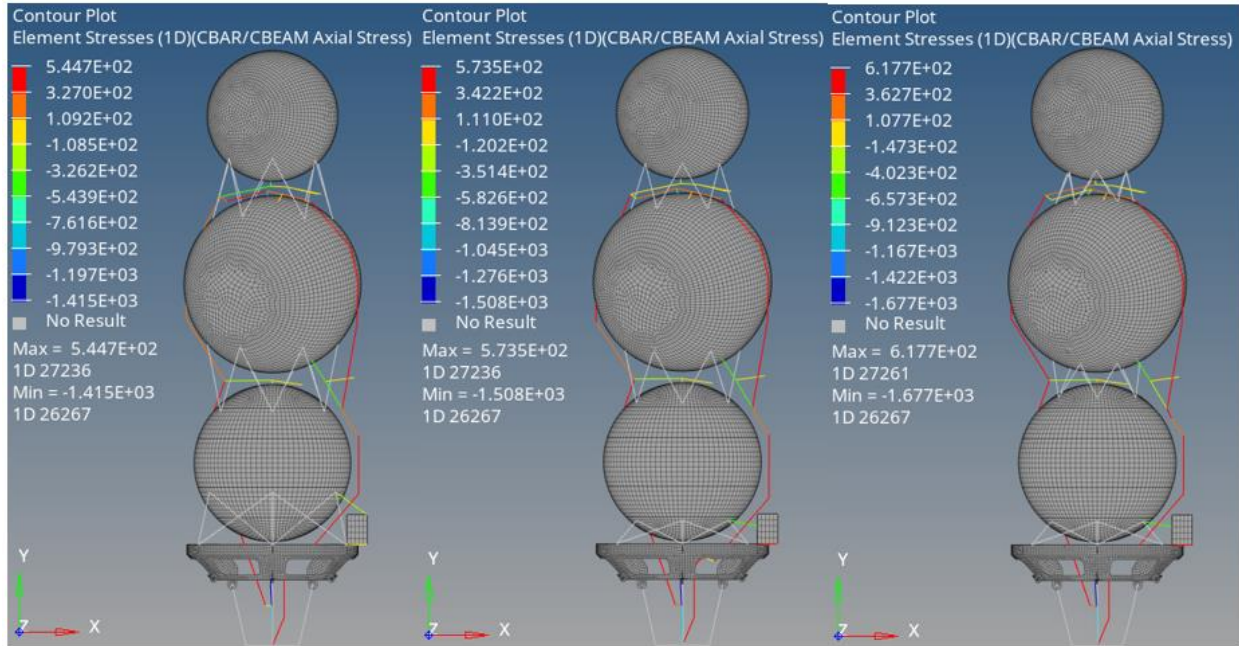
Figure 56. First Iteration, Extended Supports (Left), Original Supports (Center) and Shrunk

Supports (Right), CBAR Stresses at 3G Case

For all cases, the vertically positioned elements, and the elements going from the oxygen

tank to the engine, showed the highest values from the contour, having the highest compression

for the oxygen delivery line, and the highest tension in the methane delivery and purge lines.

From the results it was noted that a significant change in the natural frequency can only

be achieved by reducing the gap in between the tanks and the bottom palate. A second iteration

was performed, by reducing the distance of the gap in between the oxygen tank and bottom plate

(2 in), and the helium and methane tanks (1 in). The gap in between the oxygen and methane

tank was not reduced since it was too short already.

The previous discussed results showed that in the iteration where the supports are at the

original locations, are the intermediate results, in some instances, from the extended supports

case and shrunk supports case. For this set of iterations, the supports were only extended out and

shrunk in to see the results at two different ends. For the shrunk supports the rod length decreased to 6.77 in in the HE-LCH4 gap, 8.93 in in the LCH4-LOX gap and 18 the diagonal support and 8.88 in the vertical support LOX-PLATE. For the extended supports, the rod length decreased to 12.58 in in the HE-LCH4 gap, 14.90 in in the LCH4-LOX gap, and for the supports in the LOX-PLATE, they were kept at their original location. Table 6 shows the displacements, 2D stresses and 1D stresses for the two supports cases performed.

Table 7. Displacement and Stresses (Lowest to Highest) for all Load Cases and First and Last Modes of Second Iteration

Support Cases	5G	3G	5G With Pressure	Modal Analysis (First Mode)
Shrunk Elements				8.03 (Frequency)
Displacement (in)	0.021 - 0.19	0.099 - 0.89	0.045 - 0.41	NA
2D Stresses (psi)	0.19 - 17370	0.44 - 33840	0.26 - 112900	NA
1D CROD Stresses (psi)	-236.8 - 1370	-2803 - 2843	-315.4 - 2428	NA
1D CBAR Stresses (psi)	-716.9 - 174.9	-636.7 – 856.2	-1664 - 613.7	NA
Extended Elements				10.99 (Frequency)
Displacement (in)	0.022 - 0.20	0.066 - 0.59	0.027 - 0.24	NA
2D Stresses (psi)	0.19 - 17400	0.21 - 21770	0.26 - 112900	NA
1D CROD Stresses (psi)	-236.8 - 1376	-2824 - 2865	-236.8. - 2433	NA
1D CBAR Stresses (psi)	-632.7 - 160.9	-356.2 – 452.2	-1412 – 667.1	NA

*Dimensions in red mean compression stress

In the second iteration, the displacements are of low magnitude for both support cases, having magnitudes of less than one in. From table 7, the highest displacements occur at the 3G case for both supports cases, being less in the extended supports case, which is similar as in the first iteration where the displacements decrease as the supports are extended.

78
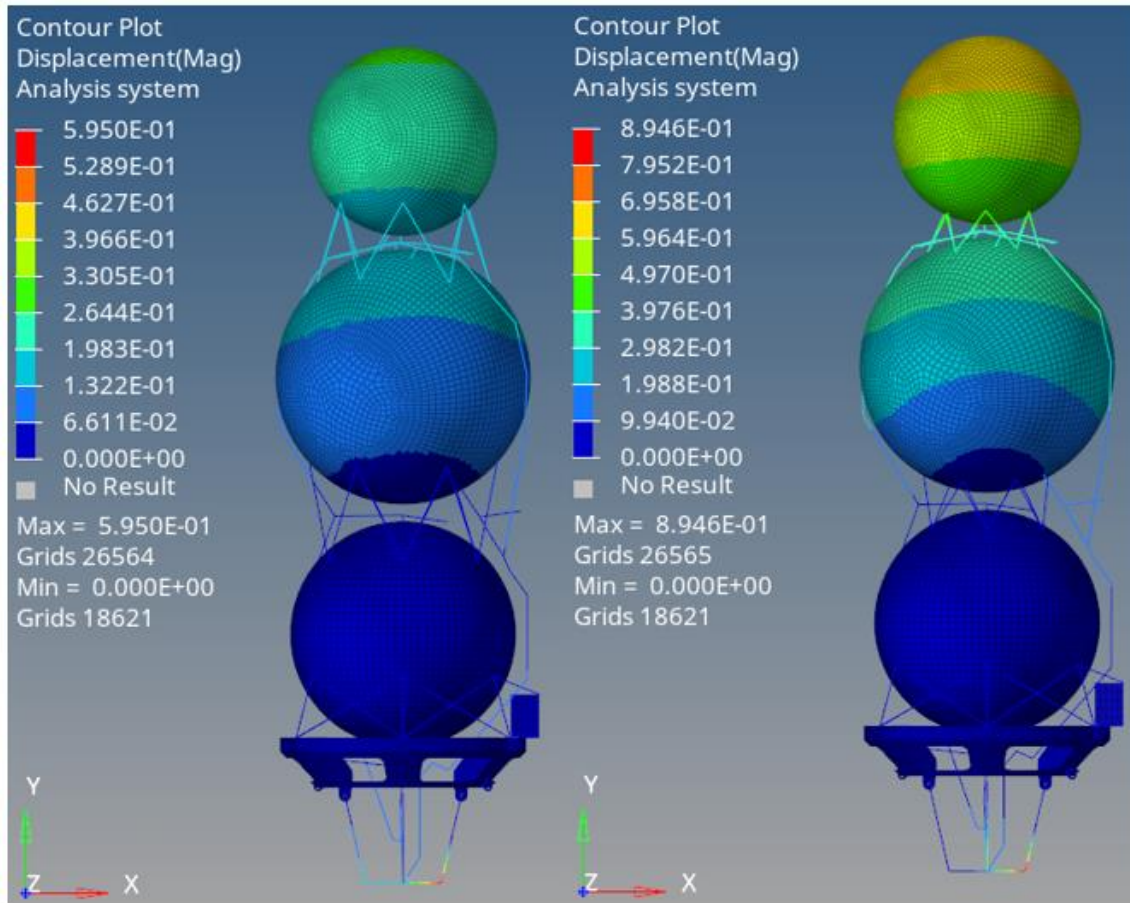
Figure 57. Second Iteration, Extended Supports (Left) and Shrunk Supports (Right) Cases,

Displacements at 3G Case

For the 2D stresses, in the second iteration, a considerable reduction in the stresses was seen for the shrunk supports case, where form being at 50350 the maximum stress, it was reduced to 33,840 psi in the second iteration for the 3G lateral load. Also, the highest stress was less at the extended supports case than at the shrunk supports case for the 3G lateral load case. Similar to the first iteration the highest displacement was located at the supports connecting the bottom plate and the engine ring.

Figure 58. Second Iteration, Extended Supports (Left) and Shrunk Supports (Right) Cases, 2D

Stresses at 3G Case

Similar to the first iteration the highest stresses were located at the wall of the oxygen tank and

bottom part of the methane tank at the spots where the rods connect to the tanks, this caused by

the 3G force that is trying to bend the structure in the x-direction.

Something interesting is that in the 5G case, for both support cases, these stresses increased at

the second iteration when they decreased, at least for the shrunk supports case, in the second

iteration at the 3G lateral load. The stresses in the 5G vertical, were around 17300 psi, while for

the 5G with pressure, there was no changes in the stresses.

Figure 59. Second Iteration, Extended Supports (Left) and Shrunk Supports (Right) Cases, 2D

Stresses at 5G With Pressure Case

For the CROD elements, the highest stresses also happen at the 3G lateral load, where they are around 2800 psi. In the 5G with pressure case, the highest stress is around 2400 psi.
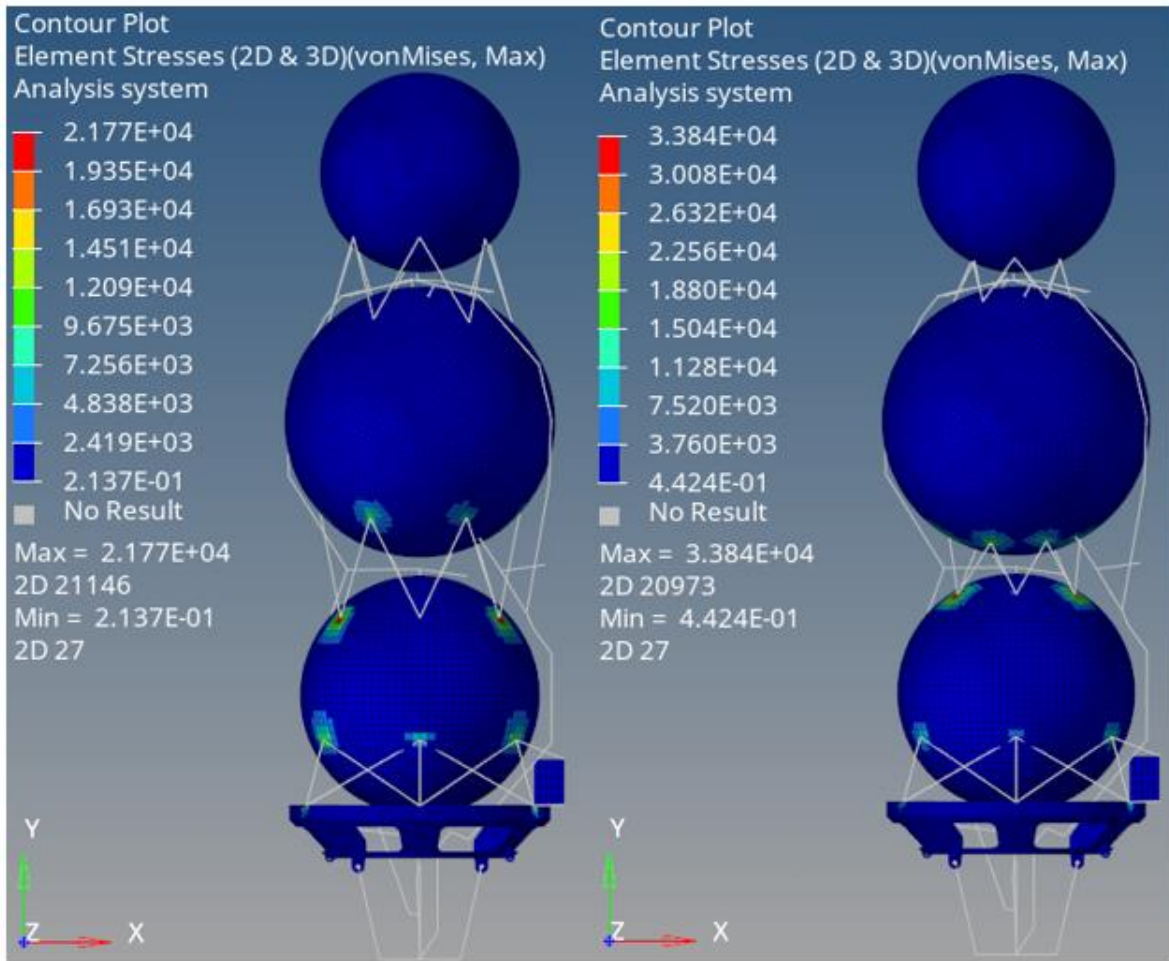
Figure 60. Second Iteration, Extended Supports (Left) and Shrunk Supports (Right) Cases,

CROD Stresses at 3G Case

The CROD elements that show the highest tension and compression are bottom plate-oxygen tank supports and some connecting the oxygen and methane tank

For the CBAR elements simulating the piping of the lander, the cases where high stresses are shown are in the 5G with pressure case, only in compression for both supports cases since tension is below 700 psi, and in the 3G lateral load case where these are above 700 psi in tension and above 500 psi in compression, but they are below those values as the supports are extended.
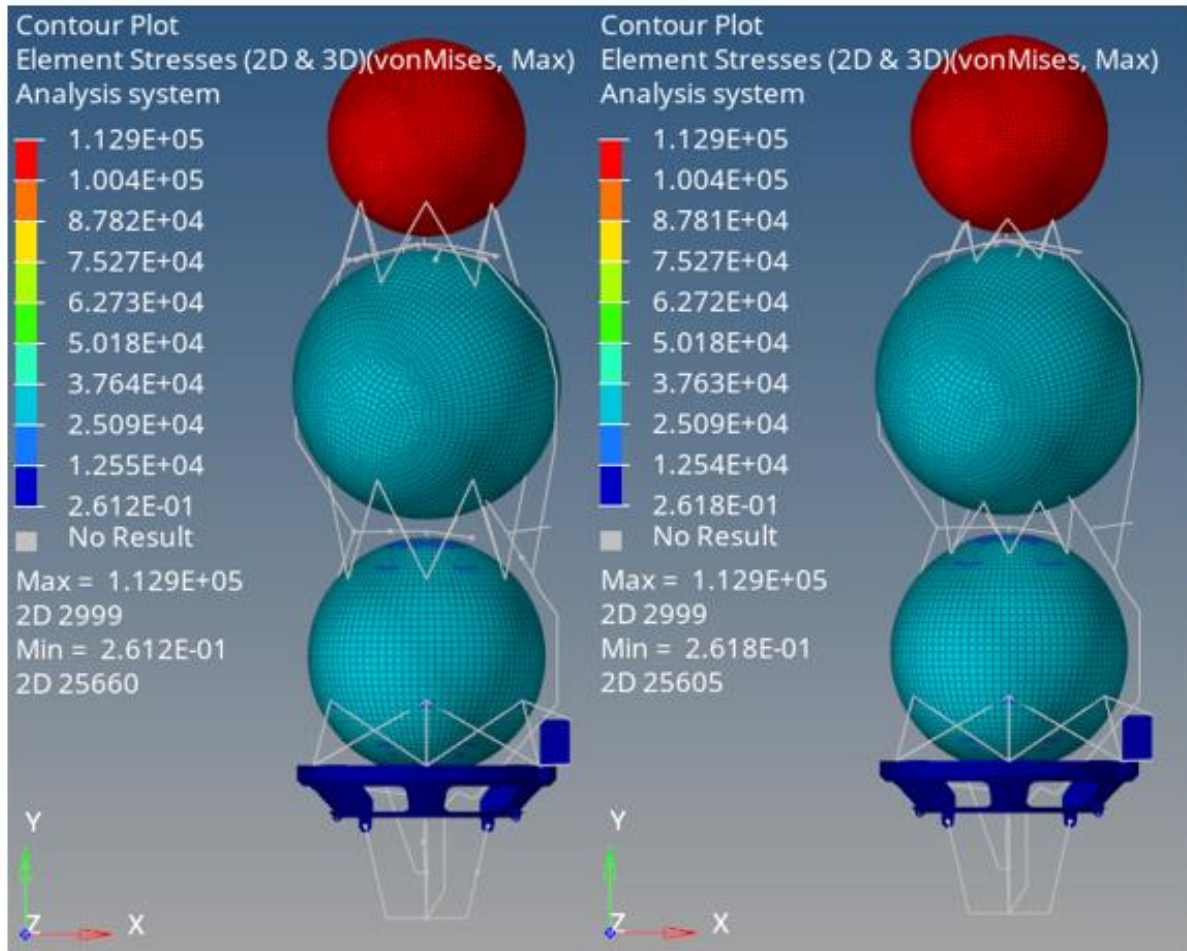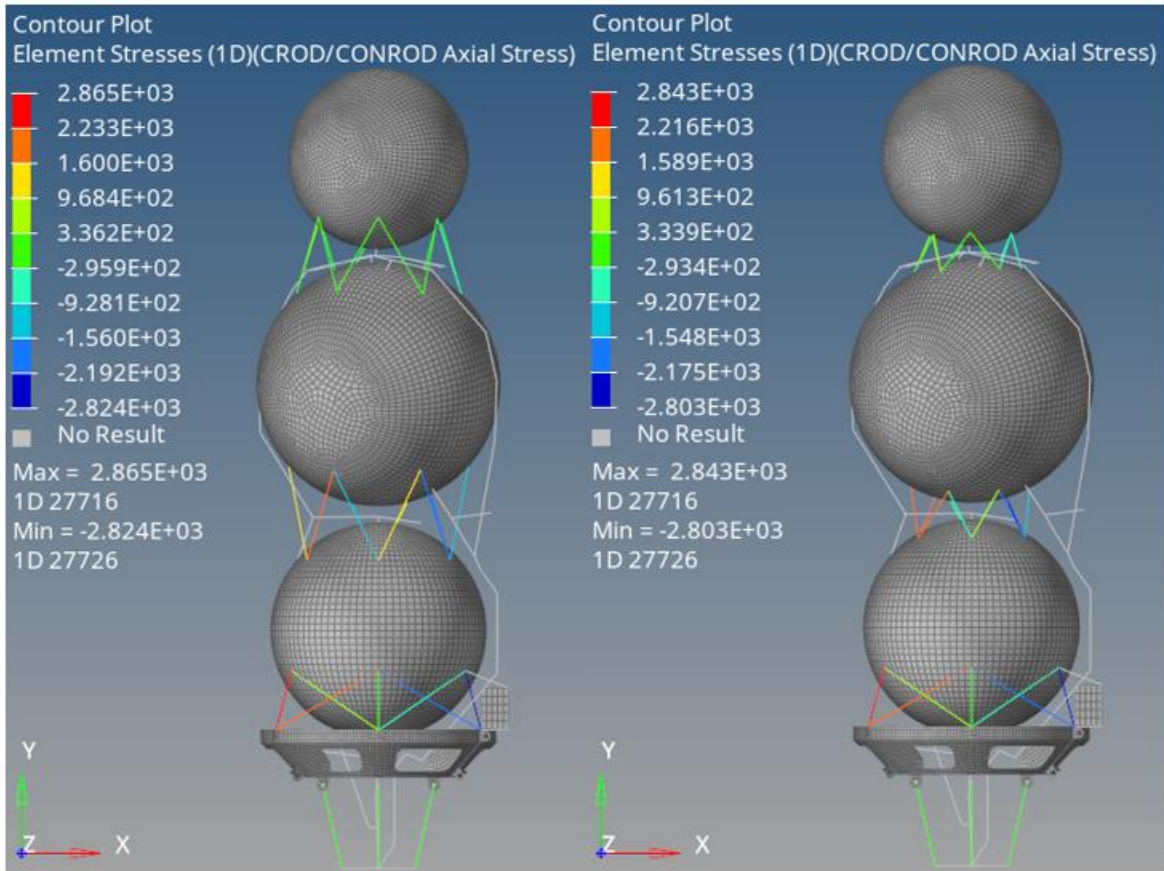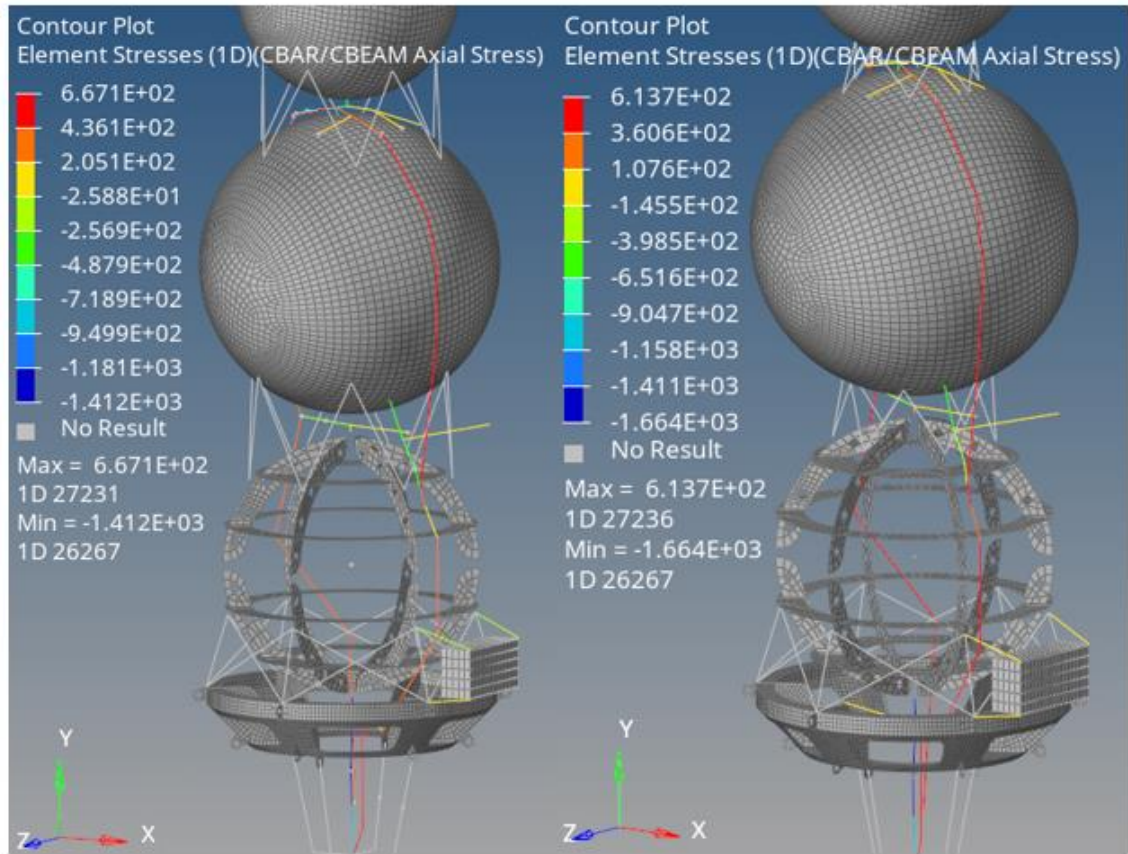
Figure 61. Second Iteration, Extended Supports (Left) and Shrunk Supports (Right) Cases,

CBAR Stresses at 5G With Pressure Case

These elements showing the highest compression are elements simulating the pipe going into the

engine from the oxygen tank, and the ones showing the highest tension are the ones vertically

positioned simulating the delivery and purge methane lines.

Chapter 4: Conclusion

From the analysis performed, it is seen that the 1D elements do not experience stresses that go beyond the allowable stress for aluminum 6061 with a factor of safety of 1.25 which is 32000 psi, except in the last modes for the second iteration. As the distance in between the tanks is decreased, from first iteration to the second iteration, the stresses in the tanks increase in the first mode of the modal analysis, this can be caused by the increase in the frequency of the first mode as the distance is decreased. In load cases, such as the 3G, these stresses go up to 50 ksi and as the supports are extended, they decrease to 20 ksi. Also, a further reduction in stresses was seen as the tanks were lowered.

From the analysis performed, it is seen that as the supports are extended out, the stresses decrease in the 1D elements, CROD and CBAR. Also, the stresses are reduced in the 2D elements as well as the supports are extended. The natural frequency also was seen to increase as the first mode was higher for the second iteration compared to the first iteration in all the support cases. The modes showed more aggressive oscillations in the structure, especially in the rods that connect the bottom plate to the engine ring and where the actuators were placed, as the frequency increased in the first mode. Even if the bending was less in the tanks and supports as the supports were extended and the tanks were lowered, as mentioned, the rods connecting the bottom plate to the engine saw more displacement and high stresses. In conclusion, the supports connecting the engine should increase in area to tolerate more stresses. Besides that, it is also encouraged to create a structure that supports the piping, especially the line where the helium delivery line and regulator are attached to. In addition, the drain and relief lines also should be supported by this structure since bending is caused by the solenoid valves. The most critical lines that should be supported should be the lines that connect to the engine, since, due to the oscillations in the rods

connecting the bottom plate and the engine ring, have high displacements and high stresses and thus also generate dangerous stresses in the outlet of the tanks, especially in the oxygen line where for the first mode, stresses above 90 ksi were spotted. It was discussed that flex hoses could be used to deliver the propellant to the engine which could reduce the stresses seen in the oxygen tank outlet, and the methane delivery line and oxygen purge and delivery lines.

For this analysis an avionics box was created referencing an atr enclosure. Due to time constrains the dimensions are not of an original atr box since the dimensions were provided late by the manufacturer. The box was placed outside the bottom plate and was supported by a 1 in X 1 in, 1/16" thickness square tube made out of aluminum 6105 found on GAINGER. The box should be supported by a structure that has more supports, even though the stresses were not of the magnitude above 5 ksi, except for the las mode in the second iteration, if the weight budget allows it, or it even can be placed inside the ring below the oxygen tank if the space allows it. The box did not show any significant stresses that are near the allowable stress for aluminum 6061.

Chapter 5: Future Work

The goal of this thesis was, besides to determine the magnitude of the stresses caused by the loads applied and to arrange the structure in a way that the maximum natural frequency could be achieved, was to compare two tentative designs for the JANUS lander vehicle, the one presented in the results section and a design where the propellant tanks are cylindrical and the pressurizing tank same as in the first iteration.
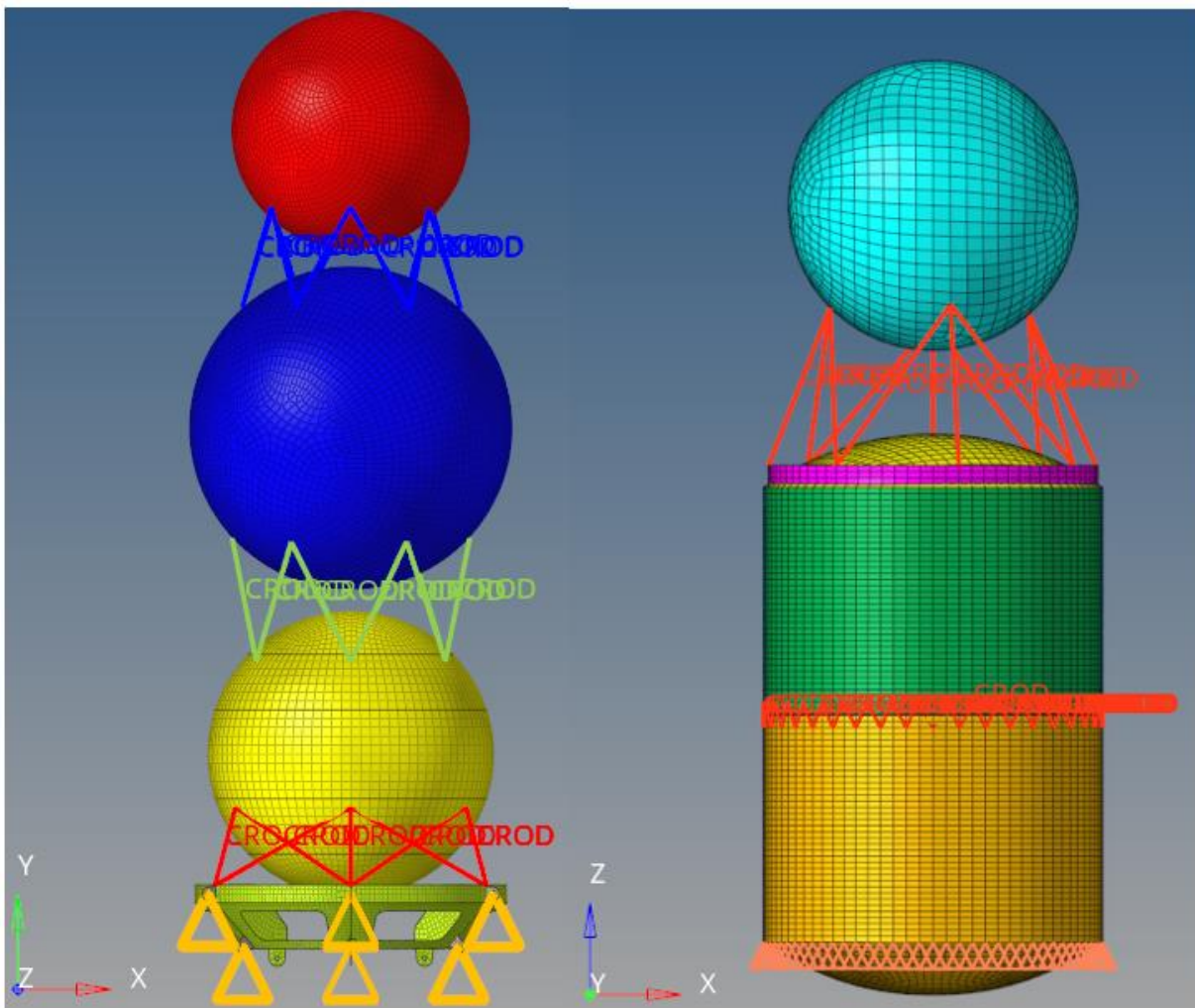

Figure 62. Tentative Designs. First Iteration (Left) and Second Iteration (Right)

Due to time constraints, both of these iterations couldn't be compared in detail, meaning that the piping, solenoid valves, regulator, avionics, gimbal, engine and bottom plate (if necessary for the second iteration) were not added to the second iteration. To have a general idea on the pros and cons of both iterations the avionics, piping, instrumentation and gimbal components were removed from the first iteration. The second iteration was fixed at the bottom edge of the orange cylinder (displayed by the orange triangles in both iterations) and a triangular pattern structure was created, similar to the one former soviet union rocket N1 had in the first three stages, as shown in figure 71 since the iteration is in an early stage of the design, missing the landing gear, avionics structure, gimbal system and propellant delivery system.
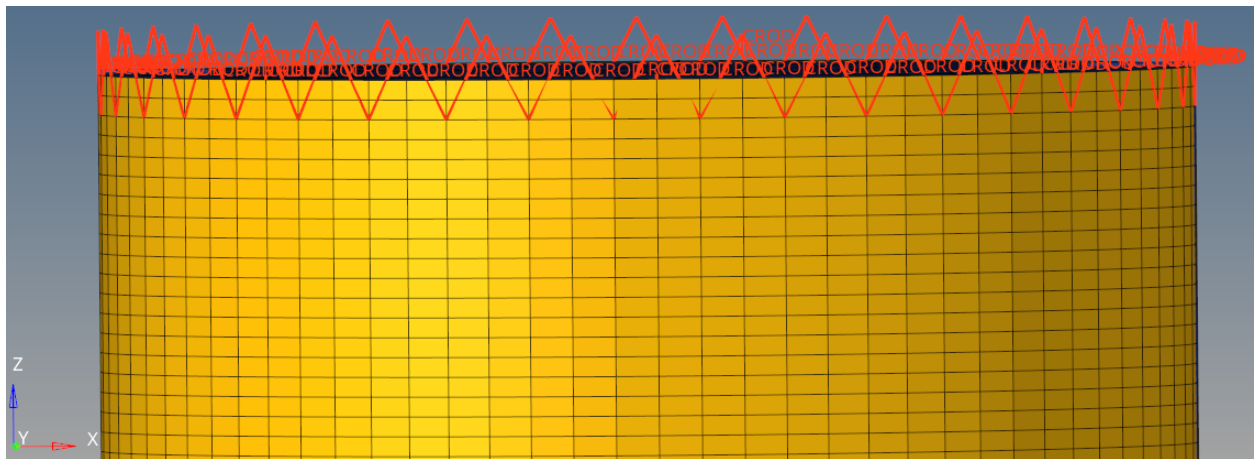
Figure 63. Connecting Rods (CROD Elements) for the second Iteration Propellant Tanks

From the results obtained, the second iteration has displacements in the 5G, 5G with pressure and 3G cases less than the ones the first iteration shows. In addition, the second iteration shows a first mode with a frequency of 89.46 compared to a frequency of 13.50 in the first iteration.

Even though the results like displacement and natural frequency seem reasonable and promising for the second iteration, 2D stresses seem not reasonable since the stresses at the

tanks, for the 5G with pressure case, show stresses of considerably less magnitude than the ones

presented in chapter 3 for the 5G with pressure case.

Figure 64. 5G With Pressure Load Case for First Iteration (Left) and Second Iteration (Rigth)

Also, the CROD elements exhibited a small stress compared to the one in the first iteration for all

cases except for the modal analysis.
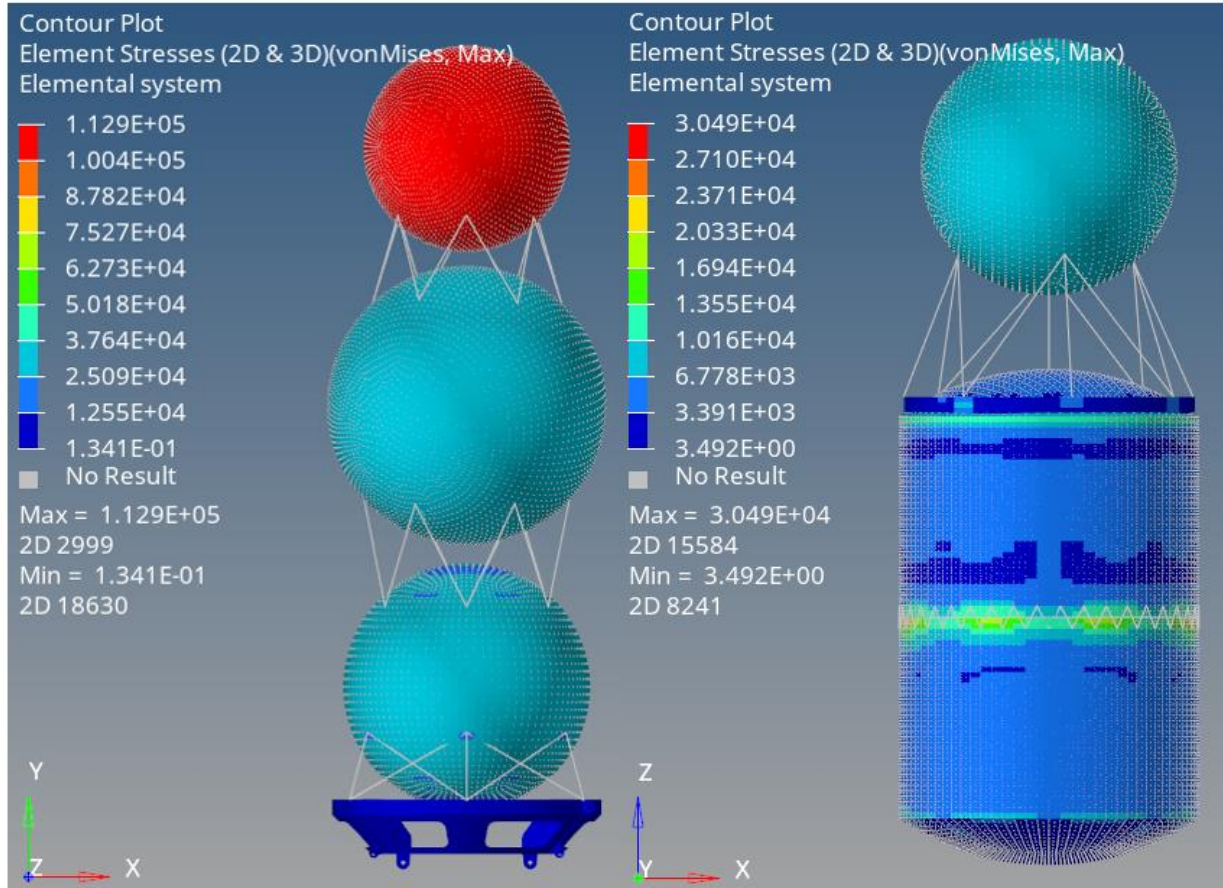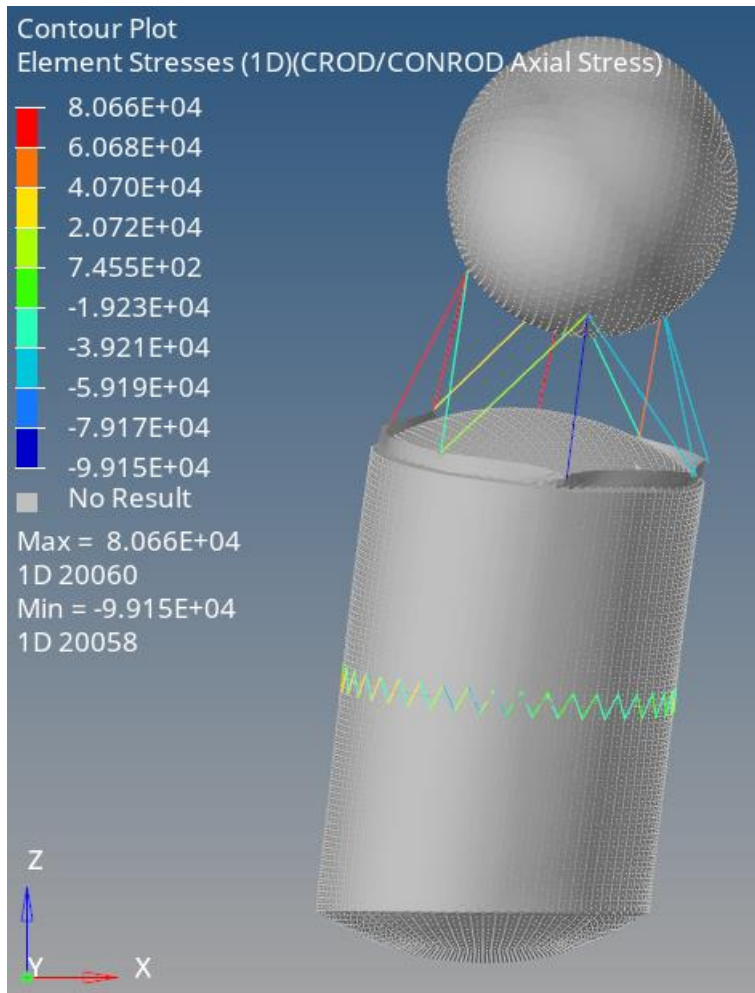
Figure 65. Second Iteration CROD Stresses at 89.46 Hz First Mode (Bending Mode)

A more detailed comparison should be made between these two iterations once components such as propellant delivery system, avionics, gimbal, landing gear (bottom plate if applicable) and engine (1D mass element) are added since these components affect the modes and also the magnitude of the stresses displayed in the analysis. Also, a "troubleshoot" of the results should be made since the stresses in the 5G with pressure case the stresses do not match.

The helium tank was analyzed individually for both iterations. The tank was constrained by few spc load types at the bottom, and a pressure of 4000 psi was applied. The same material card, property card (thickness of 0.25) with the same parameters were used, even the tank for the

second iteration was re-meshed, using more elements. The results still showed less stresses in the second iteration tank.

Figure 66. Stresses at a Pressure of 4000 psi in the First Iteration (Left) and Second Iteration (Right) Helium Tanks

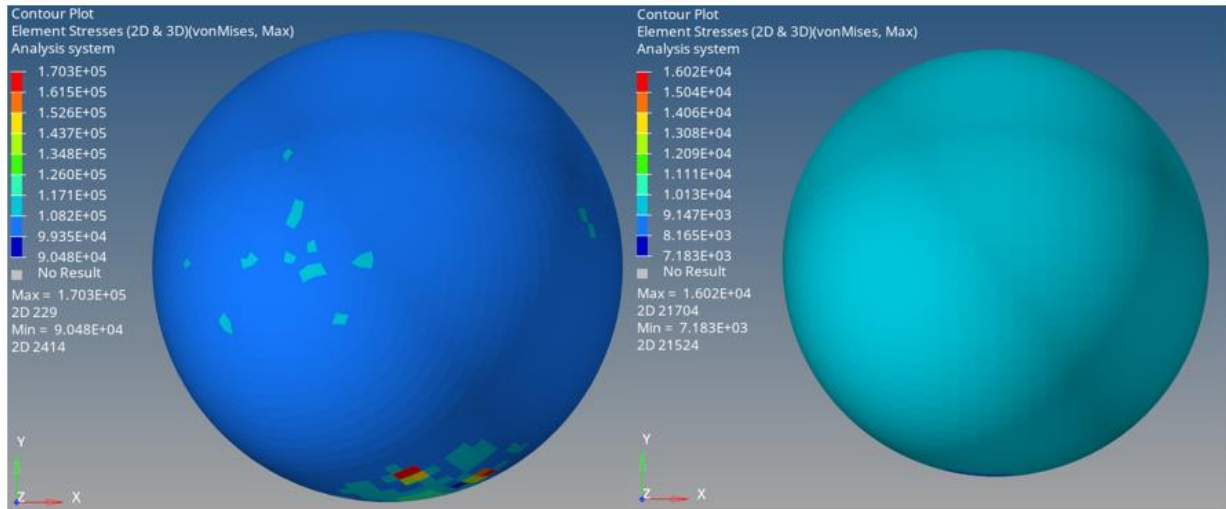A troubleshoot should be performed to determine the causes of the stresses being of a less magnitude in the second iteration helium tank.

Lastly, stronger aluminum alloys should be considered due to the high stresses that in some load cases were shown by the analysis. Aluminum 6066 and 2219 can also be considered.

References

[1] L. Mohon, "NASA Tests Methane Engine Components for Next Generation Landers," *NASA*, Oct. 28, 2015. http://www.nasa.gov/centers/marshall/news/releases/2015/nasa-tests-methane-powered-engine-components-for-next-generation-landers.html (accessed Jul. 22, 2022).

[2] W. T. Huntress, V. I. Moroz, and I. L. Shevalev, "Lunar and Planetary Robotic Exploration Missions in the 20th Century," *Space Science Reviews*, vol. 107, no. 3, pp. 541–649, Jul. 2003, doi: 10.1023/A:1026172301375.

[3] "Pioneer Program." https://space.jpl.nasa.gov/msl/Programs/pioneer.html (accessed Jul. 22, 2022).

[4] J. B. Plescia, M. S. Robinson, R. Wagner, and R. Baldridge, "Ranger and Apollo S-IVB spacecraft impact craters," *Planetary and Space Science*, vol. 124, pp. 15–35, May 2016, doi: 10.1016/j.pss.2016.01.002.

[5] "Surveyor to the Moon (1966-1968)." https://nssdc.gsfc.nasa.gov/planetary/lunar/surveyor.html (accessed Jul. 22, 2022).

[6] A. A. Siddiqi, *Beyond Earth: a chronicle of deep space exploration, 1958-2016*, Second edition. Washington, DC: National Aeronautics and Space Administration, Office of Communications, NASA History Division, 2018.

[7] "NASA Facts: Rangers and Surveyors to the Moon," *NASA Solar System Exploration*. https://solarsystem.nasa.gov/resources/2287/nasa-facts-rangers-and-surveyors-to-the-moon (accessed Jul. 22, 2022).

[8] S. Loff, "The Apollo Missions," *NASA*, Mar. 16, 2015. http://www.nasa.gov/mission_pages/apollo/missions/index.html (accessed Jul. 22, 2022).

[9] "NASA - NSSDCA - Spacecraft - Details." https://nssdc.gsfc.nasa.gov/nmc/spacecraft/display.action?id=1968-007A (accessed Jul. 22, 2022).

[10] "Milestones:Grumman Lunar Module, 1962-1972," *ETHW*, Jun. 14, 2022. https://ethw.org/Milestones:Grumman_Lunar_Module,_1962-1972 (accessed Jul. 22, 2022).

[11] "Grumman Lunar Module LM-13 at the Cradle of Aviation Museum." https://www.cradleofaviation.org/history/exhibits/exhibit-galleries/exploring_space/grumman_lunar_module_lm-13.html (accessed Jul. 22, 2022).

[12] "Apollo Lunar Module Structural Test Model," *The Franklin Institute*, Jun. 26, 2018. https://www.fi.edu/history-resources/grumman-lunar-module (accessed Jul. 22, 2022).

[13] Grumman "MAIN PROPULSION QUICK REFERENCE DATA." https://www.hq.nasa.gov/alsj/LM09_Main_Propulsion_ppMP1-22.pdf

[14] "Rocket Engine, Liquid Fuel, Apollo Lunar Module Ascent Engine | National Air and Space Museum." https://airandspace.si.edu/collection-objects/rocket-engine-liquid-fuel-apollo-lunar-module-ascent-engine/nasm_A19721169000 (accessed Jul. 22, 2022).

[15] "Rocket Engine, Liquid Fuel, Apollo Lunar Module Descent Engine | National Air and Space Museum." https://airandspace.si.edu/collection-objects/rocket-engine-liquid-fuel-apollo-lunar-module-descent-engine/nasm_A19720824000 (accessed Jul. 22, 2022).

[16] "Why Is Moment of Inertia Important?," *Raptor Scientific*, May 14, 2021. https://raptor-scientific.com/news/why-moi-is-important/ (accessed Jul. 22, 2022).

[17] S. R. Starin, and J. Eterno, "Attitude Determination and Control Systems," [online]. Accessed: Jul. 23, 2022. Available https://ntrs.nasa.gov/api/citations/20110007876/downloads/20110007876.pdf

[18] "center of gravity | Definition & Facts | Britannica." https://www.britannica.com/science/centre-of-gravity (accessed Jul. 22, 2022).

[19] A. Feldman and A. Y. Lee, "In flight estimations of Cassini spacecraft inertia tensor and thruster magnitude," Jan. 2006, Accessed: Jul. 22, 2022. [Online]. Available: https://trs.jpl.nasa.gov/handle/2014/39202

[20] "SHELLS vs. SOLIDS | Finite Element Analysis Quick Review." https://www.linkedin.com/pulse/shells-vs-solids-finite-element-analysis-quick-review-kuusisto-p-e- (accessed Jul. 22, 2022).

[21] The_Analyst, "Solid vs Shell vs Solid-Shell Elements," *FEA Tips*, Feb. 21, 2021. https://featips.com/2021/02/21/solid-vs-shell-vs-solid-shell-elements/ (accessed Jul. 22, 2022).

[22] *Automesh & Quick Edit Panel in Hypermesh (part-1)*, (Apr. 17, 2019). Accessed: Jul. 22, 2022. [Online Video]. Available: https://www.youtube.com/watch?v=yu3mhBkNbMQ

[23] "Manufacturing Solutions - Quick Edit panel." https://2022.help.altair.com/2022/hwdesktop/mfs/mfs.htm?help343.htm (accessed Jul. 23, 2022).

[24] "III Geometry in HyperMesh"https://altairuniversity.com/wp-content/uploads/2012/04/Student_Guide_59-71.pdf F_FVDFDF

[25] *When should I use tris and quads? Triangular Elements in Finite Element Modeling*, (Feb. 06, 2019). Accessed: Jul. 22, 2022. [Online Video]. Available: https://www.youtube.com/watch?v=mvUbe-Ih1CY

[26] "2D Meshing" https://www.altairuniversity.com/wp-content/uploads/2014/02/2Dmeshing.pdf (accessed Jul. 22, 2022).

[27] *Meshing in Hypermesh - Advance Meshing option for complex geometry*, (May 23, 2019). Accessed: Jul. 22, 2022. [Online Video]. Available: https://www.youtube.com/watch?v=dTjRwK9JItk

[28] "Practical Aspects of Finite Element Analysis," *Altair University*. https://altairuniversity.com/free-ebooks/free-ebook-practical-aspects-of-finite-element-simulation-a-study-guide/ (accessed Jul. 22, 2022).

[29] *Modeling rigid masses and their connections in Hypermesh*, (May 05, 2022). Accessed: Jul. 22, 2022. [Online Video]. Available: https://www.youtube.com/watch?v=hsYJK86waMQ

[30]"MAT1." https://2022.help.altair.com/2022/hwsolvers/os/topics/solvers/os/mat1_bulk_r.htm (accessed Jul. 23, 2022).

[31]"PLOAD4." https://2022.help.altair.com/2022/hwsolvers/os/topics/solvers/os/pload4_bulk_r.htm (accessed Jul. 23, 2022).

[32] "EIGRL." https://forum.altair.com/applications/core/interface/file/attachment.php?id=4132 (accessed Jul. 23, 2022).

[33]"EIGRL." https://2022.help.altair.com/2022/hwsolvers/os/topics/solvers/os/eigrl_bulk_r.htm#eigrl_bulk_r__eigrl_bulk_r_fn_gwb_2pp_h1b (accessed Jul. 23, 2022).

[34] *Setting up an FEA modal analysis*, (May 05, 2022). Accessed: Jul. 22, 2022. [Online Video]. Available: https://www.youtube.com/watch?v=fB4v-yyfpHo

[35] *Modal Analysis using Hypermesh [Optistruct Solver]*, (Aug. 02, 2020). Accessed: Jul. 22, 2022. [Online Video]. Available: https://www.youtube.com/watch?v=KV1ow8zqI2E

[36] *Performing a static g-analysis in Hypermesh/Optistruct*, (May 05, 2022). Accessed: Jul. 22, 2022. [Online Video]. Available: https://www.youtube.com/watch?v=Khz1eLaek-M

[37] A. Flores. (2021) Spacecraft Dynamics/ Rigid Body Dynamics [pdf].

[38] R. C. Hibbeler, *Mechanics of materials*, Tenth edition. Boston: Pearson, 2017.

[39] R. C. Hibbeler, *Engineering mechanics. Statics and dynamics*, Fourteenth edition. Hoboken: Pearson, 2016.

[40] "Validation Case: Modal Analysis of a Cantilever Beam | OnScale Solve Help," *OnScale*. http://https%253A%252F%252Fonscale.com%252Fhelp%252Fsolve%252Fvalidation%252Fvalidation-case-modal-analysis-cantilever-beam%252F (accessed Jul. 23, 2022).

[41] "Beam Deflection Calculator." https://www.omnicalculator.com/construction/beam-deflection (accessed Jul. 23, 2022).

Appendix

Appendix A. Masses of FEA Components of the original iteration and Fusion 360 CAD Components

Section	Current Analysis (Lbm)	Mass Budget (Lbm)
Tanks	189.218	250 (Weight Budget)
Helium Tank	85.36	85
Methane Tank	47.41	50.36
Oxygen Tank	37.21	38.21
Oxygen Tank Baffles	19.238	16.43
Main Structure	39.102	60 (Weight Budget)
Base Ring	13.767	14.29
Base Ring Ears	0.8	
Methane-to-Helium	6.05	5.976
Oxygen-to-Methane	6.629	6.216
Base Ring-to-Oxygen	11.856	N/A
TVC	65.85	60 (Weight Budget)
CBAR Connections (Gimbal System)	2.16	2.3
Actuator Mass	13.89 (Per Actuator)	14 (Per Actuator)
Engine Mass	49.8	50
Masses	900.34	
Helium Mass	61	61
Methane Mass	290.33	290.65 (for 30% FFC)
Oxygen Mass	549.01	540.34 (For 30% FFC)
Piping and Valves	51.53	75 (Weight Budget)
Pipe	17.95	
SV	33.58 (3lbs per sv)	
Total	1246.04	1270.34

Appendix B: Weight of the Supports Cases at Different Iterations

Supports Cases	HE-to-LCH4	LCH4-to-LOX	LOX-to-BOTTOM PLATE	Total Weight
Original Iteration				
Original Supports (lb)	6.05	6.629	11.856	24.535
First Iteraiton				
Original Supports (lb)	5.37	6.16	9.01	20.54
Shrunk Suppports (lb)	3.88	4.55	9.01	17.44
Extended Supports (lb)	6.91	7.61	12.71	27.23
Second Iteration				
Shrunk Supports (lb)	3.44	4.44	11.67	19.55
Extended Supports (lb)	6.44	7.61	11.67	25.72

Appendix C: FEA Analysis Components and Thicknesses and Dimensions

Components	Thickness (in)
Helium Tank	0.25
Methane Tank	0.125
Oxygen Tank	0.125
Bottom Plate	0.15
HE-LCH4 Supports	0.375 (radius)
LCH4-LOX Supports	0.375 (radius)
LOX-BOTTOM PLATE Supports	0.375 (radius)
Tubing	0.9 (Inner radius); 1 (outer radius)
Avionics Box Supports	1X1 box; 0.0625 thickness
Gimbal Supports	0.311 (radius)

Vita

Omar Vázquez was born and raised in the small town of Nombre de Dios, Durango. He moved to El Paso in 2011. After graduating from Burges High School, he completed his Associates of Science at EPCC. He transferred to UTEP in 2018. In the summer of 2018, he worked performing high pressure tests to pipes for quality control and as a welder assistant for Saulsbury Industries at Jal, New Mexico. In Spring 2020 he completed his Bachelor of Science in Mechanical Engineering then worked building concrete structures for JMG Concrete Services at Denver, Colorado for the summer of 2020. In fall 2020 he continued his education pursuing a Master of Science in Mechanical Engineering and joined the cSETR to work as a research assistant. In summer 2021 he interned at NASA Marshall Space Flight Center, working at branch ER13 performing research in Laser Powder Bed Fusion.

In Spring 2022 he accepted a full-time position as a Propulsion Test Engineer with Blue Origin at Van Horn, TX, with an expected start date in September 2022.

Contact Information: omarvazs17@gmail.com

This thesis/dissertation was typed by Omar Vázquez.